



**HAL**  
open science

## **Fourty years after the promise of “ ceramic steel? ”: zirconia-based composites with a metal-like mechanical behavior.**

J rome Chevalier, Alethea Liens, Helen Reveron, Fei Zhang, Pascal Reynaud,  
Thierry Douillard, Laura Preiss, Valter Sergio, Vanni Lugh, Mike Swain, et al.

### **► To cite this version:**

J rome Chevalier, Alethea Liens, Helen Reveron, Fei Zhang, Pascal Reynaud, et al.. Fourty years after the promise of “ ceramic steel? ”: zirconia-based composites with a metal-like mechanical behavior.. Journal of the American Ceramic Society, 2019, 10.1111/jace.16903 . hal-02371733

**HAL Id: hal-02371733**

**<https://hal.science/hal-02371733v1>**

Submitted on 15 Dec 2020

**HAL** is a multi-disciplinary open access archive for the deposit and dissemination of scientific research documents, whether they are published or not. The documents may come from teaching and research institutions in France or abroad, or from public or private research centers.

L'archive ouverte pluridisciplinaire **HAL**, est destin e au d p t et   la diffusion de documents scientifiques de niveau recherche, publi s ou non,  manant des  tablissements d'enseignement et de recherche fran ais ou  trangers, des laboratoires publics ou priv s.



**Fourty years after the promise of « ceramic steel? »:  
zirconia-based composites with a metal-like mechanical  
behavior**

Journal:	<i>Journal of the American Ceramic Society</i>
Manuscript ID	Draft
Manuscript Type:	Invited Feature Article
Date Submitted by the Author:	n/a
Complete List of Authors:	CHEVALIER, Jérôme; INSA, Materials Science Liens, Alethea; INSA, Materials Science Reveron, Helen; MATEIS-GEMPPM Insa-Lyon, Ceramics and Composites Zhang, Fei; INSA, Materials Science Reynaud, Pascal; INSA Lyon Douillard, Thierry; MATEIS, INSA Lyon, CNRS UMR5510; Preiss, Laura; INSA, Materials Science Sergo, Valter; University of Trieste, Materials and Natural Resources; University of Trieste, Lughi, Vanni; University of Trieste Swain, Michael; University of Sydney Courtois, Nicolas; Anthogyr SAS
Keywords:	zirconia, phase transformations, plasticity
Author-supplied Keyword: If there is one additional keyword you would like to include that was not on the list, please add it below::	

SCHOLARONE™  
Manuscripts

## Fourty years after the promise of « ceramic steel? »: zirconia-based composites with a metal-like mechanical behavior.

Jérôme Chevalier<sup>a,\*</sup>, Aléthéa Liens<sup>a</sup>, Helen Reveron<sup>a</sup>, Fei Zhang<sup>a</sup>, Pascal Reynaud<sup>a</sup>, Thierry Douillard<sup>a</sup>, Laura Preiss<sup>a</sup>, Valter Sergio<sup>b,c</sup>, Vanni Lughì<sup>b</sup>, Mike Swain<sup>d,e</sup>, Nicolas Courtois<sup>f</sup>

<sup>a</sup> Université de Lyon, INSA-Lyon, UMR CNRS 5510 MATEIS, 20 Avenue Albert Einstein, 69621 Villeurbanne Cedex, France

<sup>b</sup> Engineering and Architecture Dept., University of Trieste, Italy

<sup>c</sup> Faculty of Health Sciences, University of Macau, SAR Macau, China

<sup>d</sup> AMME, University of Sydney, NSW 2006 Australia

<sup>e</sup> Engineering, Don State Technical University, Rostov-on Don, Russia.

<sup>f</sup> Anthogyr SAS, 2237 avenue A. Lasquin 74700 Sallanches, France

### Abstract

40 years ago, Garvie and his Australian co-workers reported that the stress induced transformation of metastable tetragonal zirconia grains to the monoclinic symmetry could give rise to a powerful toughening mechanism. Their results even led them to consider zirconia systems as analogues of certain steels. This seminal paper generated extraordinary excitement in the ceramic community and it is still the subject of extensive research. Transformation toughening is widely used in zirconia materials and results in an increase in strength and toughness when compared to non-transformable ceramics, but the implementation into strong, tough, and sufficiently stable materials has not been fully reached. Zirconia ceramics generally fail at low strains with a much larger scatter in the strength values than metals and require statistical approaches to failure. Here we describe in details the mechanical behavior laws of ceria-doped zirconia composites exhibiting a high degree of stress-induced transformation. They present, to some extent, mechanical behavior analogous to a metal, displaying, *i*) significant amount of transformation-induced plasticity without damage, *ii*) very high flaw

---

\* Corresponding author : [jerome.chevalier@insa-lyon.fr](mailto:jerome.chevalier@insa-lyon.fr)

1  
2  
3 tolerance and *iii*) almost no dispersion in strength data. They potentially open new application  
4 avenues in situations where the advantages of ceramics were dampened by their brittle failure  
5 behavior. In particular, the consequences of such behavior for dental implants and additive-  
6 manufactured structures are highlighted.  
7  
8  
9  
10  
11  
12  
13  
14  
15  
16  
17  
18  
19  
20  
21  
22  
23  
24  
25  
26  
27  
28  
29  
30  
31  
32  
33  
34  
35  
36  
37  
38  
39  
40  
41  
42  
43  
44  
45  
46  
47  
48  
49  
50  
51  
52  
53  
54  
55  
56  
57  
58  
59  
60

For Peer Review

## I. Introduction

Zirconia ( $\text{ZrO}_2$ ) was first identified by the German chemist Martin Heinrich Klaproth in 1789 [1] as a reaction product of heating zirconium. In 1892, a more abundant source was discovered in the mineral Baddeleyite (80-98% of zirconia) [2]. An important step in the development of zirconia was published just a century ago in the *Journal of the American Ceramic Society* during its inaugural year in 1918, by Phillips, who proposed a procedure for the purification of zirconium dioxide [3]. However, it was not until 1928 that the first commercial zirconia-based product appeared, in the form of MgO-stabilized  $\text{ZrO}_2$  crucibles for metal melts [4]. Because of the tetragonal (*t*) to monoclinic (*m*) martensitic phase transformation that occurs during cooling at  $\sim 950^\circ\text{C}$  (temperature referred to as  $M_s$ , *Martensitic-Start*), accompanied by approximately 5% of volume increase [5], pure zirconia was indeed unsuitable for numerous technical applications, due to the impossibility of full-densification without catastrophic failure upon cooling and/or its poor stability when cycling at high temperatures (in the range 900-1200°C). However, it was shown that certain oxides could be added to zirconia and stabilize the high-temperature phases (cubic or tetragonal) at room temperature (see Panel A), thus allowing the use of this ceramic in a wide range of application fields. Nevertheless, for many years the use of CaO or MgO-stabilized zirconia was limited to the refractory industry. The discovery of the phase transformation toughening mechanism by Garvie and co-authors in 1975 [6] created new visions for high-performance zirconia applications. It was stated that ‘*The presence of a tetragonal phase that can revert to the stable monoclinic form has a number of important consequences. The first is a significant-increase in strength [...]. A more important contribution comes from the absorption of energy during the martensitic transformation of tetragonal particles, as in the TRIP steels*’. In other words, the *t-m* transformation at the crack tip could lead to an important transformation-induced absorption of energy. Their results, including the fact that the phase diagrams showed similar features to the one of Fe-C, even led them to consider zirconia systems as analogues of certain steels. This seminal paper created extraordinary excitement in the ceramic community and zirconia is still the subject of extensive research, debates and controversies. From a practical point of view, zirconia finds applications in a number of technical fields such as in Thermal Barrier Coatings (TBCs), bearings, fuel cell membranes, oxygen sensors, optical ferrules, and, most recently, biomedical devices. Today stabilized-zirconia is without doubt one of the most important ceramic materials because of its unique combination of properties such as high strength and fracture toughness at room temperature, high density, hardness, wear resistance, high temperature stability and low thermal

1  
2  
3 conductivity. However, it must be recognized that transformation toughening leads to an  
4 increase in strength when compared to non-transformable ceramics, but the translation into  
5 tough, strong and sufficiently stable materials has not been fully accomplished. For most  
6 industrial applications, zirconia ceramics fail by crack extension at low strains along with much  
7 larger scatter in strength than metals and this behavior imposes the use of statistical failure  
8 approaches. This is the case of the most common zirconia ceramic, stabilized with Yttria (*Y-*  
9 *TZP*, for *Yttria-Tetragonal Zirconia Polycrystal*). On the other hand, in the past [7-10] and more  
10 recently [11, 12], some Ceria-doped zirconia (*Ce-TZP*) based ceramics and composites were  
11 shown to exhibit significant amount of transformation-induced plasticity and almost no  
12 dispersion in strength data. Such materials could open new possibilities for applications where  
13 the limits of the failure properties of ceramics could be overcome, provided their mechanical  
14 behavior laws are well understood and described. The aim of the present paper is thus to  
15 describe in details the mechanical behavior of ceria-doped zirconia composites in relation to  
16 their transformation characteristics, and to discuss the transition from a conventional brittle  
17 behavior to a transformation induced ductility and, finally, to highlight the positive impact of  
18 genuine ductility on future potential applications. We here take the example of dental implants  
19 and additive-manufactured materials, for which a certain ductility and defect tolerance would  
20 be utterly beneficial.

## 34 35 36 **II. Where are we?**

37  
38  
39 Based on the established linear elastic fracture mechanics and Griffith equation, it is well known  
40 that there are two approaches to obtain reliable structural ceramic materials: controlling flaw  
41 size and/or increasing toughness and crack resistance. Indeed, for brittle materials, it is  
42 generally considered that strength  $\sigma_R$  is given by:

$$43 \sigma_R \sim \frac{K_{IC}}{\sqrt{\pi c}} \quad (1)$$

44  
45  
46 Where  $K_{IC}$  is the toughness and  $c$  is the size of the most critical defect.

47  
48  
49  
50  
51  
52  
53 With the continuing trend of seeking ever stronger materials, previous studies in the 80's  
54 proceeded to identify and reduce strength-reducing flaws by improving processing [13], for  
55 example through colloidal approaches to remove powder agglomeration and/or to induce  
56 microstructure refinement. Nevertheless, these strength enhancements were limited, as in the  
57 case of alumina ceramics, which barely exceed 600 MPa, even with careful control of grain size  
58  
59  
60

1  
2  
3 and processing defects. Subsequently in the 90's, researches placed emphasis on improving the  
4 toughness of brittle ceramics. Various methods were developed such as; *i*) phase transformation  
5 toughening in zirconia ceramics, *ii*) bridging via larger grains along with elongated  
6 morphology, *iii*) reinforcement by dispersing particles, whiskers and/or fibers, etc. [14-19].  
7  
8 Ceramics are not intrinsically tough as metals (where dislocation-based plasticity ahead of the  
9 crack tip is the key factor), but can be extrinsically toughened at the crack tip wake. This results  
10 in the generation of a crack-resistance curve (rising R-curve), which means that the toughness  
11 increases as the crack grows, eventually reaching a plateau value. However, unfortunately,  
12 strength is influenced by short-crack extension behavior and the optimal conditions  
13 (composition, grain size, transformability...) that maximize ceramic strength and toughness are  
14 not usually coincident. Consequently, the design of strong and tough materials is inevitably a  
15 matter of compromise. Therefore, over the last two decades, studies focused on strategies to  
16 obtain a better balance between strength and toughness in ceramic materials [5, 11, 12, 20-45].

17  
18 Following the extensive research studies on the development of tough and strong  
19 ceramics, bio-inspired materials have been also investigated, such as the damage-  
20 resistant materials containing a large inorganic content that widely exist in nature for  
21 structural purposes, including bone, nacre or enamel. Bio-inspired materials are  
22 tailored to have similar specific hierarchical structures as biological materials at  
23 multiple length scales [46-49]. Some remarkable enhancements in toughness were indeed  
24 achieved, for example, nacre-like 'brick-and-mortar' structures made from hybrid materials  
25 (alumina-polymethyl methacrylate) or in artificial mineral constituents, resulting in materials  
26 having long-crack fracture toughness of  $\geq 20 \text{ MPa}\cdot\sqrt{\text{m}}$  and strength of 200-500 MPa [46, 47].  
27  
28 By looking at the fracture behavior, the fracture resistance of these bio-inspired ceramics is  
29 derived from a series of extrinsic toughening mechanisms acting at various length- scales and  
30 developing a substantial R-curve effect [46-50]. These mechanisms are related to damage  
31 extension and development of a 'process zone' in which crack bridging, deflection and  
32 branching act to increase the crack resistance. Apart from the case of metal- or polymer-  
33 impregnated bio-inspired ceramics, ceramics remain 'brittle' in the sense that no ductility is  
34 observed. The term ductility is meant to convey, from a mechanical point of view, that a  
35 permanent strain remains after unloading with minimal loss in stiffness and no associated  
36 damage.

1  
2  
3 Considering the development of ‘traditional’ zirconia ceramics, the capability of obtaining  
4 genuinely “ductile” ceramics from transformation-induced plasticity has been under-explored.  
5 Some zirconia indeed exhibit pronounced R-curve behavior (high fracture toughness  $\geq 20$   
6  $\text{MPa}\cdot\sqrt{\text{m}}$  reported in some cases [14]) and a few studies have shown that Ce-TZP based  
7 ceramics might be considered as ‘ductile’, with a certain degree of transformation-induced  
8 plasticity before failure [6-10, 20, 21, 51-57 and Figure 1]. Recent studies on micro-pillars have  
9 also reported that some Y-TZP ceramics exhibit transformation-induced plasticity [58],  
10 provided the size of the tested samples was small enough and free of processing defects.  
11 Transformation-induced plasticity is thus more limited in 3Y-TZP than in Ce-TZP and has  
12 never been reported on large-sized samples.  
13  
14  
15  
16  
17  
18  
19

20  
21 Zirconia offers the possibility of utilizing different stabilizers [13, 22]. As explained in Panel  
22 A, metastable tetragonal zirconia can be retained at room temperature by alloying with  $\text{Y}_2\text{O}_3$ ,  
23  $\text{CeO}_2$  or other rare earth oxides. 3 mol.% yttria-stabilized zirconia (3Y-TZP) possesses the  
24 highest strength (800-1200 MPa) among all single-phase oxide ceramics, but only moderate  
25 fracture toughness ( $\sim 6 \text{MPa}\cdot\sqrt{\text{m}}$ ). Ce-TZP (typically 10 and 12 mol.% Ce-TZP) on the other  
26 hand exhibits higher toughness (15-20  $\text{MPa}\cdot\sqrt{\text{m}}$ ) but lower strength (typically less than 600  
27 MPa). The strength difference between Y-TZP and Ce-TZP is in part related to the fact that  
28 fully dense 3Y-TZP can be easily sintered while retaining a relatively small grain size  
29 (submicron grain size, typically as low as  $0.3 \mu\text{m}$ ), whereas the grain size of Ce-TZP generally  
30 lies above  $1.5\text{-}2.0 \mu\text{m}$ . Indeed, the mobility of grain boundaries during sintering is much higher  
31 in Ce-TZP than in Y-TZP and it is thus difficult to obtain a fine-grained, fully dense Ce-TZP.  
32 Furthermore, compared to Y-TZP, Ce-TZP has a lower critical transformation stress ( $\sigma_c^{t-m}$ ) and  
33 a higher spontaneous tetragonal-monoclinic transformation temperature  $T_0^{t-m}$ , which is  
34 associated with a larger transformation zone size around a crack [59]. Depending on the dopant  
35 concentration and the final grain size, the width of the transformation zone ( $h$ ) in Ce-TZP is in  
36 the range of  $100 \mu\text{m}$  while the transformation zone of Y-TZP is much smaller, typically a few  
37 micrometers [60]. Regarding the R-curve behavior, as shown in Figure 2 [5, 23-24], the extent  
38 of transformation toughening is proportional to  $h^{1/2}$ , while the crack extension to achieve a  
39 plateau value is a multiple (4 to 6 times) of  $h$ . In the case of Ce-TZP ceramics, this results in  
40 having a high saturation level ( $K_{Rmax}$ ). Furthermore, a crack can stably grow several times larger  
41 than the maximum transformation zone size, and, hence, Ce-TZP has high flaw tolerance  
42 characteristics [61]. Nevertheless, as explained above, since high strength can only be obtained  
43 for materials with high toughness at small crack length, the gradual increase of crack resistance  
44  
45  
46  
47  
48  
49  
50  
51  
52  
53  
54  
55  
56  
57  
58  
59  
60



1  
2  
3 (small initial slope of R-curve) in Ce-TZP gives rise to relatively modest strength compared to  
4 Y-TZP.  
5

6  
7 As a consequence, thanks to their high strength, 3Y-TZP ceramics (especially 3 mol.%) have  
8 found various high-performance applications, such as in the biomedical field, initially for hip  
9 joints (almost abandoned after 2001, due to a failure episode associated to the issue of aging  
10 described below), then for dental prostheses and implants. Moreover, high-quality commercial  
11 3Y-TZP powders are readily available, and these ceramics can be quite easily machined at  
12 different steps of the process (either in green, pre-sintered or sintered stage) and can be made  
13 more translucent. However, Y-TZP based systems may suffer from hydrothermal aging in the  
14 presence of water [59]. Aging of 3Y-TZP may be a critical problem in certain cases: this phase  
15 destabilization, occurring spontaneously (without the need of applied stresses) at room  
16 temperature and in presence of water had clearly a negative impact in the orthopedic community  
17 because of the failure of more than eight hundred 3Y-TZP Prozyr® femoral heads in 2000,  
18 commencing within months after implantation [59]. Nevertheless, the use of yttria-stabilized  
19 zirconia is booming in dental fields to make crowns, bridges and even implants, for which the  
20 optical properties (color and translucency) is another important driving force. Research is also  
21 ongoing to improve the aging stability of 3Y-TZP ceramics by adding alumina as dopant,  
22 increasing the yttria content and by a careful processing control [62-65]. Obtaining completely  
23 aging-free 3Y-TZP seems to be a difficult task due to the inherent presence of oxygen vacancies  
24 generated when  $Y^{3+}$  replaces  $Zr^{4+}$  in the cationic sub-lattice, in order to achieve charge  
25 neutrality. It is now well accepted that the presence of oxygen vacancies, stabilizing the  
26 tetragonal phase in Yttria-Zirconia system, are also the origin of aging, since they can be re-  
27 filled by hydroxyl groups in the presence of water [59]. This is in contrast to Ce-TZP, where  
28 tetragonal zirconia is stabilized by a tetravalent dopant ( $Ce^{4+}$ ) thanks to a steric effect and the  
29 absence of oxygen vacancies make this system very stable in the presence of water [59, 61]. It  
30 is worth recalling that, as explained before, not only having a high strength is important but,  
31 today, the quest is also to obtain materials with an optimal balance between strength, toughness  
32 and long-term stability, a balance that, ideally, should be tailored for each specific application.  
33 Ce-TZP systems can benefit from a high degree of transformation-induced plasticity and high  
34 toughness [5, 23-25, 51], making them highly suitable for obtaining such balance between  
35 strength, toughness and long-term stability in water-rich environments. The most critical  
36 challenges in these systems is thus to refine the microstructure, optimize the degree of phase  
37 transformation and better understand the mechanical behavior laws [66].  
38  
39  
40  
41  
42  
43  
44  
45  
46  
47  
48  
49  
50  
51  
52  
53  
54  
55  
56  
57  
58  
59  
60

1  
2  
3 It is well known that processing nanocomposites is a promising strategy for inhibiting grain  
4 growth. Introducing an immiscible second phase like alumina to pin the grain boundaries can  
5 control the grain growth of zirconia. Finer microstructures lead to higher  $\sigma_c^{t-m}$  and steeper R-  
6 curves slopes, but higher  $\sigma_c^{t-m}$  may compromise the toughening extent in zirconia ceramics. In  
7 this sense, it may be advantageous to have additional toughening effects, like adding elongated  
8 phases which can also hinder the zirconia grain growth and further improve the toughness by  
9 crack deflection [26, 67-70]. The challenge of incorporating elongated third phases is to retain  
10 the fine and uniform microstructure without turning themselves into “critical defects”. Such  
11 Ce-TZP based-composites, with high flaw tolerance and narrow strength distributions, have  
12 been reported [11, 12, 21, 22, 25-42, 71]. Without achieving the very high strength of 3Y-TZP,  
13 Ce-TZP based composites can be made strong enough for most engineering applications, with  
14 a higher toughness and reliability (*i.e.* high Weibull Modulus) and a certain degree of plasticity  
15 [5, 12, 22-25]. However, it has to be admitted that, 40 years after the introduction of the concept  
16 of ‘Ceramic steels’ and 30 years after the first studies on ductile Ce-TZP [6-10, 20, 21, 51-57],  
17 their potential has not been fully exploited. There is indeed no application of this  
18 transformation-induced plasticity feature into real ceramic products.  
19  
20  
21  
22  
23  
24  
25  
26  
27  
28  
29  
30

31 This paper therefore attempts to address the following issues:

- 32 - How can we process ultra-fine Ce-TZP based composites and how can we reach the  
33 highest degree of strength and toughness?
  - 34 - What is the mechanical behavior law of a highly transformable (ductile) zirconia  
35 composite and what can be the extent of plasticity achievable with such materials?
  - 36 - Can we talk about transformation-induced plasticity?
  - 37 - What are the benefits and drawbacks of highly transformable zirconia systems and what  
38 can be the targeted future applications?
- 39  
40  
41  
42  
43  
44  
45  
46  
47

### 48 **III. Processing challenges and experimental methods (Ce-TZP composites)**

#### 49 **General challenges in processing ultrafine ceramic composites**

50  
51 Over the past few decades, the mechanical properties of structural ceramics have been  
52 substantially improved thanks to the development of ceramic nanocomposites [15]. These  
53 composite materials are typically processed by adding fine particles/whiskers/elongated phases  
54 to different ceramic matrix (oxides and non-oxides) with the aim of refining the microstructure  
55  
56  
57  
58  
59  
60

1  
2  
3 (increasing strength and hardness) and/or to promote other toughening or high temperature  
4 strengthening mechanisms [16-19].  
5  
6

7 In the case of zirconia-based composites, the progress made to combine strength and toughness  
8 in a unique material stems not only from a better understanding of toughening/strengthening  
9 mechanisms but also from improvements achieved in the processing of nano-powders and the  
10 capability of developing complex microstructures at the nanoscale.  
11  
12  
13

14  
15 Typically, ceramic composites are processed by mixing appropriate quantities of commercial  
16 or synthesized powders in aqueous suspensions. After the dispersion step (through ball-milling,  
17 attrition milling, planetary milling, etc.), the slurry can be slip-casted onto a porous mold and  
18 then sintered (natural sintering usually at  $T > 0.5T_{\text{melting}}$ ) or dried (spray-drying or natural drying  
19 followed by dry-milling) in order to obtain a granulated powder. The latter is then pressed (by  
20 uniaxial pressing or cold isostatic pressing) and sintered or pressed and sintered at once (by hot  
21 pressing, hot isostatic pressing, Spark Plasma Sintering etc.). Ultimately, preparing ceramic  
22 composites with homogenous and controlled microstructure requires optimizing both powder  
23 synthesis and processing.  
24  
25  
26  
27  
28  
29

30  
31 Zirconia-based composites can be prepared from milling and mixing powders [72]. However,  
32 this processing route often yields to materials with coarser microstructures than those obtained  
33 with bottom-up approaches. The so-called colloidal processing based on sol-gel methods  
34 enables development of ultrafine materials, but it is more complex and, frequently, the use of  
35 expensive organic precursors such as metal alkoxides is required [73]. Since 2000 onwards  
36 various surface modification techniques have been used to produce composite powders from  
37 pure zirconia powders and inexpensive inorganic salts [74, 75]. Starting from a commercial  
38 powder, the surface of particles is first coated by precursors of second phases which are then  
39 crystallized during thermal treatment. In this manner, the mixing between the matrix ceramic  
40 particles and the precursor is realized at the nano/atomic level and composite materials with a  
41 very homogenous second phase distribution can be obtained [74, 76].  
42  
43  
44  
45  
46  
47  
48  
49

50  
51 In the case of alumina-rich composites, a modified processing route which consists in doping a  
52 commercial alumina powder with alkoxides has been used to process very homogeneous  
53 alumina-based composites. These have a relatively low quantity ( $< 5$  wt.%) of secondary  
54 intergranular nanophases of zirconia, yttrium aluminium perovskite (YAP), yttrium aluminium  
55 garnet (YAG) and/or mullite, thereby increasing the effectiveness of the reinforcement  
56 mechanisms operating in these nanocomposites and also the creep resistance [77, 78].  
57  
58  
59  
60

## Previous attempts and state of the art: processing of Ce-TZP based composites

**Table 1** shows the properties of some Ce-TZP composites developed these past 30 years. The concept of “ceramic composite” was for the first time applied in 1989 to Ce-TZP ceramics with the aim of increasing the hardness and Young modulus by adding alumina particles [32]. Since then, several authors have developed alumina/Ce-TZP composites from in-lab synthesized powders or pre-mixed and spray-dried commercial powders, which were often subjected to Cold Isostatic Pressing (CIP) and conventional sintering and in some cases to Hot Isostatic Pressing (HIP) [11, 12, 21, 25, 26, 32, 37, 38, 43, 45]. It was observed that when 20 wt.% of  $\text{Al}_2\text{O}_3$  is added to 12 mol.% Ce-TZP, the presence of alumina particles of 0.5  $\mu\text{m}$  limited the zirconia grain size from 3 to about 1  $\mu\text{m}$  [33, 34]. Very high toughness and strength values (9.8  $\text{MPa}\cdot\sqrt{\text{m}}$  and bending strength of 950 MPa) have been also reported in 1998 [35] for an intra-granular type 10Ce-TZP/30vol.%  $\text{Al}_2\text{O}_3$ /0.05 mol.%  $\text{TiO}_2$  composite in which 10-100 nm sized  $\text{Al}_2\text{O}_3$  particles were trapped within the  $\text{ZrO}_2$  grains and vice versa [36] (Figure 3).

The above 10Ce-TZP based materials were classically processed from dispersed commercial powders, which were subsequently dried, calcined, sieved, uniaxially and CIP pressed and conventionally sintered at  $T < 1550^\circ\text{C}$  for 2h. Thanks to strict control of the composition, the mechanical properties were optimized, giving rise to the US patent 7928028 and the commercial product named NANOZR (Panasonic Electric Works, Japan) with a reported bending strength of 1290 MPa and a toughness of 8.6  $\text{MPa}\cdot\sqrt{\text{m}}$  [37]. More recently, a composite of 10Ce-TZP/16vol%  $\text{MgAl}_2\text{O}_4$  combining high strength ( $\sim 900$  MPa) and very high toughness (15  $\text{MPa}\cdot\sqrt{\text{m}}$ ) was also successfully developed [38]. According to the authors, the grain size reduction achieved by developing inter-intragranular composites (10Ce-TZP and Mg-spinel grain sizes were 0.5 and 0.2  $\mu\text{m}$  respectively) increases the critical stress to induce *t-m* zirconia phase transformation, while still maintaining a high level of transformability. A further increase in toughness achieved by activating additional bridging/crack deflection mechanisms is also expected with the use of elongated second phases ( $\text{SrAl}_{12}\text{O}_{19}$ ,  $\text{LaAl}_{11}\text{O}_{18}$ ,  $\text{MgAl}_2\text{O}_4\dots$ ) [41]. Nevertheless, the exact role of such platelets on toughness, even if quite obvious in principle, has not been clearly elucidated.

In the case of alumina-rich systems, the commercial product named BIOLOX Delta (CeramTec AG, Germany) which is a Zirconia Toughened Alumina (ZTA) consisting of 80 vol.%  $\text{Al}_2\text{O}_3$ , 17 vol.%  $\text{ZrO}_2$  and 3 vol.%  $\text{SrAl}_{12}\text{O}_{19}$  platelets shows excellent stability, wear resistance and mechanical properties. Flexural strength of 1150 MPa and toughness of 5.9 - 8.5  $\text{MPa}\cdot\sqrt{\text{m}}$  were

1  
2  
3 reported [79, 80]. Small quantities of  $Y_2O_3$  (0.6 wt.%) and  $Cr_2O_3$  (0.3 wt.%) are also added to  
4 the raw materials in order to increase zirconia stability, and hardness and wear resistance,  
5 respectively [71] (Figure 4). Ceria has also been used to improve the stability of zirconia in  
6 ZTA materials [40] as well as other elongated phases such as  $CeMgAl_{11}O_{19}$  (obtained by co-  
7 precipitation methods and mixed with zirconia and alumina powders [41]) or  $LaAl_{11}O_{18}$   
8 (crystallized in-situ during sintering from  $La_2O_3$  [42]).  
9

10  
11  
12 In the case of zirconia-rich systems, Cutler et al. developed in the 90's tri-phasic 12Ce-  
13 TZP/ $Al_2O_3$ / $SrAl_{12}O_{19}$  composites, with Ce-TZP grains of 1-3  $\mu m$ , equiaxed  $Al_2O_3$  grains of  
14 0.1-1  $\mu m$  and  $SrAl_{12}O_{19}$  platelets of 1-3  $\mu m$  in length [21]. Depending on the composition,  
15 fracture strength in the range 500-700 MPa and fracture toughness of 10-15  $MPa\sqrt{m}$  were  
16 measured. These composites were processed by mixing  $Al_2O_3$ , Ce-TZP (12 mol.%) and  $SrZrO_3$ ,  
17 the latter being the source of  $SrAl_{12}O_{19}$  platelets. Zirconia-based composites may be also  
18 processed by the alkoxide route described above, allowing a fine tuning of microstructure and  
19 composition [77, 81-83].  
20  
21  
22

23  
24  
25 At this stage, it is pertinent to address the issue of the redox behavior of Cerium. Cerium ions  
26 can present both the  $Ce^{+4}$  and  $Ce^{+3}$  oxidation state. As stabilizing agent for zirconia, for reasons  
27 already recalled in section II,  $Ce^{+4}$  is preferred to  $Ce^{+3}$  [84-86]. The internal part of  
28 ceria/zirconia composites can however undergo the  $Ce^{+4}/Ce^{+3}$  reduction even when sintered in  
29 air, and this may be detrimental for the structural stability of the component (this fact can be  
30 detected even with the naked eye, since the zirconia parts with Cerium oxide in the  $Ce^{+3}$  state  
31 ( $Ce_2O_3$ ) tend to have a greyish color rather than the pale yellow of Ce-TZP with  $Ce^{+4}$ ;  
32 ultimately, though, the presence of  $Ce^{+3}$  can be confirmed by X-Ray Photoelectron  
33 Spectroscopy (XPS) analysis [87]. Indeed all processing/firing conditions of Ce-TZP  
34 composites must be designed in order to avoid  $Ce^{+3}$  appearance, but practically, the issue is  
35 relevant only for dense pieces thicker than about 1 cm: below this dimension, if sintered in air  
36 with a convenient cooling rate,  $Ce^{+4}$  is the dominant oxidation state [88].  
37  
38  
39  
40  
41  
42  
43  
44  
45  
46  
47  
48  
49

### 50 51 **The two approaches to process Ce-TZP - $Al_2O_3$ - $SrAl_{12}O_{19}$ composites presented in this** 52 **work** 53

54  
55 The above-mentioned literature shows that tri-phasic systems are promising to obtain Ce-TZP-  
56 based composites with high toughness and high strength, thanks to a careful microstructural  
57 engineering. The combination of this approach with post-doping strategies (e.g. surface  
58 modification of a Ce-TZP powder with inorganic precursors, which then gives rise to composite  
59  
60

1  
2  
3 nano-powders) allows a further degree of refinement, as shown in previous studies [11, 12, 74,  
4 75, 77].

### 7 ***Post-doping route***

9  
10 In order to obtain ultrafine tri-phasic ceramics, composite powders were prepared by an  
11 innovative surface coating route, developed at the Politecnico di Torino by Palmero et al. [11]:  
12 commercial zirconia powders were coated by inorganic precursors of the second phases which  
13 crystallize on the surface of the zirconia particles under appropriate thermal treatment.  
14 basically, a commercial 10 mol.% ceria-stabilized zirconia powder (Daiichi Kigenso Kagaku  
15 Kogyo Co. LTD, Japan), referred to as 10Ce-TZP, was employed as raw material. The powder  
16 was then dispersed in a water-based slurry, which was then doped by a drop-wise addition of  
17 nitrates of Aluminum, Strontium and Cerium to obtain composite powders having the following  
18 composition after thermal treatments: 84 vol.% ZrO<sub>2</sub>, 8 vol.% Al<sub>2</sub>O<sub>3</sub>, 8 vol.% SrAl<sub>12</sub>O<sub>19</sub>  
19 (referred to as ZA<sub>8</sub>Sr<sub>8</sub>) and with different degrees of ceria in the zirconia phase. Composite  
20 powders were then obtained by drying the slurry with the precursors attached at the surface of  
21 the zirconia particles and then with further thermal treatments yielding the secondary alumina  
22 and aluminate phases. The powders were then dispersed in water and slip-casted, under  
23 conditions reported in [11]. An example of the microstructure obtained with these composite  
24 powders is shown in Figure 5: zirconia grains (Z) of  $0.6 \pm 0.2 \mu\text{m}$ , alumina grains (A) of  $0.3 \pm$   
25  $0.1 \mu\text{m}$  and strontium aluminate grains (S) with a mean length of  $0.6 \pm 0.2 \mu\text{m}$  and aspect ratio  
26 (length/width) of  $5 \pm 2$  were developed after conventional sintering at 1450°C-1h. The method  
27 thus allows a very precise and easy tuning of the ceria content, as well as ultrafine  
28 microstructures not previously achieved, and it has been patented [89]. However, industrial  
29 needs require easier processing, with more conventional powder-mixing and pressing  
30 techniques: therefore a more standard route was also attempted as a benchmark, as explained  
31 below.

### 48 **Standard powder-mixing route**

50  
51 Zirconia-based composites with 11.0 and 11.5 mol.% CeO<sub>2</sub> contents obtained by industrial  
52 processing (*i.e.* isostatic pressing of a spray dried composite powder composed of 84 vol.% Ce-  
53 TZP, 8 vol.% Al<sub>2</sub>O<sub>3</sub> and 8 vol.% SrAl<sub>12</sub>O<sub>19</sub> and conventional sintering) were also investigated  
54 [22]. For all the composites sintered conventionally at 1450°C-1h (Figure 6), the grain size of  
55 zirconia (Z) was  $1.0 \pm 0.3 \mu\text{m}$ , the grain size of alumina (A) was  $0.3 \pm 0.1 \mu\text{m}$ , the length of the  
56 aluminate platelets was  $1.7 \pm 0.5 \mu\text{m}$  and their aspect ratio (length/width)  $5 \pm 2$  [22]. The  
57  
58  
59  
60

1  
2  
3 industrial processing of the studied composites led to a larger size of the zirconia and aluminate  
4 elongated phases, in comparison to those developed by a surface modification strategy and slip-  
5 casting.  
6  
7

### 9 **Choice of samples for testing**

10  
11 Due to the difficulty in obtaining large batches of materials through the post-doping method,  
12 the characterization of these samples was limited to: *i*) spontaneous transformation  
13 temperatures  $T_{t-m}$ , *ii*) biaxial bending strength and *iii*) toughness (Single-Edge-V-Notched  
14 Beam (SENVB)). The effect of the composition (mainly the Ceria content) and of the sintering  
15 temperature on these properties were also thoroughly investigated.  
16  
17  
18  
19

20  
21 On the other hand, to determine the mechanical behavior laws of more transformable  
22 composites and to characterize the mechanical properties with different testing geometries  
23 (biaxial bending, four-point bending, pure tension, load to failure of dental implants,  
24 compression of additive-manufactured samples), a large series of samples was processed by the  
25 powder-mixing route, in a pilot-plant.  
26  
27  
28  
29

30  
31 Piston-on-three balls biaxial bending strength was determined from samples with a diameter of  
32 15 mm machined on both sides in order to have opposing flat surfaces, with a thickness of  $1.2$   
33  $\pm 0.2$  mm. For toughness and four-point bending strength measurements, ceramics were  
34 machined on all sides to a rectangular cross section of  $(4.0 \times 3.0) \pm 0.2$  mm x 50 mm. Final  
35 machining of tensile surfaces was performed by grinding with a 16  $\mu$ m diamond grinding tools  
36 (CNC with DMU60 mono BLOCK®, DMG, Germany). The notches (SENVB) were  
37 introduced using a diamond-loaded cutting wheel 300  $\mu$ m in thickness across the 3 mm wide  
38 surface perpendicular to the length of the bar, and then sharpened using a razor blade and 3  $\mu$ m  
39 diamond polishing grit (notch depth in the range of 0.8–1.2 mm, notch-tip radius of less than  
40 10  $\mu$ m). In order to minimize the effect of residual stresses developed during sample  
41 preparation, an annealing treatment was applied (1200°C-30 min). According to the ISO  
42 standard 6872 [90] no annealing treatment was applied for biaxial strength measurements. The  
43 cross-head speed was set to 0.5 mm/min (for toughness) or 1 mm/min (for strength) until failure.  
44 In addition, in order to better characterize the *t-m* phase transformation during subsequent steps  
45 of loading, the tensile surface of a number of samples of each composition was polished using  
46 1  $\mu$ m diamond paste before being submitted to load-unload tests.  
47  
48  
49  
50  
51  
52  
53  
54  
55  
56  
57  
58  
59  
60

1  
2  
3 Tensile test were also performed on machined “bone-shaped” samples (total length of 60 mm,  
4 central diameter 2.5 mm and terminal diameter 5 mm) on a hydraulic MTS tensile machine. A  
5 clamping hydraulic pressure of 5 MPa was used to prevent the samples from sliding inside the  
6 jaws. The tests were performed at a speed of 0.05 mm/min. Both load-unload and load to failure  
7 tests were performed on the tensile samples. Strain was measured directly on the samples by  
8 means of a displacement transducer.  
9

10  
11  
12  
13  
14 As introduced before, and to highlight ceramics exhibiting a relatively high degree of ductility,  
15 dental implant prototypes and additive-manufactured samples were also prepared and tested.  
16 Both processing and testing will be described in [section V](#).  
17  
18

#### 21 IV. Mechanical behavior of ductile Ce-TZP-Al<sub>2</sub>O<sub>3</sub>-SrAl<sub>12</sub>O<sub>19</sub> composites

##### 23 Dopant concentration and microstructural effects on transformation and 24 strength/toughness relations 25 26

27  
28 The development of zirconia-based composites with a significant amount of ductility implies a  
29 sufficient propensity towards *t-m* transformation at ambient temperature. Adjusting the  
30 *transformation-ability* is possible via the amount of dopant (ceria content) and microstructure  
31 control (zirconia grain size). The *t-m* transformation temperature ( $T_{t-m}$ ) was measured on  
32 cylinders suspended above a liquid nitrogen bath, progressively cooled below ambient. The  
33 surface temperature of the samples was monitored with thermocouples during cooling and the  
34 temperature at which the samples spontaneously cracked (generalized transformation) was  
35 recorded. [Figure 7](#) shows the evolution of the spontaneous *t-m* transformation temperature  
36 (without any applied stress) of sintered ceria-doped zirconia / 8 vol.% Al<sub>2</sub>O<sub>3</sub> / 8 vol.% SrAl<sub>12</sub>O<sub>19</sub>  
37 composites as a function of the ceria content in the zirconia phase and the sintering temperature,  
38 for the two types of processing methods described above (*i.e.* post-doping and powder mixing  
39 respectively). As expected and already discussed in the literature on other zirconia systems,  $T_{t-m}$   
40 decreases with increasing amount of stabilizer [\[91-94\]](#) and with a refinement of the  
41 microstructure, [\[10, 91-95\]](#), which, in turn, can be obtained through a decrease of the sintering  
42 temperature and/or by a modification of the powder synthesis (post-doping route, as proposed  
43 in [\[43, 92\]](#) giving a much finer, sub-micron microstructure). As  $T_{t-m}$ , and thus the  
44 transformability, decreases with the amount of stabilizer,  $K_{IC}$  obviously decreases with the  
45 amount of CeO<sub>2</sub> in the zirconia phase, as shown in [Figure 8](#), obtained for the composites  
46 processed through the post-doping route. On the other hand, [Figure 8](#) also shows that measured  
47  
48  
49  
50  
51  
52  
53  
54  
55  
56  
57  
58  
59  
60



1  
2  
3 strength passes through a maximum. This peculiar behavior cannot be explained solely by  
4 standard fracture mechanics equations, but rather by invoking a transition to a ‘ductile’ behavior  
5 (transformation before failure) for low stabilizer content and a ‘brittle’ response (crack  
6 propagation and transformation around the propagating crack) for higher stabilizer amount.  
7 This is in line with the results and analyses of Swain and co-workers [20, 96] and with those  
8 reported in other earlier studies dealing with monolithic Ce-TZP (see Panel A).  
9

10  
11  
12 The limitation of the strength in highly transformable zirconia-based materials is governed by  
13 the critical stress necessary to induce the  $t$ - $m$  zirconia phase transformation. This is shown in  
14 Panel B, for which we show that for a high transformability, the mechanical behavior law can  
15 be approximated as almost purely elastic-plastic. In other words, the critical stress for  
16 transformation  $\sigma_c^{t-m}$  corresponds roughly to the elastic limit  $\sigma_y$  and thus (for a purely elastic-  
17 plastic behavior) to the maximum acceptable stress  $\sigma_{max1}$  :

$$\sigma_{max1} \sim \sigma_y \sim \sigma_c^{t-m} \quad (2)$$

18  
19  
20 In this regime, the higher the amount of stabilizer, the higher the critical stress for  
21 transformation and thus the higher the possible strength. In contrast, for a larger amount of  
22 stabilizer, failure precedes transformation:  $t$ - $m$  transition occurs only when a crack propagates  
23 from a stress concentration site such as a pre-existing processing flaw. We move then to the  
24 more classical theory of phase transformation toughening (transformation around a propagating  
25 crack) and the Irwin-Griffith equation, for which the maximum acceptable stress  $\sigma_{max2}$  is given  
26 by:  
27

$$\sigma_{max2} \sim \frac{K_{IC}}{\sqrt{\pi c}} \quad (3)$$

28  
29  
30 In this regime, which is also consistent with eqn. (1) for brittle ceramics, strength decreases  
31 when the stabilizer amount increases. This is schematically illustrated in Figure 8.b. A  
32 maximum in strength is obtained when  $\sigma_{max1} = \sigma_{max2}$ . This maximum can also be optimized by  
33 careful process control and decrease in defect size. In other words, the lower the defect size  
34 induced by the process, the higher the maximum in the strength-toughness relation. The load  
35 displacement curves of biaxial bending samples (see Figure 9), with different amounts of CeO<sub>2</sub>  
36 also illustrate the different mechanical behavior of ductile (10 and 10.5 mol.%) and brittle (11.5  
37 mol.%) composites. Load-unload tests illustrate the inelastic strains in the ductile composites  
38  
39  
40  
41  
42  
43  
44  
45  
46  
47  
48  
49  
50  
51  
52  
53  
54  
55  
56  
57  
58  
59  
60

1  
2  
3 after unloading, with no apparent modification of the stiffness (no apparent damage). This latter  
4 aspect is addressed in detail hereafter.  
5  
6

7  
8 As microstructural features are almost identical in these samples with different ceria amounts,  
9 the strength variation is attributed to the different degree of zirconia stabilization. In less-  
10 stabilized samples (containing 10.0 and 10.5 mol.% ceria), zirconia transformation starts before  
11 crack propagation and the strength depends on the critical transformation stress  $\sigma_c^{t-m}$ . For higher  
12 ceria contents (*i.e.* 11.0 and 11.5 mol.% ceria), as zirconia becomes less transformable, the  
13 transformation is hindered and it occurs only around the crack as it propagates from a pre-  
14 existing processing flaw. The maximum strength is obtained for the intermediate (10.5 mol.%)  
15 ceria content, for which the critical stress for t-m transformation,  $\sigma_c^{t-m}$  and the defect-related  
16 strength are equal, *i.e.* when  $\sigma_c^{t-m} \sim \sigma_{max1} \sim \sigma_{max2}$ . Incidentally, this shows that small variations  
17 in dopant content (as well as microstructural features) play a critical role on the mechanical  
18 behavior laws in these systems, which emphasizes again the influence of processing robustness  
19 on the final properties.  
20  
21  
22  
23  
24  
25  
26  
27  
28

29  
30 **Figure 10.a** shows the superposition of an optical microscopy image (Nomarski contrast) and  
31 a monoclinic/tetragonal Raman maps obtained by analyzing the tensile surface of a biaxial  
32 tested disc (10.5 mol.% ceria) after unloading. These maps were already described in [12]. A  
33 large transformation zone is observed (few millimeters in diameter), in which the monoclinic  
34 content can reach 60 vol.%, with compressive stresses as high as 1GPa, measured after  
35 unloading (**Figure 10.b**). The stress values of **Figure 10.b** are determined for the *t-zirconia*  
36 phase. Stress partitioning between the different phases is to be expected; indeed a detailed stress  
37 analysis on partly transformed Ce-TZP/Al<sub>2</sub>O<sub>3</sub> composites has indicated that the overall average  
38 stress, intended as the hydrostatic stress in each phase weighted over the volume fraction of that  
39 phase, is indeed very highly compressive in transformed regions [97]. It is noted that these  
40 compressive stresses were (and generally are) measured after unloading and not *in-situ*. It is  
41 more likely a saturation of the maximum tensile stress at the transformation stress  $\sigma_c^{t-m}$  which  
42 occurs in the region of very localized highest applied stresses (*i.e.* starting from the center), is  
43 associated with a redistribution of the stress field, as schematically depicted in **Figure 10.c**.  
44 This shielding of the applied stress is quite similar to that occurring in metals, when plasticity  
45 occurs in regions of high applied stresses. This stress shielding explains, in part (**see Panel B**),  
46 the apparent very high biaxial flexural strength. A schematic picture of stress variations across  
47 the diameter of the disc, from the center to the border, comparing conventional non-  
48  
49  
50  
51  
52  
53  
54  
55  
56  
57  
58  
59  
60

1  
2  
3 transformable ceramic and with transformable ceramics, during loading and after unloading, is  
4 shown in **Figure 10.c**. Such a shielding effect may have important beneficial implications in  
5 structures for which the stress field is heterogeneous, with stress concentrations in some areas  
6 such as around the notches associated with the screw thread in dental implants. On the other  
7 hand, such benefits are only possible if this is true plasticity and if no damage (micro-cracking)  
8 is associated with the transformation. The question is all the more important in that the  $t$ - $m$   
9 transformation is associated with both hydrostatic and deviatoric components (quite large  
10 volume expansion and shear strains).  
11  
12  
13  
14  
15  
16  
17

### 18 **Is it real plasticity?**

19  
20  
21 **Figure 11 a.** shows the stress-strain curve of a  $\text{ZA}_8\text{Sr}_8\text{Ce}_{11}$ -1450°C (84 vol.%  $\text{ZrO}_2$  doped with  
22 11 mol.% of Ceria, 8 vol.%  $\text{Al}_2\text{O}_3$ , 8 vol.%  $\text{SrAl}_{12}\text{O}_{19}$ , sintered at 1450°C) composite tested in  
23 tension, processed here by the powder-mixing method with the aim of obtaining a sufficient  
24 number of test specimens. As more comprehensively discussed in **Panel B** this curve shows  
25 that the composite processed under these conditions exhibits a significant amount of plasticity  
26 for a ceramic before failure (plastic strain of  $\sim 0.5\%$ ). Such a degree of plasticity is related to  
27 the capability of the material to transform at low applied stresses, associated with a high  $T_{t-m}$   
28 temperature ( $-42^\circ\text{C}$ , see **Figure 7**), quite close to ambient. Load-unload sequences were  
29 conducted at difference stages during the test to evaluate the evolution of the stiffness versus  
30 applied strain. A small decrease of the Young's modulus versus applied strain (*i.e.* versus the  
31 proportion of transformed monoclinic phase in the material) is observed in the last few load-  
32 unload cycles, which could be attributed either to the presence of micro-cracks or to the fact  
33 that  $m$  zirconia exhibits a lower stiffness than that of the  $t$  phase (**Figure 11.b**). Unfortunately,  
34 no experimental data exists in the literature about Young's modulus of ceria-doped monoclinic  
35 zirconia and numerical simulations may give different conclusions depending on the binding  
36 potentials assumed for atomistic scale simulations [98]. To assess the key question of the  
37 absence or presence of micro-cracks (and damage) associated to the transformation, thin foils  
38 taken from a transformation band were prepared by Focused Ion Beam (FIB) milling and  
39 examined by Scanning Electron Microscopy (SEM) and Transmission Electron Microscopy  
40 (TEM) (**Figure 12**). SEM images show that the transformation zone does not exhibit micro-  
41 cracks, as it was concluded in the past on Mg-PSZ by Liu et al. [52], except at few grain  
42 boundaries located at the surface. These micro-cracks are limited to 1 micron depth. Below 1  
43 micron depth, no micro-cracks are observed. TEM characterization confirmed that no micro-  
44  
45  
46  
47  
48  
49  
50  
51  
52  
53  
54  
55  
56  
57  
58  
59  
60

(or nano-) cracks were present inside the transformation bands, except locally at the surface. The mechanical behavior law can therefore be considered as purely elasto-plastic, which is in agreement with a previous paper by Zhe et al. [57] (see also Panel B). The presence of a few micro-cracks localized at the surface of the transformation bands cannot explain by itself neither the small variation in Young's modulus, which can then be attributed to a less stiff monoclinic phase, nor the amount of plastic strain observed. However, further static/cyclic fatigue tests are necessary to assess whether micro-cracks of very small dimensions at the surface could be detrimental in the long term.

### **Transformation Induced Plasticity (TRIP) : relation between transformation bands and plastic strain**

Figure B-5 a. shows the features of transformation bands in the composite processed by the mixing route, just after failure by 4-point bending. The bands are clearly visible on the tensile side of the samples. It is interesting to note that the bands are not randomly, but regularly, dispersed. They are absent on the compressive side of the samples(not shown).

Knowing the size of the transformation bands and their density at the surface, as well as the  $t$ - $m$  transformation ratio in the bands, it may be possible to calculate the macroscopic strain associated to the transformation. Both Raman spectroscopy and Transmission Kikuchi Diffraction (TKD) in a Scanning Electron Microscope (not shown here) revealed that only a portion ( $V_m \approx 25 \text{ vol.}\% \pm 5\%$ ) of the tetragonal grains were transformed toward the monoclinic symmetry in the bands during the 4 point bending tests (which is below the measured monoclinic content in the transformed zone in biaxial bending). Being  $V_{ZrO_2}$  the fraction of zirconia in the composite (84 vol.%) and  $d_{tb}$  the density of transformation bands (% of surface transformed) at failure, the strain due to the  $t$ - $m$  transformation induced plasticity is given by :

$$\varepsilon = V_m \cdot V_{ZrO_2} \cdot d_{tb} \cdot (\varepsilon_{vol} + \varepsilon_{shear}) \quad (4)$$

In this equation,  $\varepsilon_{vol}$  and  $\varepsilon_{shear}$  are the volume and shape strain amplitudes of the  $t$ - $m$  transformation respectively. More precisely,  $\varepsilon_{vol}$  is the strain (in the direction of tensile stress) induced by the volume expansion of the grains and  $\varepsilon_{shear}$  is the shear of the lattice associated to the  $t$ - $m$  transformation.

1  
2  
3 Taking only the shape strain amplitude  $\varepsilon_{vol}$  with a value of 0.0167 [59] (*i.e.* neglecting the shear  
4 component of the transformation) and a density of transformation bands (area of the bands  
5 divided by the total area in tension) from **Figure B-5 a.** equal to 0.10, gives a macroscopic  
6 strain of 0.035%, which is far lower than observed experimentally and calculated by the inverse  
7 method described in **Panel B** (0.55% plastic strain). Therefore, the shear component of the  
8 transformation is the major part of the observed total strain. Taking a shape strain amplitude of  
9 0.16 [59, 99] then gives a macroscopic strain of 0.37%, which, given the uncertainties in the  
10 estimations of  $V_m$ ,  $V_{ZrO_2}$  and  $d_{tb}$  is in line with the measured macroscopic strain.  
11  
12  
13  
14  
15  
16  
17

18 The shear component is often neglected in the analysis of the deformation induced by the *t-m*  
19 transformation [8, 99]. The current analysis clearly shows that it is the Transformation Induced  
20 Plasticity (TRIP) effect in zirconia which is the most important contribution to the deformation.  
21 Future work may seek to investigate textures of the transformation grains inside transformation  
22 zones.  
23  
24  
25  
26  
27

### 28 **Flaw tolerance**

29  
30 Using the stress superposition argument, the transformation zone in zirconia systems can be  
31 considered as a process zone, in which the externally applied stress is “shielded” (that is  
32 reduced) by the stress caused by the transformation of tetragonal grains to monoclinic  
33 symmetry. The concept of a process (‘plastic’) zone ahead of the crack tip as defined by Ashby  
34 [100] is thus relevant to calculate the flaw size above which a given material behaves as fragile  
35 or ductile. **Figure 13** is a chart of fracture toughness versus yield stress, often used to compare  
36 material’s behavior in relation to the risk of brittle failure. The diagonal lines show the process  
37 zone size diameter,  $d$ , where:  
38  
39  
40  
41  
42  
43  
44

$$45 \quad d = \frac{K_{Ic}^2}{\pi\sigma_y^2} \quad (5)$$

46  
47  
48 The evaluation of the process zone diameter from the toughness (see **Figure 8**) and elastic limit  
49 measured for a Ceria content of 11 mol.% (*i.e.*  $\sim 10\text{MPa}\cdot\sqrt{\text{m}}$  and 500 MPa respectively, see  
50 **Panel B**) gives a process zone diameter of around 100 microns, in line with the transformation  
51 zone observed in this system [98] and **section II**. The same consideration for 3Y-TZP ceramics  
52 would give a process zone diameter of one to few microns, which is again in line with  
53 transformation zones generally observed in this material [60]. Such a simple consideration  
54  
55  
56  
57  
58  
59  
60

allows also to predict that  $\text{ZA}_8\text{Sr}_8\text{Ce}_{11}$ -1450°C composites processed through the standard powder-mixing route would remain ductile even if processing defects of around 100 microns are present. **Figure 14** illustrates the very high flaw tolerance of such ductile ceramics, by showing two tensile stress-strain curves obtained on samples with and without a large processing defect ( $\sim 150 \mu\text{m}$  observed on the fracture surface). The stress-strain curve is not significantly affected (although the strain to failure is somewhat lower).

**Figure 15** is a Weibull plot obtained for the  $\text{ZA}_8\text{Sr}_8\text{Ce}_{11}$ -1450°C composite (processed through conventional powder-mixing) and for a benchmark, medical grade (HIPed) 3Y-TZP using two loading configurations (4-point bending and biaxial piston-on-three-balls testing). From the probability-stress curves, typical Weibull moduli between 12 and 17 are extrapolated for 3Y-TZP, while values around 30 are observed for the Ce-TZP based composite. Such high Weibull moduli were previously reported [12, 22, 101] for highly transformable Ce-TZP systems. The difference between 4-point bending and piston-on-three-balls mechanical behavior cannot be imputed to a size effect in the Weibull analysis (different volumes of samples) but rather to a difference in stress distribution and, hence, to transformation features, as discussed in **Panel B**. It has to be recognized that 4-point bending strength of 3Y-TZP remains almost twice higher than the Ce-based composite and that the benefit of using a ‘ductile’ or ‘fragile’ zirconia ceramic may depend on the actual loading configuration (application, displacement or load controlled, heterogeneous or homogeneous stress distribution), size and geometry of the product and defects generated through the processing. Admittedly, the same comparison *i.e* between 3Y-TZP and the optimal grade of composites processed by post-doping route would be conclusive, but this was impossible at the time of writing, due to the limits in processing large batches of powders by this synthesis method.

## V. Potential Applications of ductile ceramics: case study on implants and additive-manufactured ceramics

### Advantages and drawbacks

#### Case study 1: dental implants with a high tolerance to surface modifications

Implant prototypes were processed from the  $\text{ZA}_8\text{Sr}_8\text{Ce}_{11}$  zirconia powder described previously (powder mixing). The powder was granulated by spray drying and cold-isostatically pressed (300 MPa) in the form of cylindrical bars of diameter 5.1 mm. Bars were sintered at 1450°C

1  
2  
3 for 1 hour and then machined in the sintered state to final shape (see **Figure 16**) by hard milling-  
4 turning process on a 5 axis Computer Numerical Control (CNC) milling center. Prototypes were  
5 machined to a final diameter of 3.4 mm, which represents the lowest and most challenging  
6 dimension for ceramic implants. It is generally accepted that machined surfaces are not optimal  
7 to favor bone integration [102-106] and there is a consensus to consider that a certain surface  
8 roughness  $R_a \sim 1-1.5$  microns improves osseointegration and mechanical anchorage with bone  
9 [102-106]. Several strategies are thus explored to obtain such rough surfaces, the most common  
10 being sandblasting and chemical etching. Other surface modifications are today proposed for  
11 ceramic implants, as laser patterning [107-109] or injection molding in matrices [110] with the  
12 targeted roughness. As sandblasting followed potentially by chemical etching is the most  
13 commonly developed strategy, such treatments were tested in this case study. Sandblasting was  
14 conducted with 150  $\mu\text{m}$  alumina particles at 3.5 bars, leading to a roughness ( $S_a$ ) of 1.3 microns  
15 (measured using a white-light optical interferometer). When followed by etching (in  $\text{HF}/\text{HNO}_3$   
16 for 3h at Room Temperature (RT)),  $S_a$  was decreased to 1.0 micron, but an additional surface  
17 topography was created at the grain scale (see **Figure 17**). An additional thermal treatment was  
18 conducted on some of the prototypes to release potential residual stresses associated to different  
19 surface treatments. This annealing was performed at 1350°C, (*i.e.* above the  $m-t$  transformation  
20 and below the sintering temperature).

21  
22  
23  
24  
25  
26  
27  
28  
29  
30  
31  
32  
33  
34  
35 Load to failure tests on hard machined 3.4 mm diameter implants were performed following  
36 ISO14801 geometrical prescription [111], so as to follow the most usual and severe testing  
37 method for dental implants. The implants were embedded in an epoxy resin having a stiffness  
38 similar to bone (RenCast CW 5156/HY5158, with a Young's modulus of 5.8 GPa). The  
39 embedding level was 3 mm below the intended initial bone crest position around the implant to  
40 simulate bone resorption, as specified in ISO 14801. The implants were loaded to failure at 30°  
41 angulation with respect to the vertical axis at a crosshead speed of 5 mm/min. 4 implants were  
42 tested for each surface feature. Several surface states were compared: as machined (hard milling  
43 process on a 5 axis CNC milling center), machined + sandblasted (alumina particles) or  
44 machined + sandblasted + chemically etched.

45  
46  
47  
48  
49  
50  
51  
52  
53 **Figure 17.a** shows the load to failure values obtained on the prototypes as a function of the  
54 surface treatments conducted. They are compared to publically available data for other ceramic  
55 (3Y-TZP based) implants [112-117]. Values are similar irrespective of the surface treatments,  
56 ranging from 336 N in average after machining down to 286 N following sandblasting, etched  
57 and then annealed prototypes in which residual machining/sandblasting stresses were relieved.  
58  
59  
60

1  
2  
3 These values appear quite modest when compared to data already reported by manufacturers of  
4 3Y-TZP implants ( $\sim 350 - 450$  N [112 - 121]). On the other hand, load to failure results were  
5 very reproducible and the strength of implants was minimally affected by the type of surface  
6 treatment conducted. Given the limit of the study and the difficulty to compare implant  
7 strengths from public datasheets, especially because they have different sizes, designs and  
8 surface features, our results are consistent with the main advantages and drawbacks of such  
9 'ductile' ceramics: mechanical resistance is modest and associated with the moderate elastic  
10 limit of the material tested ( $\approx 500$  MPa). As a reminder, implants were processed using a  
11 transformable  $\text{ZA}_8\text{Sr}_8\text{Ce}_{11}$ -1450°C composite, processed by a standard powder-mixing route.  
12 Given the obtained load to failure value of 295 N for the most common surface treatment  
13 (sandblasting followed by etching), these implants of 3.4 mm made with the Ce-zirconia  
14 composite would be likely restricted to lateral incisor teeth and at least 4.0 mm diameter would  
15 be necessary for other locations [122]. On the other side, thanks to the benefits of flaw tolerance,  
16 variability in strength is very low, insuring a high reproducibility and reliability in strength data  
17 and a strong robustness against processing variability and surface treatments. At this stage, it  
18 must be noted that the prototype implants were not Hot-Isostatically-Pressed as is the case of  
19 most commercial 3Y-TZP implants to limit the risk of large defects. Another competitive  
20 argument for using Ce-zirconia composites is their resistance to Low Temperature Degradation  
21 (aging). Some prototype implants were aged in an autoclave at 134°C-2 bars for 5 hours  
22 following ISO 13356 [123]. They showed no evolution, neither in monoclinic content nor  
23 change in mechanical strength after the aging treatment. Doping with ceria leads to an absence  
24 of susceptibility toward chemically induced Low Temperature Degradation (aging) as ceria  
25 addition does not create oxygen vacancies in the lattice, which are associated to water-species  
26 diffusion and further destabilization in yttria-doped zirconia with time [59, 61], while 3Y-TZP  
27 commercial implants aged, although not visible by XRD but by Raman  
28 spectroscopy. Admittedly, there are some signs that large residual stresses, as introduced by a  
29 previous t-m transformation, might result in stress-driven (rather than chemical-driven) aging  
30 in Ce-TZP composites [124].

31  
32 Such ductile composites may be seen as a potential option for manufacturing robust dental  
33 implants, with an acceptable maximum strength for a zirconia-based ceramic (around 600 MPa  
34 in 4-point bending configuration), but a high degree of flaw resistance, reliability and stability.  
35 Certainly, decreasing the ductility to a certain extent (but still in the 'ductile' range of the  
36 strength-toughness relationship) would further improve the mechanical resistance of the  
37  
38  
39  
40  
41  
42  
43  
44  
45  
46  
47  
48  
49  
50  
51  
52  
53  
54  
55  
56  
57  
58  
59  
60



1  
2  
3 implants. Again, as for mechanical testing, further development of composites processed  
4 through post-doping route or any method enabling finer microstructures, at a larger, industrial  
5 scale, would be welcome for practical applications.  
6  
7

## 9 **Case study 2: mechanical properties of additive-manufactured scaffolds**

10  
11 In recent years, Additive Manufacturing (AM) techniques have expanded fast, because they  
12 enable the customization of complex shapes and may reduce the duration and complexity of the  
13 manufacturing process. However, AM of ceramics has many challenges because, compared to  
14 metals, ceramics are less tolerant to processing-induced defects, while currently AM results in  
15 larger material defects than other well-established industrial technologies. For example, 3Y-  
16 TZP commonly exhibits strengths higher than 1 GPa when processed by Cold Isostatic Pressing,  
17 while values in the range of 550-850 MPa were reported when shaped by stereolithography  
18 [125]. Hence, the ductile Ce-TZP based composites described above may have greater potential  
19 for AM, as scaffolds for which defects are inherent to the structure targeted or even as dense  
20 materials for which defects are undesired but generally present.  
21  
22  
23  
24  
25  
26  
27  
28

29  
30 Dense samples and scaffolds were printed using a robotic assisted deposition device (3D inks,  
31 Tulsa, OK, USA), often referred as robocasting or Direct-Ink-Writing. The printable paste was  
32 prepared by mixing the 33 vol.%  $\text{ZA}_8\text{Sr}_8\text{Ce}_{11}$  zirconia powders in a 25 wt.% Pluronic® F127-  
33 based hydrogel solution. Mixing was performed using SpeedMixer (DAC 150.1 FWZ-K,  
34 Flacktek, Germany) at 2500 rpm and the paste was degassed by centrifugal loading at 5000 rpm  
35 for 10 min before placing in the syringes. Dense biaxial bending disks and 3D porous structures  
36 were built-up by extruding the paste through conical tips of 400  $\mu\text{m}$  diameter at a speed of 10  
37 mm/s on flat Teflon-sprayed substrates in 95 % humidity and at 25°C.  
38  
39  
40  
41  
42  
43

- 44 - Disks for biaxial bending were obtained by depositing the filaments in one direction.  
45 Distance between the filaments was 320  $\mu\text{m}$  (80% of the filament) in the XY plane and  
46 336  $\mu\text{m}$  (84% of the filament) in the Z direction. The starting filament was placed with  
47 160  $\mu\text{m}$  offset with the previous layer in order to fill the gap between filaments.  
48
- 49 - Cylindrical 3D porous structures were deposited with strut-to-strut distance of 800  $\mu\text{m}$   
50 (in the XY plane) and distance between the filaments in the Z direction was 320  $\mu\text{m}$   
51 (*i.e.*, 20 % overlap).  
52
- 53 - Two 3D structures with different porosities were printed: one with a reinforcing dense  
54 rim and one without rim reinforcement.  
55  
56  
57  
58  
59  
60

1  
2  
3 Following printing, the structures were dried for 60 hours at a temperature of 60°C while at the  
4 same time decreasing the humidity from 95% to 30%. De-binding and sintering were performed  
5 at 600°C for 3 h and 1350°C for 1 h, respectively.  
6  
7

8  
9 Samples of cylindrical 3D structures ( $\varnothing$  10 mm x 10 mm in height after sintering) were used  
10 for compression tests at 0.5 mm/min, while disks ( $\varnothing$  12 mm x 1.5 mm in thickness after  
11 sintering) were used in piston-on-three-balls bending.  
12  
13

14  
15 The robocasting method did not develop full density struts after sintering and in case of ‘dense’  
16 biaxial disks only 86 % of theoretical density was achieved. **Figure 18** shows the architecture  
17 of the 3D porous structures (with and without the reinforcing rim) and the microstructure of the  
18 materials at two scales. Interestingly, although the samples obtained exhibited a relatively high  
19 degree of residual micro-porosity (14 %), biaxial flexural strength reached  $850 \pm 22$  MPa (N=8).  
20 We also observed dramatic improvements in the compressive strength of the 3D porous scaffold  
21 made from this composite, when compared to the literature, even with high porosities (40 % -  
22 60 %) (**Figure 19**). Values obtained for these samples are well above those reported so far in  
23 the literature [126-136]. Therefore, such metal-like behavior and defect-tolerant properties of  
24 the investigated  $\text{ZA}_8\text{Sr}_8\text{Ce}_{11}$  material appear to be an excellent option for additive  
25 manufacturing technologies. These preliminary results will be complemented by further  
26 analysis of defect size – strength relations in this system, as well as a comparison with Y-TZP  
27 processed under the same conditions, in an upcoming paper. Another consequence of these  
28 results is that, contrary to most brittle ceramics including Y-TZP, it is possible to process porous  
29 biocompatible structures with a lower stiffness, which is favorable in terms of decreasing stress-  
30 shielding with bone, without compromising strength. This can also be exploited for implants in  
31 contact with bone, for which the high stiffness of ceramics is generally considered a drawback.  
32  
33  
34  
35  
36  
37  
38  
39  
40  
41  
42  
43  
44  
45

## 46 **VI. Perspectives and Concluding remarks**

47

48  
49 Even though, as was sometimes reported in previous literature, transformation-induced ductility  
50 of some zirconia ceramics has been certainly under-exploited to date. The high flaw tolerance  
51 and higher reliability, along with the associated absence of chemically-driven low-temperature  
52 aging, the present work has shown Ceria-doped zirconia based ceramics and composites may  
53 be tailored so as to achieve high strength and toughness (for the ‘optimum’ of the strength-  
54 toughness relation), or a larger propensity of transformation induced plasticity associated with  
55 still higher toughness. Such ceramic composites with a toughness of more than  $10\text{-}15 \text{ MPa}\sqrt{\text{m}}$ ,  
56  
57  
58  
59  
60

1  
2  
3 a rising R-Curve and an elastic limit of 500 MPa, may compete with bio-inspired ceramics,  
4 which are considered today at the forefront of ceramic research, while being readily accessible  
5 using conventional ceramic processes. Better than competing, the combination of phase  
6 transformation toughening with a clever microstructural architecture may reveal an interesting  
7 field of research, as gradients of transformation from the surface towards the core of a material  
8 may be achieved. Laminated structures through tape casting or additive manufacturing or even  
9 the combination with self-diagnostic ability by the incorporation of a conductive network or  
10 wires inside structures without compromising strengths thanks to the defect-tolerant character  
11 of the base-ceramic can be also designed. This paper has confirmed that toughness (and thus  
12 ductility) cannot be increased to values exceeding  $10 \text{ MPa}\sqrt{\text{m}}$  without compromising strength,  
13 which still remains modest when compared to 3Y-TZP materials. The future of such  
14 composites, in order to achieve maximum strength will certainly rely on our capacity to process,  
15 with scalable methods, ultra-fine and homogeneous powders and materials, which may then  
16 provide even greater potential in term of strength-toughness relations. The concept of strength  
17 limitation of transformation-toughened zirconia alloys discussed in the 80's still remains, but  
18 the effect of micro- (nano-) structure on such strength-toughness relations is still a matter of  
19 scientific and technological interest.  
20  
21  
22  
23  
24  
25  
26  
27  
28  
29  
30  
31  
32  
33  
34  
35  
36  
37  
38  
39  
40  
41  
42  
43  
44  
45  
46  
47  
48  
49  
50  
51  
52  
53  
54  
55  
56  
57  
58  
59  
60

## Panel A. Zirconia Systems: Phase Transformation Toughening and Strength-Toughness Relationship

Transformation toughening was first described in TRIP (Transformation-Induced Plasticity) steels and wear-resistant cast irons (1968) [137]. The same phenomenon was then observed in a ceramic material (CaO-partially stabilized zirconia) in 1975 by Garvie et al. [6] and two years later, by Gupta et al. [138] in zirconia containing low percentage of yttria. In these stabilized-zirconia systems, toughening is based on the retention of the metastable tetragonal phase at room temperature: when a crack propagates, the concentrated stress field at the crack tip enables *t*-crystals to transform into a stable *m*-phase and, the associated volume expansion, generates localized compressive stresses, which act against the applied stress intensity factor. This tetragonal-to-monoclinic phase transformation, which can be triggered by shear and/or hydrostatic tensile stresses [139], leads to a significant increase of the strength, due to the increase of the work of fracture rather than the reduction of the defect size, as classically observed in brittle ceramics. Depending on the cation (Ca, Mg, Y, Ce, rare earths oxides...) and the quantity of stabilizing agent added to zirconia, different materials can be developed. If an amount of transformable tetragonal phase is present within a matrix of cubic zirconia, one refers to *Partially Stabilized Zirconia* or PSZ. If zirconia is fully tetragonal following sintering one refers to *Tetragonal Zirconia Polycrystals* or TZP. The term 'TZP' is sometimes incorrectly used for yttria stabilized systems with 3-4 mol.% yttria, while phase diagram and current knowledge of these systems show that they are not fully tetragonal. Finally, *Fully Stabilized Zirconia* or FSZ is developed when the concentration of dopant is high enough for complete cubic stabilization (case of 8Y-FSZ) [140, 141].

In case of ceramics, the stress-shielding effect resulting from the transformation-induced strains near the crack tip was estimated using a linear elastic fracture mechanics model developed by McMeeking and Evans in 1982 [142]. A second model based on energy considerations, developed by Budiansky et al. in 1983 [143], allowed computation of the work of fracture due to the *t-to-m* transformation in zirconia. However, neither of these two models describes with precision the shape, size and volume of the transformation zone at the crack tip. Recently, a two-dimensional elastic phase field model proposed by Mamivand et al. [144] has simulated correctly the phase transformation nucleation at the crack tip and the development of compressive stresses, which lead to crack closure while the crack is under tensile loading. In the 80's, Swain and co-workers [20, 96] showed that the mechanical properties of TZP materials depend on the contribution of the toughening mechanism: (a) at lower toughness (generally less

1  
2  
3 than 8-10 MPa. $\sqrt{m}$  as in 3Y-TZP system [137], see Fig. A-1) toughening contribution is modest  
4 and the strength is limited by the flaw-size following the Griffith relationship (brittle behavior  
5 and transformation follows crack growth) while (b) at higher toughness (case of 9-10 Ce-TZP  
6 systems showing ductile-like behavior, see Fig. A-1), the strength is limited by the critical  
7 transformation stress to induce the *t-m* zirconia phase transformation taking place before crack  
8 propagation.  
9

10  
11  
12  
13  
14 The critical stress to trigger the *t-m* transformation ( $\sigma_c^{t-m}$ ) is primarily a function of the grain  
15 size and the type and quantity of stabilizing agent but can be also modified by residual stresses  
16 due to thermal expansion mismatch between grains and/or the presence of secondary phases.  
17 For a given dopant concentration,  $\sigma_c^{t-m}$  decreases with increasing grain sizes (grains smaller  
18 than a critical size cannot undergo the phase transformation under a given stress field) and at  
19 similar grain size and dopant concentration, the degree of stabilization depends on the type of  
20 dopant (*e.g.* adding yttria creates oxygen vacancies, which is the most efficient means to  
21 stabilize the tetragonal phase, while ceria relies only on lattice parameter changes [145, 146]).  
22 Obviously, for a given type of dopant, the lower the dopant concentration the lower the  $\sigma_c^{t-m}$ .  
23  
24  
25  
26  
27  
28  
29

30  
31 In composites,  $\sigma_c^{t-m}$  decreases if residual tensile stresses are generated or increase when zirconia  
32 is put under compression. The magnitude and sign of internal residual stresses depends on *i*)  
33 secondary phase compositions, *ii*) the associated thermal expansion coefficients and *iii*) the  
34 presence of a preexisting *t-m* transformation [97].  
35  
36  
37

38  
39 The plot of strength versus fracture toughness for various PSZ and TZP systems (see Fig. A-2)  
40 shows that in Y-TZP, Ce-TZP and Mg-PSZ transformable zirconia, increasing toughness above  
41 8-10 MPa. $\sqrt{m}$  is associated with a decrease in strength. This toughness values represent the  
42 frontier between the two different behaviors proposed by Swain and Rose [20]: it should be  
43 taken into account when designing zirconia-toughened-based engineering ceramics. In practical  
44 terms, if the objective is to develop maximum strength, it will be necessary to limit the  
45 transformability of the material while improving the processing, machining and final surface  
46 treatments applied to the product in order to reduce the critical flaw size. On the contrary, if the  
47 material to be developed must be flaw and damage tolerant (that is less sensitive to processing,  
48 machining and surface modifications), it will be more beneficial to increase the transformability  
49 and to adapt the product design to guarantee the maximum strength that will be limited by the  
50  $\sigma_c^{t-m}$ . Practically, in the latter materials, the *t-m* phase transformation will take place before  
51 failure.  
52  
53  
54  
55  
56  
57  
58  
59  
60

1  
2  
3 Among the more classical transformable zirconia systems, Y-TZP shows the highest  
4 mechanical strength (more than 1 GPa) but relatively moderate toughness [147, 148]. On the  
5 contrary, Ce-TZP can be very transformable (high fracture toughness) but at a lower maximum  
6 strength [149, 150]. In Ce-TZP the optimum fracture strength was observed for ceramics  
7 containing 10-12 mol.% CeO<sub>2</sub> (about 500-600 MPa). This relative modest strength (in  
8 comparison to Y-TZP) is mostly related to the larger grain size of Ce-TZP. Therefore, from the  
9 late 1980s, many researchers have worked on hindering grain growth in Ce-TZP by adding one  
10 or more secondary phases (Al<sub>2</sub>O<sub>3</sub>, MgAl<sub>2</sub>O<sub>3</sub>, SrAl<sub>12</sub>O<sub>19</sub>...), developing Ce-TZP-based  
11 composites with strengths higher than 1 GPa [12, 35, 38, 43-45].  
12  
13  
14  
15  
16  
17  
18

19 Another important feature shown in Fig. A-2 is that the addition of a secondary phase to Y-  
20 TZP increases also the strength to 2.4 GPa, as reported by Tsukuma and Ueda [151] in 2Y-TZP  
21 composites containing 20-40 wt.% of alumina. According to these authors, the improvement of  
22 the strength from 1.4 GPa (pure 2Y-TZP) to 2.4 GPa is related to the presence of smaller flaws  
23 and the suppression of crack initiation by alumina. The effectiveness of Y-TZP additions to  
24 Al<sub>2</sub>O<sub>3</sub> has also been studied and maximum bending strengths of ~1.6 GPa and toughness of 6.5  
25 MPa√m were reached with 70 vol.% of Al<sub>2</sub>O<sub>3</sub>-3Y-TZP systems [152]. 3Y-TZP is one of the  
26 most commonly used ceramics to boost the strength of Zirconia Toughened Alumina (ZTA).  
27  
28  
29  
30  
31  
32  
33  
34  
35  
36  
37  
38  
39  
40  
41  
42  
43  
44  
45  
46  
47  
48  
49  
50  
51  
52  
53  
54  
55  
56  
57  
58  
59  
60

## Panel B. Mechanical behavior laws of highly transformable zirconia ceramics - importance of the test methods

Different methods are proposed in standards and publications for the strength measurements of ceramics. Among them, three- or four-point and biaxial bending tests are the most popular. They are schematized in the [Appendix](#). They provide the advantage, for ceramics, to create tensile stresses on one side of the sample, without having to proceed with more difficult, pure tensile tests. The biaxial flexural strength tests also have the advantage of not being sensitive to the specimen edge preparation as is the case for three- and four-point bending tests. ISO standards for dental ceramics (ISO 6872 [\[90\]](#)), and more specifically for zirconia as an implant material (ISO 13356 [\[123\]](#)), specify the use of bending tests to obtain strength data, using linear elastic equations. However, with non-linear behavior, and this is the case of very transformable zirconia, stresses and strain cannot be calculated simply and directly from load and displacement hypothesizing a purely elastic behaviour. As already indicated by Fett and Munz [\[9\]](#) and later by Rauchs et al. [\[10\]](#), plastic deformation on the tensile side of the bending samples leads to an overall stress re-distribution and to overestimated values of the tensile stress, and thus of real strength, when using elastic-behavior equations given in the [Appendix](#). In the case of biaxial bending tests with supporting balls, additional errors associated with indentation of the material by the balls is generally not considered but may be significant and compromise (underestimate) the measurement of beam deflection.

[Figure B-1](#) shows apparent stress-strain curves obtained on a  $\text{ZA}_8\text{Sr}_8\text{Ce}_{11}$ -1450°C composite processed through conventional powder mixing (thus exhibiting high transformability) with different loading configurations, when both stress and strain are calculated through standard equations considering elastic hypotheses in the case of the bending tests. The  $\text{ZA}_8\text{Sr}_8\text{Ce}_{11}$ -1450°C composition was chosen as a model material with transformation before failure and a high level of transformation-induced plasticity. It is noted that the displacements were accurately measured by Linear Voltage Displacement Transducer (LVDT) just under the samples in bending tests and with an extensometer in the case of tension. A significant indentation of the samples by the supporting balls was noted in biaxial bending and taken into consideration in the actual measured displacement. [Figure B-2](#) illustrates a load-displacement curve of a ball of the same diameter as the one used for biaxial bending on a flat  $\text{ZA}_8\text{Sr}_8\text{Ce}_{11}$ -1450°C support, for a maximum load applied on the ball similar to that reached during biaxial bending. A permanent penetration of the ball of 20  $\mu\text{m}$  is observed. This shows that under

1  
2  
3 biaxial bending, a portion of the measured displacements is due to indentation effects. From a  
4 practical point of view, strength calculation following ISO standards would result in values of  
5 roughly 400 MPa in tension, 540 MPa in 3 or 4-point bending and more than 1GPa in biaxial  
6 bending.  
7  
8  
9

10  
11 Tensile tests are very sensitive to misalignment and lead to a larger scatter of results (as  
12 schematized by the dashed area in **Figure B-1**). On the other hand, stresses calculated in  
13 bending overestimate true values of strength and do not capture relevant mechanical behavior  
14 laws without further analysis. Finite Element Methods (FEM) can be used to simulate a load-  
15 displacement response during a loading test, by integrating a given stress-strain (constitutive)  
16 mechanical behavior law of the material. **Figure B-3** shows the load-displacement curve  
17 experimentally measured during a 4-point bending test and the ones calculated from the  
18 knowledge of the stress-strain curves determined in tension. Plasticity was modeled as cast-iron  
19 behavior, which considers plasticity with isotropic hardening in tension and only elasticity (no  
20 transformation) in compression.  
21  
22  
23  
24  
25  
26  
27  
28

29  
30 The simulations based on stress-strain curves obtained through the tensile tests are consistent  
31 with the experimental load-displacement curve, especially for the upper stress-strain curve (best  
32 alignment), but do not fully match with it. In fact, a simulation of tensile tests by FEM shows  
33 that small misalignments, even imperceptible, may lead to stress gradients and thus  
34 transformation (plasticity) onset near the upper and lower edges of the narrowing of the sample.  
35 This was checked with Raman Spectroscopy where the onset of phase transformation was  
36 heterogeneous in the case of the strongest misalignment, as shown in **Figure B-4**. In other  
37 words, bending stresses super-impose onto the applied tensile stresses and lead to a certain  
38 under-estimation of the real tensile stress. An alternate approach to the issue stems from the  
39 following question: what would be the strain–stress curve to enter in the FEM simulation to fit  
40 the experimental load-displacement curve in bending? The best fit was obtained with a cast-  
41 iron model, exhibiting a yield (transformation) stress of 500 MPa in tension with minimal  
42 hardening (maximum stress of 540 MPa) and a pure elastic behavior in compression. This result  
43 is important since it shows that the effective stress-strain curve does not show significant  
44 hardening and that the mechanical behavior law of such highly transformable ceramic is almost  
45 purely elastic-plastic in tension. It shows also that 4-point bending does not over-estimate the  
46 real strength significantly as the maximum stress determined is of 540 MPa. On the other hand,  
47 it shows that tensile tests may underestimate yield and maximum stresses if very careful  
48 attention is not given to misalignment. Finally, it shows that biaxial bending should be avoided,  
49  
50  
51  
52  
53  
54  
55  
56  
57  
58  
59  
60



1  
2  
3 as it overestimates strength to an unacceptable extent, unless a similar inverse approach is  
4 performed (considering an elastic-plastic, cast-iron mechanical behavior law instead of pure  
5 elasticity). Though not shown here, this approach has been adopted in our case, and taking the  
6 stress-strain curve obtained through the analysis of the 4-point bending test (inverse method)  
7 agrees exceptionally well with the experimental load-displacement curve, provided that the  
8 penetration of the supporting balls into the material is also considered.  
9

10  
11  
12  
13  
14 From a general point of view, the mechanical behavior law is the same whatever the type of  
15 loading condition (*i.e.* transformation starts when the maximum tensile stress reaches a critical  
16 value - here 500 MPa – and the behavior can then be described by a cast-iron model without  
17 strain hardening). The difference between biaxial bending, 4-point bending and tension is not  
18 due to a different intrinsic mechanical behavior law, but different loading configurations, which  
19 in turn generates a different transformation zone and associated different stress distribution, as  
20 explained by Touaiher et al. [152] and highlighted in the main core of the text (see also **Figure**  
21 **10**). The features of the transformation zones in 4-point and biaxial bending are illustrated in  
22 **Figure B-5 a**. Transformations bands, perpendicular to the main tensile stress direction, are  
23 visible and increase rapidly in number and depth between the onset of transformation and the  
24 end of the test (fracture) for the 4-point bending configuration. A much larger zone is observed  
25 in piston-on-three ball (**Figure B-5.b**), starting on the tensile side of the sample and increasing  
26 progressively in size with increasing load. This large transformation acts to shield the applied  
27 tensile stresses and leads to stress redistribution, which explains the high loads that can  
28 withstand the samples in this configuration.  
29  
30  
31  
32  
33  
34  
35  
36  
37  
38  
39  
40

41 In practical terms, such considerations may have two implications:  
42

- 43 - The use of Biaxial bending in the conditions of the ISO standards should be avoided in  
44 highly transformable zirconia ceramics, because it overestimates to a large extent the  
45 real strength of the material if elastic equations are used to compute stresses,  
46  
47
- 48 - From a product point of view, the benefits of the transformation-induced plasticity  
49 depend on the loading conditions, with a better potential reinforcement for complex  
50 loading configurations and stress distribution. If pure tension is considered, the load  
51 necessary for transformation and for failure will be almost the same. On the other hand,  
52 if peak stresses are generated, as it is the case of biaxial bending, transformation will  
53 shield the applied stresses and allow a redistribution of the stress field through a large  
54 portion of the material.  
55  
56  
57  
58  
59  
60

## Acknowledgements

The research leading up to these results was undertaken in the framework of the *LONGLIFE* project (<http://www.longlife-project.eu>) funded by the European Community's Seventh Framework Program (FP7/2007-2013) under the grant agreement n. 280741 and *SISCERA* project (<http://siscera-project.eu>) also funded by E.U. (H2020-FTIPilot-2016, grant agreement n. 737954). Even if this paper concentrates on mechanical properties of the materials, the research effort conducted by our other partners in the field of powder synthesis and processing is deeply appreciated and acknowledged. In particular, we warmly thank our colleagues and friends from Politecnico di Torino, Marta Fornabaio, Paola Palmero, Laura Montanaro, from Swerea IVF, Erik Adolfsson, and Doceram AG, Tobias Fuerderer and Sven Schomer. We also deeply thank our colleagues from INSA, Sylvain Meille, Laurent Gremillard, Arnaud Doko, and Christian Olagnon, who took part on some of these projects at different steps of their achievements. V.S. and V.L. thank Alois Bonifacio for his contribution in the analysis of the Raman mapping data. We acknowledge the CLYM (Centre Lyonnais de Microscopie), supported by the CNRS, the "Grand Lyon" and the Rhône-Alpes Region for the access to the FIB/SEM device used in this study. Some of the Raman data shown were collected by Francesca Russo Cirillo for her undergraduate thesis, and her work is gratefully acknowledged.

## References

1. Dann GE. Martin Heinrich Klaproth: (1743-1817.) Ein deutscher Apotheker und Chemiker. Sein Weg und seine Leistung. Berlin: Akademie-Verlag; 1958.
2. The use of zirconia as a refractory material. *Nature*. 1917; 99 (2488):375-376.
3. Phillips AJ. The partial purification of zirconium oxide. *J Am Ceram Soc*. 1918;1(11):791-800.
4. Ryshkewitch E, inventor; Degussa, assignee. A process for Overpass of zirconia in the plastic state. *Deutsch Patent 519796C*. 1926 Dec 18.
5. Hannink RHJ, Kelly PM., Muddle BC. Transformation toughening in ZrO<sub>2</sub>-containing ceramics. *J Am Ceram Soc*. 2000;83(3):461-487.
6. Garvie RC, Hannink RHJ, Pascoe RT. Ceramic Steel. *Nature*. 1975; 258(5538):703-704.
7. Grathwohl G, Liu T. Crack Resistance and Fatigue of Transforming Ceramics: II, CeO<sub>2</sub>-Stabilized Tetragonal ZrO<sub>2</sub>. *J Am Ceram Soc*. 1991;74(12):3028–3034.
8. Gogotsi GA, Zavadava VP, Swain MV. Mechanical Property Characterization of a 9 mol% Ce-TZP Ceramic Material -I. Flexural Response. *J Eur Ceram Soc*. 1995;15(12):1185-1192.
9. Fett T, Munz D. Influence of time-dependent phase transformations on bending tests. *Mat Sci Eng A-Struct*. 1996; 219(1-2): 89–94.
10. Rauchs G, Fett T, Munz D, Oberacker R. Tetragonal-to-monoclinic phase transformation in CeO<sub>2</sub> -stabilised zirconia under uniaxial loading. *J Eur Ceram Soc*. 2001;21(12):2229-2241.
11. Palmero P, Fornabaio M, Montanaro L, Reveron H, Esnouf C, Chevalier J. Towards long lasting zirconia-based composites for dental implants. Part I: Innovative synthesis, microstructural characterization and in vitro stability. *Biomaterials*. 2015;50:38-46.
12. Reveron H, Fornabaio M, Palmero P, et al. Towards long lasting zirconia-based composites for dental implants: Transformation induced plasticity and its consequence on ceramic reliability. *Acta Biomater*. 2017; 48:423-432.
13. Evans AG. Structural Reliability:A Processing-Dependent Phenomenon. *J Am Ceram Soc*. 1982;65(3):127-137.
14. Evans AG. Perspective on the Development of High-Toughness Ceramics. *J Am Ceram Soc*. 1990;73():187-206.
15. Niihara K. New Design Concept of Structural Ceramics. *J Ceram Soc Jpn*. 1991;99(10):974-982.
16. Jaafar M, Reveron H, Esnouf C, Fantozzi G. Highly creep-resistant alumina–SiC nanocomposites processed by spark plasma sintering. *Scripta Mater*. 2013;68(2):134-137.
17. Bai X, Huang C, Wang J, Zou B, Liu H. Fabrication and characterization of Si<sub>3</sub>N<sub>4</sub> reinforced

- 1  
2  
3  $\text{Al}_2\text{O}_3$ -based ceramic tool materials. *Ceram Int.* 2015;41(10):12798-12804.
- 4  
5 18. Gogotsi Y. Particulate silicon nitride-based composites. *J Mat Sci.* 1994;29(10):1573-4803.
- 6  
7 19. Yin Z, Huang C, Zou B, Liu H, Zhu H, Wang J. Preparation and characterization of  $\text{Al}_2\text{O}_3/\text{TiC}$   
8 micro-nano-composite ceramic tool materials. *Ceram Int.* 2013;39(4):4253-4262.
- 9  
10 20. Swain V, Rose LRF. Strength Limitations of Transformation-Toughened Zirconia Alloys. *J Am*  
11 *Ceram Soc.* 1986;69(7):511-518.
- 12  
13 21. Cutler RA, Mayhew RJ, Prettyman KM, Virkar AV. High-Toughness Ce-TZP/ $\text{Al}_2\text{O}_3$  Ceramics  
14 with Improved Hardness and Strength *J Am Ceram Soc.* 1991;74(1):179-86.
- 15  
16 22. Touaiher I, Saadaoui M, Chevalier J, Preiss L, Reveron H. Fracture behavior of Ce-  
17 TZP/alumina/aluminate composites with different amounts of transformation toughening.  
18 Influence of the testing methods. *J Eur Ceram Soc.* 2018;38(4):1778-1789.
- 19  
20 23. Dietrich M. What Can We Learn from R-Curve Measurements? *J Am Ceram Soc.*  
21 2007;90(1):1-15.
- 22  
23 24. Yu CS, Shetty DK. Transformation yielding, plasticity and crack-growth-resistance (R-curve)  
24 behaviour of  $\text{CeO}_2$ -TZP. *J Mater Sci.* 1990;25(4):2025-2035.
- 25  
26 25. Readey MJ, McCallen CL. Microstructure, Flaw Tolerance, and Reliability of Ce-TZP and  
27 Y-TZP Ceramics. *J Am Ceram Soc.* 1995;78(10):2769-2776.
- 28  
29 26. Tsai JF, Chon U, Ramachandran N, Shetty DK. Transformation Plasticity and Toughening in  
30  $\text{CeO}_2$ -Partially-Stabilized Zirconia-Alumina (Ce-TZP/ $\text{Al}_2\text{O}_3$ ) Composites Doped with  $\text{MnO}$ .  
31 *J Am Ceram Soc.* 1992;75(5):1229-1238.
- 32  
33 27. Eichler J, Hoffman M, Eisele U, Rödel J. R-curve behaviour of 2Y-TZP with submicron grain  
34 size. *J Eur Ceram Soc.* 2006;26(16):3575-3582.
- 35  
36 28. Yu CS, Shetty DK. Transformation Zone Shape, Size, and Crack-Growth-Resistance  
37 [R-Curve] Behavior of Ceria-Partially-Stabilized Zirconia Polycrystals. *J Am Ceram Soc.*  
38 1989;72(6):921-928.
- 39  
40 29. Nawa M, Kurizoe N, Okamoto Y, Ueno A. Transformation-induced plastic deformation in Ce-  
41 TZP/alumina nanocomposite generated during fatigue tests at room temperature. *J Eur Ceram*  
42 *Soc.* 2014;34(16):4337-4345.
- 43  
44 30. Benzaid R, Chevalier J, Saadaoui M, et al. Fracture toughness, strength and slow crack growth  
45 in a ceria stabilized zirconia-alumina nanocomposite for medical applications. *Biomaterials.*  
46 2008;29(27):3636-3641.
- 47  
48 31. Ramachandran N, Chao LY, Shetty DK. R-Curve Behavior and Flaw Insensitivity of  
49 Ce-TZP/ $\text{Al}_2\text{O}_3$  Composite. *J Am Ceram Soc.* 1993;76(4):961-969.
- 50  
51  
52  
53  
54  
55  
56  
57  
58  
59  
60

- 1
- 2
- 3 32. Sato T, Endo T, Shimada M. Postsintering Hot Isostatic Pressing of Ceria-Doped Tetragonal
- 4 Zirconia/Alumina Composites in an Argon Oxygen Gas Atmosphere. *J Am Ceram Soc.*
- 5 1989;72(5):761-764.
- 6
- 7
- 8 33. Tsai JF, Yu CS, Shetty DK. Fatigue Crack Propagation in Ceria-Partially-Stabilized Zirconia
- 9 (Ce-TZP)-Alumina Composites" *J Am Ceram Soc.* 1990;73(10):2992-3001.
- 10
- 11 34. Yu CS, Shetty DK, Shaw MC, Marshall DB. Transformation Zone Shape Effects on Crack
- 12 Shielding in Ceria-Partially-Stabilized Zirconia (Ce-TZP)/Alumina Composites. *J Am Ceram*
- 13 *Soc.* 1992;75(11):2991-2994.
- 14
- 15 35. Nawa M, Nakamoto S, Sekino T, Niihara K. Tough and strong Ce-TZP/Alumina
- 16 nanocomposites doped with Titania. *Ceram Int.* 1998;24(10):497-506.
- 17
- 18 36. NANOZR brochure. Panasonic Healthcare. Available from <https://www.phchd.com>
- 19
- 20 37. Nawa M, Nakanishi H, Suehiro Y, inventors; Panasonic Electric Works Co., Ltd. (Osaka, JP)
- 21 assignee. ZrO<sub>2</sub>-Al<sub>2</sub>O<sub>3</sub> composite ceramic material and production method therefor. US Patent
- 22 7928028. 2004 March 23.
- 23
- 24 38. Apel E, Ritzberger C, Courtois N, et al. Introduction to a tough, strong and stable Ce-
- 25 TZP/MgAl<sub>2</sub>O<sub>4</sub> composite for biomedical applications. *J Eur Ceram Soc.* 2012;32(11):2697-
- 26 2703.
- 27
- 28 39. Mazaheri M, Mari D, Hesabi ZR, Schaller R, Fantozzi G. Multi-walled carbon
- 29 nanotube/nanostructured zirconia composites: Outstanding mechanical properties in a wide
- 30 range of temperature. *Compos Sci Technol.* 2011;71(7):939-945.
- 31
- 32 40. Yang G, Li JC, Wang GC, Yashima M, Min SL, Chen TC. Investigation on strengthening and
- 33 toughening mechanisms of Ce-TZP/Al<sub>2</sub>O<sub>3</sub> nanocomposites. *Metall Mater Trans A.*
- 34 2006;37(6):1969-1975.
- 35
- 36 41. Guo R, Guo D, Chen Y, Yang Z, Yuan Q. In situ formation of LaAl<sub>11</sub>O<sub>18</sub> rodlike particles in
- 37 ZTA ceramics and effect on the mechanical properties. *Ceram Int.* 2002;28(7):699-704.
- 38
- 39 42. Magnani G, Brillante A. Effect of the composition and sintering process on mechanical
- 40 properties and residual stresses in zirconia-alumina composites. *J Eur Ceram Soc.*
- 41 2005;25(15):3383-3392.
- 42
- 43 43. Kern F. A comparison of microstructure and mechanical properties of 12Ce-TZP reinforced
- 44 with alumina and in situ formed strontium- or lanthanum- hexaaluminate precipitates. *J Eur*
- 45 *Ceram Soc.* 2014;34(2):413-423.
- 46
- 47 44. Cutler RA, Lindemann JM, Ulvensøen JH, Lange HI. Damage-resistant SrO-doped Ce-
- 48 TZP/Al<sub>2</sub>O<sub>3</sub> composites. *Mater Design.* 1994;15(3):123-133.
- 49
- 50 45. Burger W, Richter HG. High strength and toughness alumina matrix composites by
- 51
- 52
- 53
- 54
- 55
- 56
- 57
- 58
- 59
- 60

- 1  
2  
3 transformation toughening and “in situ” platelets reinforcement (ZPTA)-the new generation  
4 of bioceramics. *Key Eng Mat.* 2011;192-195:545-548.
- 5  
6 46. Munch E, Launey ME, Alsen DH, Saiz E, Tomsia AP, Ritchie RO. Tough, Bio-Inspired Hybrid  
7 Materials. *Science.* 2008;322(5907):1516-1520.
- 8  
9 47. Bouville F, Maire E, Meille S, Van de Moortèle B, Stevenson AJ, Deville S. Strong, tough and  
10 stiff bioinspired ceramics from brittle constituents. *Nat Mater.* 2014;13:508-514.
- 11  
12 48. Le Ferrand H, Bouville F, Niebel TP, Studart AR. Magnetically assisted slip casting of  
13 bioinspired heterogeneous composites. *Nat Mater.* 2015;14:1172-1179.
- 14  
15 49. Wegst, UGK, Bai H, Saiz E, Tomsia AP, Ritchie RO. Bioinspired structural materials. *Nat*  
16 *Mater.* 2014;14:23-36.
- 17  
18 50. Launey ME, Ritchie RO. On the Fracture Toughness of Advanced Materials. *Adv Mater.*  
19 2009;21(20):2103-2110.
- 20  
21 51. Hannink RHJ, Swain MV. Metastability of the Martensitic Transformation in a 12mol% Ceria-  
22 Zirconia Alloy - I Deformation and Fracture Observations. *J Am Ceram Soc.* 1989;72(8):90-  
23 98.
- 24  
25 52. Liu SY, Chen IW. Fatigue Deformation Mechanisms of Zirconia Ceramics. *J Am Ceram Soc.*  
26 1992;75(5):1191-1204.
- 27  
28 53. Liu T, Mai YW, Swain MV, Grathwohl G. Effects of grain size and specimen geometry on the  
29 transformation and R-curve behaviour of 9Ce-TZP ceramics. *J Mater Sci.* 1994;29(3):835-843.
- 30  
31 54. Reyes-Morel PE, Chen IW. Transformation plasticity of CeO<sub>2</sub>-stabilized tetragonal zirconia  
32 polycrystals: I, Stress assistance and autocatalysis. *J Am Ceram Soc.* 1988;71(5):343-353.
- 33  
34 55. Wang JS, Tsai JF, Shetty DK, Virkar AV. Effect of MnO on the microstructures, phase stability,  
35 and mechanical properties of ceria-partially-stabilized zirconia (Ce-TZP) and Ce-TZP-Al<sub>2</sub>O<sub>3</sub>  
36 composites. *J Mater Res.* 1995;5(9):1948-1957.
- 37  
38 56. Lankford J. Plastic Deformation of Partially Stabilized Zirconia. *J Am Ceram Soc.* 1983;66(11):  
39 C212-C213.
- 40  
41 57. Zhe X, Wang C, Hendry A. Dislocation-Related Plasticity of Ceria-Stabilized Zirconia  
42 Polycrystals. *J Am Cer Soc.* 1996;79(6):1726-1728.
- 43  
44 58. Camposilvan E, Anglada M. Size and plasticity effects in zirconia micropillars compression.  
45 *Acta Mater.* 2016;103:882-892.
- 46  
47 59. Chevalier J, Gremillard L, Virkar AV, Clark DR. The Tetragonal-Monoclinic Transformation  
48 in Zirconia: Lessons Learned and Future Trends. *J Am Ceram Soc.* 2009;92(9):1901-1920.
- 49  
50 60. Shimozono T, Ikeda J, Pezzotti G. Evaluation of transformation zone around propagating cracks  
51 in zirconia biomaterials using Raman microprobe spectroscopy. *Key Eng Mater.* 2006;309-  
52  
53  
54  
55  
56  
57  
58  
59  
60

- 311:1207-1210.
61. Chevalier J, Gremillard L. Ceramics for medical applications: A picture for the next 20 years. *J Eur Ceram Soc.* 2009;29(7):1245-1255.
  62. Rossi M, Rainforth W, McComb DW, Scott AJ, Brydson R. The role of trace additions of alumina to yttria-tetragonal zirconia polycrystals (Y-TZP). *Scripta Mater.* 2001;45(6):653-660.
  63. Tsubakino H, Nozato R, Hamamoto M. Effect of Alumina Addition on the Tetragonal-to-Monoclinic Phase Transformation in Zirconia- 3 mol% Yttria". *J Am Ceram Soc.* 1991;74(2):440-443.
  64. Chevalier J, Deville S, Münch E, Jullian R Lair F. Critical effect of cubic phase on aging in 3mol% yttria-stabilized zirconia ceramics for hip replacement prosthesis. *Biomaterials.* 2004;25(24):5539-5545.
  65. Paul A, Vaidhyanathan B, Binner JGP. Hydrothermal Aging Behavior of Nanocrystalline Y-TZP Ceramics. *J Am Ceram Soc.* 2011;94(7):2146-2152.
  66. Lughì V, Sergo V. Low temperature degradation -aging- of zirconia: a critical review of the relevant aspects in dentistry. *Dent Mater.* 2010;26(8):807-820.
  67. Maschio S, Pezzotti G, Sbaizero O. Effect of LaNbO<sub>4</sub> addition on the mechanical properties of Ceria-Tetragonal Zirconia Polycrystal Matrices. *J Eur Ceram Soc.* 1998;18(12):1779-1785.
  68. Miura M, Hongoh H, Yogo T, Hirano S, Fujii T. Formation of plate-like lanthanum-β-Aluminate crystal in Ce-TZP matrix. *J Mater Sci.* 1994;29(1):262-268.
  69. Ori S, Kojima T, Hara T, Uekawa N, Kakegawa K. Fabrication of Ce-TZP/β-hexaaluminate composites using amorphous precursor of the second phase. *J Ceram Soc Jpn.* 2012;120:111-115.
  70. Yamaguchi T, Sakamoto W, Yogo T, Fujii T, Hirano TS. In situ formation of Ce-TZP/Ba hexaaluminate composites. *J Ceram Soc Jpn.* 1999;107:814-916.
  71. Chevalier J, Grandjean S, Kuntz M, Pezzotti G. On the kinetics and impact of tetragonal to monoclinic transformation in an alumina/zirconia composite for arthroplasty applications", *Biomaterials.* 2009;30(29):5279-5282.
  72. Thuan WH, Chen Z, Wang TC, Cheng CH, Kuo PS. Mechanical properties of Al<sub>2</sub>O<sub>3</sub>/ZrO<sub>2</sub> composites. *J Eur Ceram Soc.* 2002;22(16):2827-2833.
  73. Rafferty A, Alsebaie AM, Olabi AG, Prescott T. Properties of zirconia toughened-alumina prepared via powder processing and colloidal processing routes. *J Colloid Interf Sci.* 2009;329(2):310-315.
  74. Yuan Z, Vleugels J, Van Der Biest O. Synthesis and characterization of CeO<sub>2</sub>-coated ZrO<sub>2</sub> powder-based TZP. *Mater Lett.* 2000;46(5):249-254.

- 1
- 2
- 3 75. Palmero P, Naglieri V, Chevalier J, Fantozzi G, Montanaro L. Alumina-based nanocomposites
- 4 obtained by doping with inorganic salt solutions: application to immiscible and reactive
- 5 systems. *J Eur Ceram Soc.* 2009;29(1):59-66.
- 6
- 7
- 8 76. Torrecillas R, Diaz Rodriguez LA, inventors; CSIC, assignee. Nanostructured composite
- 9 material of stabilized zirconia with cerium oxide and doped alumina with zirconia, use, and
- 10 procedure for obtaining same. United States patent US8546285B2. 2013 Oct 1.
- 11
- 12
- 13 77. Schehl M, Díaz L.A, Torrecillas R. Alumina nanocomposites from powder–alkoxide mixtures.
- 14 *Acta Mater.* 2002;50(5):1125-1139.
- 15
- 16
- 17 78. Bartolomé JF, De Aza AH, Martín A et al., Alumina/Zirconia Micro/Nanocomposites: A New
- 18 Material for Biomedical Applications With Superior Sliding Wear Resistance. *J Am Ceram*
- 19 *Soc.* 2007;90(10):3177-3184.
- 20
- 21
- 22 79. Palmero P, de Barra E, Cambier F. *Advances in ceramic biomaterials : Materials, Devices and*
- 23 *Challenges.* Woodhead Publishing; 2017.
- 24
- 25 80. Benazzo F, Falezio F, Dietrich M. *Bioceramics and alternative bearings in joint arthroplasty:*
- 26 *11<sup>th</sup> biolox symposium-proceeding, ceramics in orthopaedics.* Springer Science and Business
- 27 *Media; 2006.*
- 28
- 29
- 30 81. De Aza AH, Chevalier J, Fantozzi G, Schehl M, Torrecillas R. Slow-crack growth behavior of
- 31 zirconia toughened alumina ceramics processed by different methods *J Am Ceram Soc.*
- 32 2003;86(1):115-120.
- 33
- 34
- 35 82. Deville S, Chevalier J, Fantozzi G et al. Low temperature ageing of zirconia toughened alumina
- 36 ceramics and its implcation in biomedical implants. *J Eur Ceram Soc.* 2003;23(15):2975-2982.
- 37
- 38
- 39 83. Goyos L, Diaz LA, TorrecillasR. Alumina-Ceria-TZP nano composites obtained in an alcohol
- 40 medium by two different processing routes. Paper presented at: *ECCMIS 15<sup>th</sup>.* 2012 Jun 24-28;
- 41 Venice, Italie. p. 24-28.
- 42
- 43
- 44 84. Rouanet A. Etude du système zircone oxide de cerium à haute temperature. *C R Hebd Seances*
- 45 *Acad Sci.* 1968;18(C908).
- 46
- 47 85. Leonov AI, Keler EK, Andreeva AB. The system  $\text{La}_2\text{O}_3\text{-ZrO}_2$ ,  $\text{Ce}_2\text{O}_3\text{-ZrO}_2$  and  $\text{Nd}_2\text{O}_3\text{-ZrO}_2$ .
- 48 *Izv Akad Nauk USSR Neorg Mater.* 1966;2:1047-1054. (pp. 893-897 on the English edition).
- 49
- 50 86. Heussner KH, Claussen N. Strengthening of ceria-doped tetragonal zirconia polycrystals by
- 51 reduction-induced phase transformation. *J Am Ceram Soc.* 1989;72(6):1044-1046.
- 52
- 53 87. Sergo V, Schmid C, Meriani S, Evans AG. Mechanically Induced Zone Darkening of
- 54 Alumina/Ceria-Stabilized Zirconia Composites. *J Am Ceram Soc.* 1994;77(11):2971-2976.
- 55
- 56 88. Sergo V, Meriani S, Magistris A, Chiodelli G. Thermally Induced Changes in the
- 57 Ceria/Zirconia System. *Thermochim Acta.* 1988;133:113-118.
- 58
- 59
- 60



- 1
- 2
- 3 89. Montanaro L, Palmero P, Chevalier J, Reveron H, Fuerderer T, inventors ; Politec di Torino et
- 4 al., assignee. Procedimento di produzione di compositi ceramici multifasici a base di zirconia.
- 5 Italien patent TO2014A00145. 2014 Feb 21.
- 6
- 7
- 8 90. International Organization for Standardization. ISO 6872:2015. \_Dentistry-Ceramic materials
- 9 \_ . Geneva: ISO; 2015.
- 10
- 11 91. Becher PF, Swain MV, Ferber MK. Relation of transformation temperature to the fracture
- 12 toughness of transformation-toughened ceramics. *J Mater Sci*. 1987;22(1):76-84.
- 13
- 14 92. Alexander KB, Becher PF, Wang X, Hsueh C. Internal Stresses and the Martensite Start
- 15 Temperature in Alumina-Zirconia Composites: Effects. *J Am Ceram Soc*. 1995;78(2):291-269.
- 16
- 17 93. Becher PF, Swain MV. Grain-Size-Dependent Transformation Behavior in Polycrystalline
- 18 Tetragonal Zirconia. *J Am Ceram Soc*. 1992;75(3):493-502.
- 19
- 20 94. Li LF, Yang K, Li YY. Microstructure and toughening of Ce-TZP ceramics at low temperatures.
- 21 In: Balachandran UB, Hartwig KT, Gubser DU, Bardos VA, editors. *Advances in Cryogenic*
- 22 *Engineering Materials*. Boston: Springer, 2000; p.259-266.
- 23
- 24 95. Li B, Zhe X, Ishii K, Sasaki Y. Trasformation characteristics of Ce-TZP during shape memory
- 25 cycles. *Mater Trans JIM*. 1997;38(10):906-909.
- 26
- 27 96. Swain MV. Inelastic deformation of Mg-PSZ and its significance for strength-toughness
- 28 relationship of zirconia toughened ceramics. *Acta Metall*. 1985;33(11):2083-2091.
- 29
- 30 97. Sergo V, Clarke DR, Pompe W. Deformation Bands In Ceria-Stabilized Tetragonal
- 31 Zirconia/Alumina: I. Measurement of Internal Stresses. *J Am Ceram Soc*. 1995;78(3):633-640.
- 32
- 33 98. Gebresilassie AG. Atomic scale simulations in zirconia : Effect of yttria doping and
- 34 environment on stability of phases. *Mechanics of materials [physics.class-ph]*. Université de
- 35 Lyon, 2016.
- 36
- 37 99. Chevalier J, Cales B, Drouin JM. Low-Temperature Aging of Y-TZP Ceramics. *J Am Ceram*
- 38 *Soc*. 1999;82(8):2150-2154.
- 39
- 40 100. Ashby MF. *Materials Selection in Mechanical Design*, 3rd ed. Waltham, MA: Butterworth-
- 41 Heinemann; 2005.
- 42
- 43 101. Lambrigger M. Evaluation of Weibull master curves of zirconia ceramics and zirconia/alumina
- 44 composites. *J Mater Sci Lett*. 1997;16(11):924-926.
- 45
- 46 102. Wennerberg A, Albrektsson T, Wennerberg AT. Suggested guidelines for the topographic
- 47 evaluation of implant surfaces. *Int J Oral Maxillofac Implant*. 2000;15:331-344.
- 48
- 49 103. Wennerberg A, Albrektsson T. On Implant Surfaces: A Review of Current Knowledge and
- 50 Opinions. *Int J Oral Maxillofac Implant*. 2009;24:63-74.
- 51
- 52 104. Sennerby L, Dasmah A, Larsson B, Iverhed M. Bone tissue responses to surface-modified
- 53
- 54
- 55
- 56
- 57
- 58
- 59
- 60

- 1  
2  
3 zirconia implants: a histomorphometric and removal torque study in the rabbit. *Clin Implant*  
4 *Dentistry Related Res.* 2005;7:13-20.
- 5  
6 105. Depprich R, Zipprich H, Ommerborn M, et al. Osseointegration of zirconia implants compared  
7 with titanium: an in vivo study. *Head Face Med.* 2008;4(30):1-8.
- 8  
9 106. Yamashita D, Machigashira M, Miyamoto M, et al. Effect of surface roughness on initial  
10 responses of osteoblast-like cells on two types of zircon2009;28:461-470.
- 11  
12 107. Kurella A, Dahotre NB. Review paper: Surface modification for bioimplants: The role of laser  
13 surface engineering. *J Biomater Appl.* 2005;20(1):5-50.
- 14  
15 108. Roitero E, Lasserre F, Anglada M, Mücklich F, Jiménez-Piqué E. A parametric study of laser  
16 interference surface patterning of dental zirconia: Effects of laser parameters on topography  
17 and surface quality. *Dent Mater.* 2017;33(1):e28–e38.
- 18  
19 109. Roitero E, Lasserre F, Roa JJ, Anglada M, Mücklich F, Jiménez-Piqué E. Nanosecond-laser  
20 patterning of 3Y-TZP: Damage and microstructural changes. *J Eur Ceram Soc.*  
21 2017;37(15):4876-4887.
- 22  
23 110. Park YS, Chung SH, Shon WJ. Peri-implant bone formation and surface characteristics of rough  
24 surface zirconia implants manufactured by powder injection molding technique in rabbit tibiae.  
25 *Clin Oral Implants Res.* 2013;24(5):586-591.
- 26  
27 111. International Organization for Standardization. ISO 14801:2008. *Dentistry-Implants-Dynamic*  
28 *fatigue test for endosseous dental implants*. Geneva: ISO; 2008.
- 29  
30 112. Rosa LB, Batiglion C, Siéssere S, et al. Bite force and masticatory efficiency in individuals  
31 with different oral rehabilitations. *Open J Stomatol.* 2012;2(1):21-26.
- 32  
33 113. Ferrario VF, Sforza C, Serrao G, Dellavia C, Tartaglia GM. Single tooth bite forces in healthy  
34 young adults. *J Oral Rehabil.* 2004;31(1):18-22.
- 35  
36 114. Biswas BK, Bag S, Pal S. Biomechanical Analysis Of Normal And Implanted Tooth Using  
37 Biting Force Measurement. *Int J Eng Appl Sci.* 2013;4(2):17-23.
- 38  
39 115. Luraschi J, Schimmel M, Bernard JP, Gallucci GO, Belser U, Müller F. Mechanosensation and  
40 maximum bite force in edentulous patients rehabilitated with bimaxillary implant-supported  
41 fixed dental prostheses. *Clin Oral Implants Res.* 2012;23(5):577-583.
- 42  
43 116. Jofré J, Hamada T, Nishimura M, Klattenhoff C. The effect of maximum bite force on marginal  
44 bone loss of mini-implants supporting a mandibular overdenture: A randomized controlled trial.  
45 *Clin Oral Implants Res.* 2010;21(2):243-249.
- 46  
47 117. Fontijn-Tekamp FA, Slagter AP, Van Der Bilt A, et al. Biting and chewing in overdentures,  
48 full dentures, and natural dentitions. *J Dent Res.* 2000;79(7):1519-1524.
- 49  
50 118. <https://www.straumann.com>
- 51  
52  
53  
54  
55  
56  
57  
58  
59  
60

- 1
- 2
- 3 119. <https://zsystems.com>
- 4
- 5 120. <https://www.zeramex.com>
- 6
- 7 121. <https://www.camlog.fr>
- 8
- 9 122. International Organization for Standardization. ISO3950:2016. *Dentistry-Designation system for teeth and areas of the oral cavity*. Geneva:ISO; 2016.
- 10
- 11
- 12 123. International Organization for Standardization. ISO 13356:2015. *Implants for surgery- Ceramic materials based on yttria-stabilized tetragonal zirconia (Y-TZP)*. Geneva:ISO; 2015.
- 13
- 14
- 15 124. Harrer W, Schwentenwein M, Lube T, Danzer R. Fractography of zirconia-specimens made using additive manufacturing (LCM) technology. *J Eur Cer Soc.* 2017;37(14):4331-4381.
- 16
- 17
- 18 125. Goyos-Ball L, García-Tuñón E, Fernández-García E, et al. Mechanical and biological evaluation of 3D printed 10CeTZP-Al<sub>2</sub>O<sub>3</sub> structures. *J Eur Ceram Soc.* 2017;37(9):3151-3158.
- 19
- 20
- 21
- 22 126. Tarafder S, Balla VK, Davies NM, Bandyopadhyay A, Bose S. Microwave-sintered 3D printed tricalcium phosphate scaffolds for bone tissue engineering. *J Tissue Eng Regen M.* 2013;7(8):631-41.
- 23
- 24
- 25
- 26
- 27 127. Khalyfa A, Vogt S, Weisser J, et al. Development of a new calcium phosphate powder-binder system for the 3D printing of patient specific implants. *J Mater Sci-Mater M.* 2007;18(5):909-916.
- 28
- 29
- 30
- 31
- 32 128. Miranda P, Pajares A, Saiz E, Tomsia AP, Guiberteau F. Fracture modes under uniaxial compression in hydroxyapatite scaffolds fabricated by robocasting. *J Biomed Mater Res A.* 2007;83(3):646-655.
- 33
- 34
- 35
- 36
- 37 129. Farzadi A, Solati-Hashjin M, Asadi-Eydivand M, Abu Osman NA. Effect of layer thickness and printing orientation on mechanical properties and dimensional accuracy of 3D printed porous samples for bone tissue engineering. *Plos One.* 2014;9(9):e108252.
- 38
- 39
- 40
- 41
- 42 130. Zocca A, Colombo P, Gomes CM, Günster J. Additive Manufacturing of Ceramics: Issues, Potentialities, and Opportunities. *J Am Ceram Soc.* 2015;98(7):1983-2001.
- 43
- 44
- 45
- 46 131. Fielding GA, Bandyopadhyay A, Bose S. Effects of silica and zinc oxide doping on mechanical and biological properties of 3D printed tricalcium phosphate tissue engineering scaffolds. *Dent Mater.* 2012;28(2):113-122.
- 47
- 48
- 49
- 50
- 51 132. Kolan KC, Leu MC, Hilmas GE, Brown RF, Velez M. Fabrication of 13-93 bioactive glass scaffolds for bone tissue engineering using indirect selective laser sintering. *Biofabrication.* 2011;3(2):025004.
- 52
- 53
- 54
- 55
- 56 133. Chu TMG, Orton DG, Hollister SH, Feinberg SE, Halloran JW. Mechanical and in vivo performance of hydroxyapatite implants with controlled architectures. *Biomaterials.* 2002;23(5):1283-1293.
- 57
- 58
- 59
- 60

134. Genet M, Houmard M, Eslava S, Saiz E, Tomsia AP. A two-scale Weibull approach to the failure of porous ceramic structures made by robocasting: possibilities and limits. *J Eur Ceram Soc.* 2013;33(4):679-688.
135. Deville S, Saiz E, Tomsia AP. Freeze casting of hydroxyapatite scaffolds for bone tissue engineering. *Biomaterials.* 2006;27(32):5480-5489.
136. Gerberich WW, Hemings PL, Merz MD, Zackay VF. Preliminary toughness results on TRIP steel. *Trans Am Soc Metal.* 1968;61:843-847.
137. Gupta TK, Bechtold JH, Kuznickii RC, Cadoff LH, Rossing BR. Stabilization of tetragonal phase in polycrystalline zirconia. *J Mater Sci.* 1977;12:2421-2426.
138. Chen IW, Reyes Morel PE. Implications of transformation plasticity in ZrO<sub>2</sub>-containing ceramics : I, Shear and dilatation effects. *J Am Ceram Soc.* 1986;69(3):181-189.
139. Claussen N. Microstructural Design of Zirconia-Toughened Ceramics (ZTC). In: Claussen N, Ruhle M, Heuer AH, editors. *Advances in Ceramics, Vol. 12. Science and Technology of Zirconia 11.* Columbus OH: American Ceramic Society, 1984; p. 325-351.
140. Heuer AH. Transformation toughening in ZrO<sub>2</sub> -containing ceramics. *J Am Ceram Soc.* 1987;70(10): 689-698.
141. McMeeking RM, Evans AG. Mechanics of Transformation-Toughening in Brittle Materials. *J Am Ceram Soc.* 1982;65(5):242-246.
142. Budiansky B, Hutchinson JW, Lambropoulos JC. Continuum theory of dilatant transformation toughening in ceramics. *Int J Solids Struct.* 1983;19:337-355.
143. Mamivanda M, Asle Zaeem M, El Kadiriab H. Phase field modeling of stress-induced tetragonal-to-monoclinic transformation in zirconia and its effect on transformation toughening. *Acta Mater.* 2014;64:208-219.
144. Maekawa H, Kawata K, Xiong YP, Sakai N, Yokokawa H. Quantification of local oxygen defects around Yttrium ions for yttria-doped ceria-zirconia ternary system. *Solid State Ionics.* 2009;180(4-5): 314-319.
145. Li P, Chen IW, Penner-Hahn JE, Tien TY. X-ray Absorption Studies of Ceria with Trivalent Dopants. *J Am Ceram Soc.* 1991;74(5): 958-967.
146. Tsukuma K, Kubota Y, Tsukidate T. Thermal and mechanical properties of Y<sub>2</sub>O<sub>3</sub>-stabilized tetragonal zirconia polycrystals. In: Claussen N, Ruhle M, Heuer AH, editors. *Advances in Ceramics, Vol. 12. Science and Technology of Zirconia 12.* Columbus OH: American Ceramic Society, 1984; p.382-390.
147. Gross V, Swain MV. Mechanical Properties and Microstructure of Sintered and Hot Isostatically Pressed Yttria-Partially Stabilized Zirconia. *J Aust Ceram Soc.* 1986;22:1-12.

- 1  
2  
3 148. Tsukuma K, Shimada M. Strength, fracture toughness and Vickers hardness of CeO<sub>2</sub>- stabilized  
4 tetragonal ZrO<sub>2</sub> polycrystals (Ce-TZP). *J Mater Sci.* 1985;20(4):1178-1184.  
5  
6 149. El Attaoui H, Saâdaoui M, Chevalier J, Fantozzi G. Static and cyclic crack propagation in Ce-  
7 TZP ceramics with different amounts of transformation toughening. *J Eur Ceram Soc.*  
8 2007;27(2-3):483-486.  
9  
10 150. Tsukuma K, Ueda K, Matsushita K, Shimada M. High-Temperature Strength and Fracture  
11 Toughness of Y<sub>2</sub>O<sub>3</sub>-Partially-Stabilized ZrO<sub>2</sub>/Al<sub>2</sub>O<sub>3</sub> Composites. *J Am Ceram Soc.* 1985;68(2):  
12 C56-C58.  
13  
14 151. Tsukuma K, Takahata T. Mechanical Property and Microstructure of TZP and TZP/Al<sub>2</sub>O<sub>3</sub>  
15 Composites. Paper presented at MRS; 1986. *MRS Proceedings.* 1986;78:12-135.  
16  
17 152. Touaiher I, Saâdaoui M, Chevalier J, Reveron H. Effect of loading configuration on strength  
18 values in a highly transformable zirconia-based composite. *Dent Mater.* 2016;32(9):e211-e219.  
19  
20 153. Fünfschilling S, Fett T, Hoffmann M, et al. Bridging stresses from R-curve of silicon nitrides.  
21 *J Mater Sci.* 2009;44(14):3900-3904.  
22  
23  
24  
25  
26  
27  
28  
29  
30  
31  
32  
33  
34  
35  
36  
37  
38  
39  
40  
41  
42  
43  
44  
45  
46  
47  
48  
49  
50  
51  
52  
53  
54  
55  
56  
57  
58  
59  
60

## Symbols and abbreviations

### Materials denomination

- Y-TZP : Ytria-stabilized Tetragonal Zirconia Polycrystal (yttria-doped zirconia)
- Ce-TZP : Ceria-stabilized Tetragonal Zirconia Polycrystal (ceria-doped zirconia)
- 3Y-TZP : 3 mol.% Ytria-stabilized Tetragonal Zirconia Polycrystal
- YAP: Yttrium Aluminium Perovskite
- YAG: Yttrium Aluminium Garnet
- ZTA: Zirconia-Toughened Alumina
- $ZA_8Sr_8$ : 84 vol.%  $ZrO_2$ , 8 vol.%  $Al_2O_3$ , 8 vol.%  $SrAl_{12}O_{19}$
- Z: Zirconia grains
- A: Alumina grains
- S: Strontium aluminate grains
- PSZ: Partially Stabilized Zirconia
- TZP: Tetragonal Zirconia Polycrystals
- FSZ: Fully Stabilized Zirconia
- Mg-PSZ: Magnesia Partially Stabilized Zirconia
- TCP: Tri-Calcium Phosphate
- DLM: dianhydro-D-glucitol [bis(dilactoylmethacrylate)]
- TTCP: Tetra Calcium Phosphate
- HA: Hydroxyapatite
- CaP: Calcium Phosphate

### Zirconia phases denomination

- t : tetragonal
- m : monoclinic

### Mechanical parameters

- $\sigma_R$  : strength
- $K_{IC}$  : toughness
- c : critical defect size
- $\sigma_c^{t-m}$ : critical transformation stress
- $\Delta K_{cT}$ : transformation toughening
- $K_{app}$ : applied stress intensity factor
- $a_{ss}$ : crack extension at the steady-state
- $K_R$  : R-Curve (increase of crack resistance versus crack size)
- $K_{Rmax}$ : saturation level (plateau value) of the R-Curve
- $\sigma_{max1}$  : maximum strength (for highly transformable ceramics)
- $\sigma_y$  : yield strength
- $\sigma_{max2}$  : maximum strength (for low transformability ceramics)
- $\epsilon$ : plastic strain due to *t-m* transformation
- $\epsilon_{vol}$ : dilatation strain induced by the volume expansion of the grains

- $\epsilon_{\text{shear}}$ : shear strain associated to the *t-m* transformation

### Physical parameters and phenomena

- $M_s$  : martensitic start
- $T_0^{t-m}$ : spontaneous tetragonal-monoclinic transformation temperature
- $h$  : width of the transformation zone
- $T$ : Temperature
- $T_{\text{melting}}$ : melting temperature
- $T_{t-m}$ : t-m transformation temperature
- $V_m$  : Volume fraction of monoclinic phase
- $V_{\text{ZrO}_2}$ : Volume fraction of zirconia in the studies composite (here 84 vol.%)
- $D_{tb}$ : density of transformation bands (% of surface transformation at failure)
- $d$ : Process zone size (diameter)
- $S_a$  : Roughness parameter
- TRIP : Transformation Induced Plasticity
- LTD : Low Temperature Degradation

### Tests and experimental methods

- CIP: Cold Isostatic Pressing
- HIP: Hot Isostatic Pressing
- XPS: X-Ray Photoelectron Spectroscopy
- SEVNB: Single-Edge-V-Notched Beam
- CNC: Computer Numerical Control
- FIB : Focused Ion Beam
- SEM : Scanning Electron Microscopy
- TEM : Transmission Electron Microscopy
- HAADF : High Angle Annular Dark Field
- AM : Additive Manufacturing
- LVDT: Low Voltage Displacement Transducer
- FEM: Finite Element Methods
- FEA: Finite Element Analysis
- M: Hard Machining
- S: Sandblasting
- E: Etching
- A: Annealing
- DIW: Direct Ink Writing
- 3DP: 3D – Printing
- SLS: Selective Laser Sintering
- SLA: Stereolithography

### Applications

- TBCs : Thermal Barrier Coatings

## FIGURES AND TABLES CAPTIONS

### FIGURES CAPTIONS

**Figure 1.** Transformation-induced plasticity in 9 mol % Ce-TZP, as shown by different papers: **(a)** Stress-strain diagrams in four-point bending test of 9Ce-TZP sintered at various conditions [7]. **(b)** Cyclic load-displacement in four-point bending test [8]. **(c)** Stress-strain curve with acoustic emission signal in four-point bending test. The acoustic emission signals were produced by the burst formation of transformation bands at the onset of elastic-plastic deformation [10]. **(d)** Load-displacement in double cantilever beam test [53]. Note that only works using 9Ce-TZP were representatively shown in this figure, but several works also showed the transformation-induced plasticity effect on other zirconia ceramics including Ce-TZP, Ce-TZP-based composite and Mg-PSZ [9, 20, 21, 26, 52, 54-57, 28-31].

**Figure 2.** **(a)** R-curve illustration of zirconia ceramics. Extent of crack-shielding due to stress-induced transformation (*i.e.* transformation toughening  $\Delta K_{CT}$ ) is proportional to  $h^{1/2}$ , which then depends on the critical stress for phase transformation ( $\sigma_c$ ) in the relationship of  $h \propto (K_{app}/\sigma_c)^2$ , where  $K_{app}$  is the applied stress intensity factor. As a consequence of the tangency condition, the strength is directly related to the slope of the R-curve [5, 23]. **(b)** R-curves of 12Ce-TZP [23, 24] with two different cracks (natural crack and macrocrack) and **(c)** R-curves of Y-TZP materials (2Y-TZP and 3T-TZP [27]) compared with  $\text{Si}_3\text{N}_4$  [153]. Ce-TZP has high  $\Delta K_{CT}$  and  $a_{ss}$  (crack extension at the steady-state or plateau value,  $K_{RMax}$ ) resulting in high fracture toughness and defect tolerant characteristics, whereas, 3Y-TZP has steep slope in R-curve, contributing to its high strength.

**Figure 3.** Microstructural features of 10Ce-TZP-alumina based composites developed by Nawa et al. [35] from which the commercial product NANOZR derives [36].

**Figure 4.** Microstructural features of BIOLOX Delta<sup>®</sup> ZTA composite [71].

**Figure 5.** **(a)** TEM (STEM-HAADF) and **(b)** SEM microstructural features of  $\text{ZA}_8\text{Sr}_8$  composites [11, 12] prepared at the lab-scale from powder post-doping route and then through slip-casting and sintering (1450°C-1h). Z stands for Zirconia grains, A for Alumina grains and S for Strontium aluminate grains.

**Figure 6.** SEM microstructural features of  $\text{ZA}_8\text{Sr}_8$  composites prepared at the industrial level from powder mixing and then spray-drying granulation, CIP and sintering (1450°C-1h) [22]. Z stands for Zirconia grains, A for Alumina grains and S for Strontium aluminate grains.

**Figure 7.** Evolution of the spontaneous *t-m* transformation temperature (*i.e.* without any applied stress) of Ceria-doped zirconia / alumina / Strontium Aluminate composites as function of the



1  
2  
3 Ceria content in the zirconia phase and of the sintering temperature, for two types of powder-  
4 synthesis methods.  
5

6  
7 **Figure 8.** (a) Biaxial strength and toughness as function of the ceria content for ZA<sub>8</sub>Sr<sub>8</sub>Ce<sub>11</sub>-  
8 1450°C composite obtained by post-doping route. (b) Schematic illustration of the “ductile-  
9 brittle” transition in Ce-TZP composites.  $\sigma_R$  stands for the maximum strength,  $K_{IC}$  the  
10 toughness,  $c$  the critical defect size,  $\sigma_c^{t-m}$  the critical transformation stress,  $\sigma_y$  the yield strength,  
11  $c_0$  and  $c_1$  two different defect sizes with  $c_1 < c_0$ .  
12  
13

14 **Figure 9.** Biaxial bending load-unload-displacement curves for different ceria-containing Ce-  
15 TZP composites obtained by post-doping and after a sintering at 1450°C. A clear difference in  
16 the mechanical behavior is observed depending on the Ceria concentration.  
17  
18  
19

20 **Figure 10.** (a) Superposition of an optical microscopy image (Nomarski contrast) and a  
21 monoclinic/tetragonal Raman map obtained by analyzing the tensile surface of a biaxially tested  
22 disc (10.5 mol.% ceria). (b) Corresponding stress distribution obtained by Raman mapping.  
23 Results were obtained on Ce-TZP processed by post-doping route and after a sintering at  
24 1450°C. (c) Schematic picture of stress variations along the distance from the center for a  
25 conventional non-transformable ceramic and for the transformable Ce-TZP ceramic tested here.  
26 The residual stress field represented here is the difference between the stress field of the elasto-  
27 plastic material and the purely elastic case.  
28  
29  
30  
31  
32

33 **Figure 11.** (a) Stress-strain load-unload curve of a ZA<sub>8</sub>Sr<sub>8</sub>Ce<sub>11</sub>-1450°C composite obtained by  
34 the mixing route during a tensile test, exhibiting a significant amount of plasticity before failure  
35 (b) Corresponding variations of the Young’s modulus as function of the applied strain  
36 (measurements performed during re-loading).  
37  
38  
39

40 **Figure 12.** (a) Location of the FIB lift-out of the thin foils inside a transformation band. (b)  
41 Preparation of the TEM foil by FIB. (c) SEM image of the prepared TEM foil showing micro-  
42 cracks of approximately 1  $\mu\text{m}$  at the upper surface and no micro-cracks inside the foil. (d) TEM  
43 image of the central part of the foil showing that no micro-cracks are visible. TEM foil was  
44 prepared on a ZA<sub>8</sub>Sr<sub>8</sub>Ce<sub>11</sub>-1450°C composite obtained by mixing route.  
45  
46  
47  
48

49 **Figure 13.** Fracture toughness versus yield strength chart for different materials. Blue figures  
50 are referring to 3Y-TZP ceramics while orange figures refer to Ce-TZP composites. The  
51 diagonal lines show the process-zone size diameter,  $d$ , in mm.  
52  
53  
54

55 **Figure 14.** Tensile Stress-Strain curve of two different Ce-TZP composite samples  
56 (ZA<sub>8</sub>Sr<sub>8</sub>Ce<sub>11</sub>-1450°C obtained by mixing route). Sample 1 doesn’t show any internal defect  
57 whereas sample 2 exhibits a large internal defect of  $\sim 150 \mu\text{m}$ . It can be noted that sample 2  
58 does not show any significant decrease of the mechanical properties compared to sample 1,  
59 even though it contains a large internal defect, illustrating the large flaw tolerance.  
60

1  
2  
3  
4  
5  
6  
7  
8  
9  
10  
11  
12  
13  
**Figure 15.** Weibull plot: probability of failure as function of the calculated stress for Ce-TZP composite:  $\text{ZA}_8\text{Sr}_8\text{Ce}_{11}$ -1450°C obtained by mixing route (round orange symbols) compared to 3Y-TZP (blue square symbols) obtained with two different loading conditions: 4 point bending test (full symbols) and biaxial bending tests using a piston-on-3-balls set up (half black symbols). The Ce-TZP composite shows a very high Weibull modulus compared to 3Y-TZP explaining its lower sensitivity to the presence of defects. Clearly the overall strengths of Ce-TZP composites are relatively lower than 3YTZP.

14  
15  
16  
17  
**Figure 16.** Image of a prototype dental implant made of the Ce-TZP composite ( $\text{ZA}_8\text{Sr}_8\text{Ce}_{11}$ -1450°C-mixing route) and machined in the sintered state.

18  
19  
20  
21  
22  
23  
24  
25  
26  
27  
**Figure 17. (a)** Load to failure of implant prototypes as function of the surface treatments for the  $\text{ZA}_8\text{Sr}_8\text{Ce}_{11}$ -1450°C composite obtained by mixing route. Available data for 3Y-TZP dental implants fall in the dashed region. “M” stands for hard machining, “S” for sandblasting (with 150  $\mu\text{m}$  alumina particles), “E” for etching (in HF/HNO<sub>3</sub> for 3h) and “A” for annealing at 1350°C for one hour respectively. 3 to 4 samples were tested in each conditions. **(b)** and **(c)** SEM image of a dental implant prototype after sandblasting. **(d)** and **(e)** SEM image of a dental implant prototype after sandblasting + etching.

28  
29  
30  
31  
32  
33  
**Figure 18.** Additive-manufactured (Robocasting) lattice structures (top 3 optical pictures) and microstructure of  $\text{ZA}_8\text{Sr}_8\text{Ce}_{11}$  (11Ce-TZP/ $\text{Al}_2\text{O}_3$ /  $\text{SrAl}_{12}\text{O}_{19}$ ) composite (bottom 2 SEM pictures).

34  
35  
36  
37  
38  
39  
40  
41  
42  
43  
44  
45  
46  
47  
**Figure 19.** Compressive strength of  $\text{ZA}_8\text{Sr}_8\text{Ce}_{11}$  scaffolds achieved by Direct Ink Writing (DIW) for two porosity contents. Higher strength was obtained with the scaffold with a rim and the scaffold without rim had lower compressive strength. Comparison with literature values of porous ceramics made from additive manufacturing and freeze casting techniques is reported for comparison [126-135]. *TCP* stands for TriCalciumPhosphate, *DLM* for dianhydro-D-glucitol [bis(dilactoylmethacrylate), *TTCP* for TetraCalciumPosphate, *3DP* for 3D printing, *HA* for hydroxyapatite, *CaP* for CalciumPhosphate, *SLS* for selective laser sintering and *SLA* for stereolithography.

48  
49  
50  
51  
52  
53  
**Figure A-1.** Strength-toughness relationship for zirconia materials. Linear curves are predicted from Griffith equation considering different flaw-sizes (5-100 microns, Y-TZP) whereas the hyperbolic curve is predicted theoretically using the expression proposed by Swain and Rose [20].

54  
55  
56  
57  
**Figure A-2.** Summary of the strength-toughness results for various PSZ and TZP systems and for 2Y-TZP-20 wt.% $\text{Al}_2\text{O}_3$  composites [20, 151].

58  
59  
60  
**Figure B-1.** Apparent ‘stress-strain’ curves obtained on the  $\text{ZA}_8\text{Sr}_8\text{C}_{11}$ -1450°C composite obtained by mixing route with different loading configurations, when both stress and strain in

1  
2  
3 bending are calculated through standard equations considering elastic hypotheses. The dashed  
4 area corresponds to the variation obtained with tensile tests.  
5  
6

7  
8 **Figure B-2.** Applied load as function of the penetration depth after a 1 ball-indentation test on  
9 the  $\text{ZA}_8\text{Sr}_8\text{Ce}_{11}$ -1450°C composite obtained by mixing route. For an applied load of 350 N, a  
10 permanent penetration depth of the ball of approximately 20  $\mu\text{m}$  is observed. This displacement  
11 should be subtracted from the displacement measured by the LVDT.  
12

13  
14 **Figure B-3. (a)** Experimental (solid black line) and FEA-simulated load-displacement curves  
15 in 4 point bending for the  $\text{ZA}_8\text{Sr}_8\text{Ce}_{11}$ -1450°C composite obtained by mixing route. FEA-  
16 simulated curves are obtained by using a CAST-IRON material's model (elastic in compression  
17 and elasto-plastic in tension) and effective load-displacement curve recorded in tension (Figure  
18 **(b)**, red and orange symbols). In blue, the results of the inverse method, showing that the  
19 behavior can be well described by an elasto-plastic behavior, with a yield stress of 500 MPa  
20 and almost no hardening.  
21  
22

23  
24 **Figure B-4.** Effect of misalignment on the onset of transformation and apparent yield stress  
25 measured in tension on  $\text{ZA}_8\text{Sr}_8\text{Ce}_{11}$ -1450°C composite obtained by mixing route. **(a)**  
26 Experimental Stress-strain curve with the lowest apparent yield (transformation) stress in all  
27 out set of data. **(b)** Monoclinic content versus position along the sample measured by Raman  
28 spectroscopy for two opposite line-scans along the same sample. **(c)** Finite Element Simulation  
29 of maximal principal stress in a tensile sample with a parasite misalignment of 30 microns.  
30  
31  
32

33  
34 **Figure B-5.** Specific features of the transformation zones observed by optical microscopy  
35 (Nomarski contrast) on  $\text{ZA}_8\text{Sr}_8\text{Ce}_{11}$ -1450°C composite obtained by mixing route in pure  
36 bending **(a)** and biaxial bending **(b)**  
37  
38

### 39 TABLES CAPTIONS

40  
41  
42 **Table 1.** The properties of some Ce-TZP composites developed in the past compared to 3Y-  
43 TZP and Ce-TZP ceramics.  
44  
45  
46  
47  
48  
49  
50  
51  
52  
53  
54  
55  
56  
57  
58  
59  
60

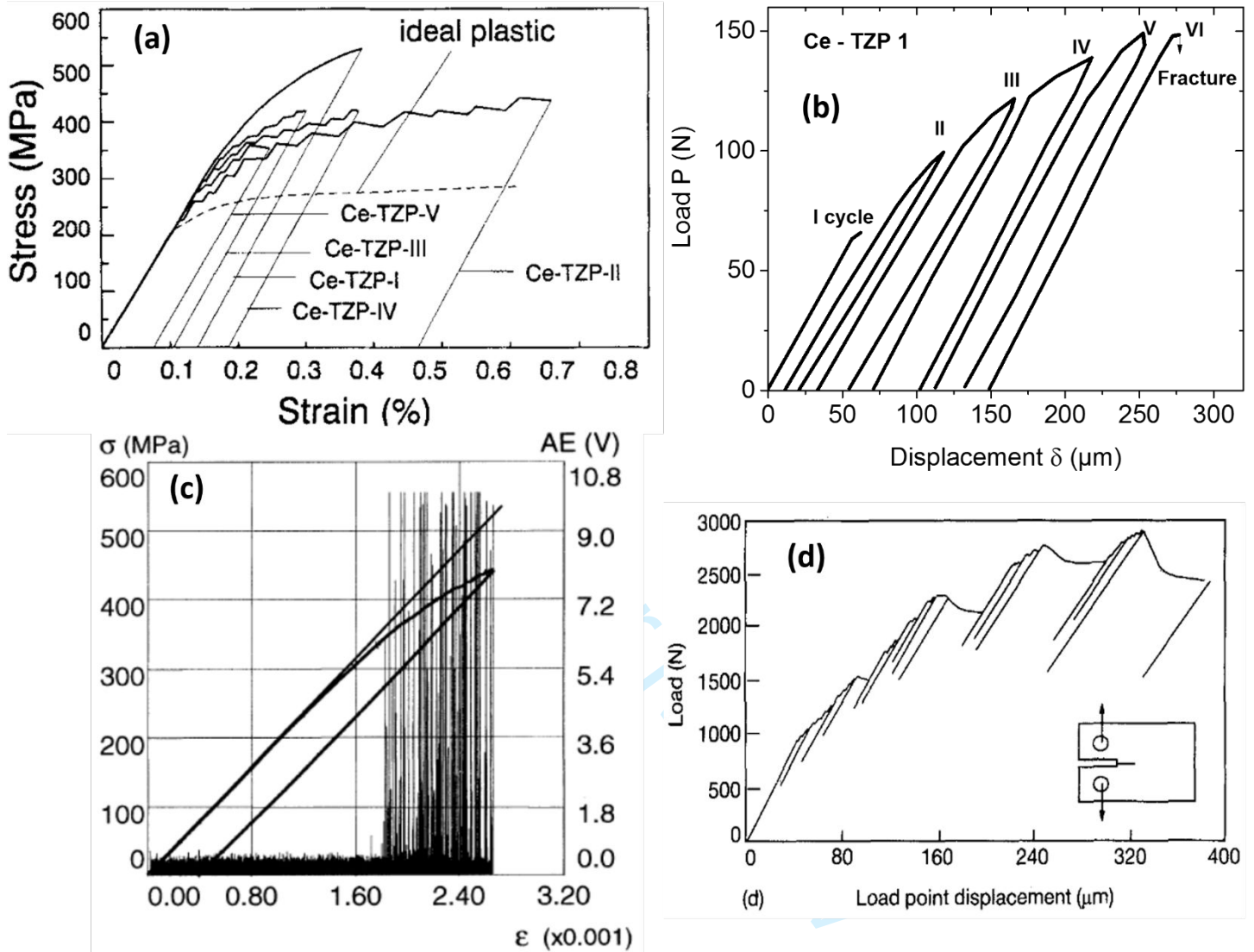


Figure 1.

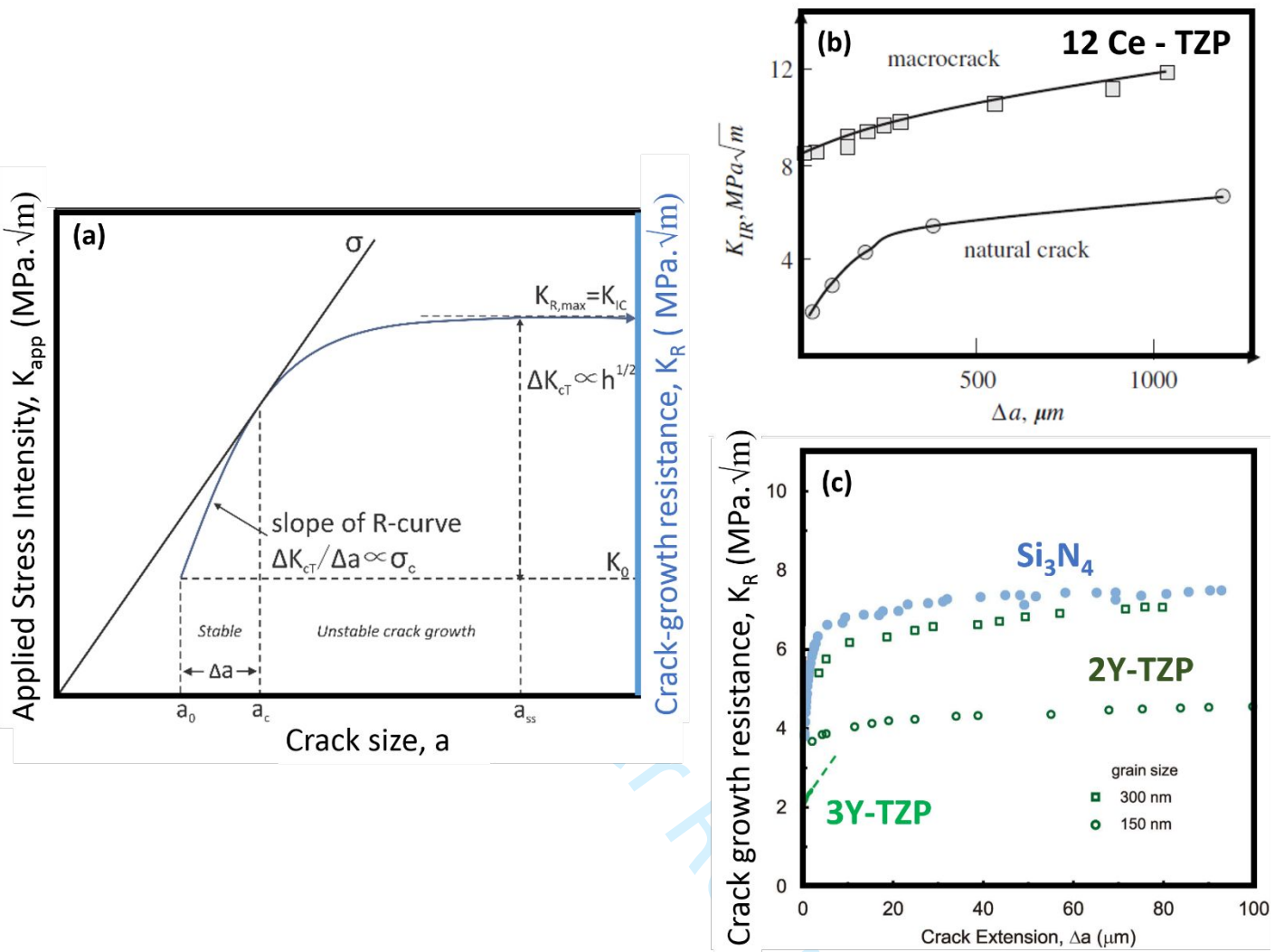


Figure 2.

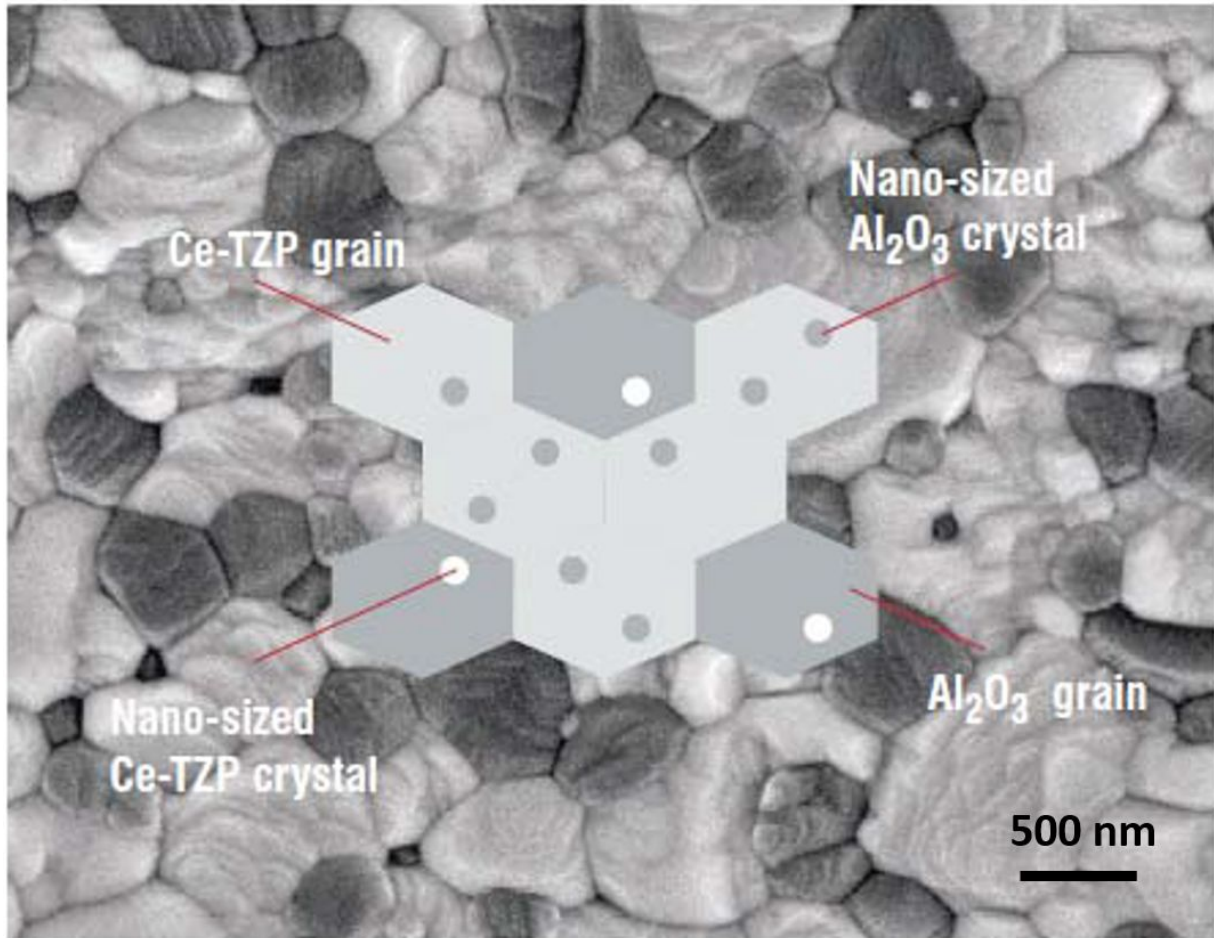


Figure 3.

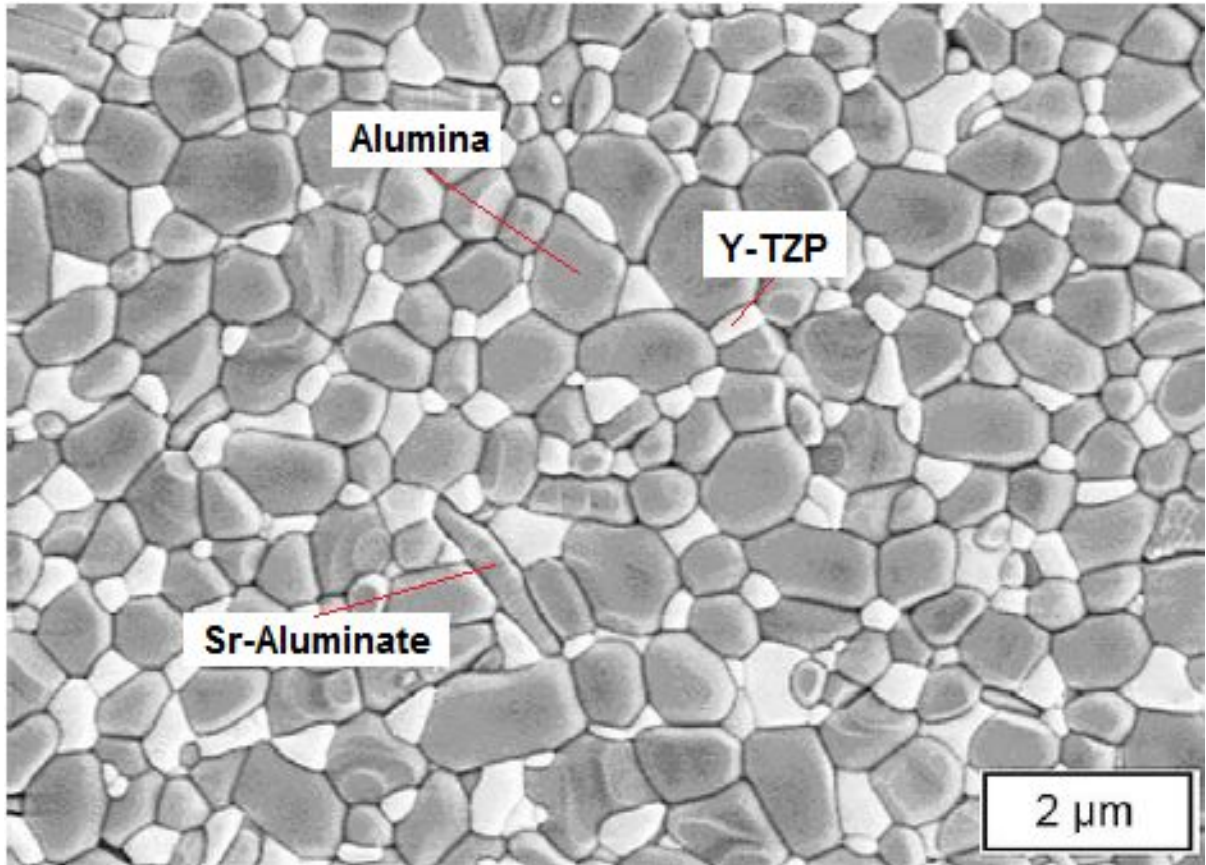


Figure 4.

1  
2  
3  
4  
5  
6  
7  
8  
9  
10  
11  
12  
13  
14  
15  
16  
17  
18  
19  
20  
21  
22  
23  
24  
25  
26  
27  
28  
29  
30  
31  
32  
33  
34  
35  
36  
37  
38  
39  
40  
41  
42  
43  
44  
45  
46  
47  
48  
49  
50  
51  
52  
53  
54  
55  
56  
57  
58  
59  
60

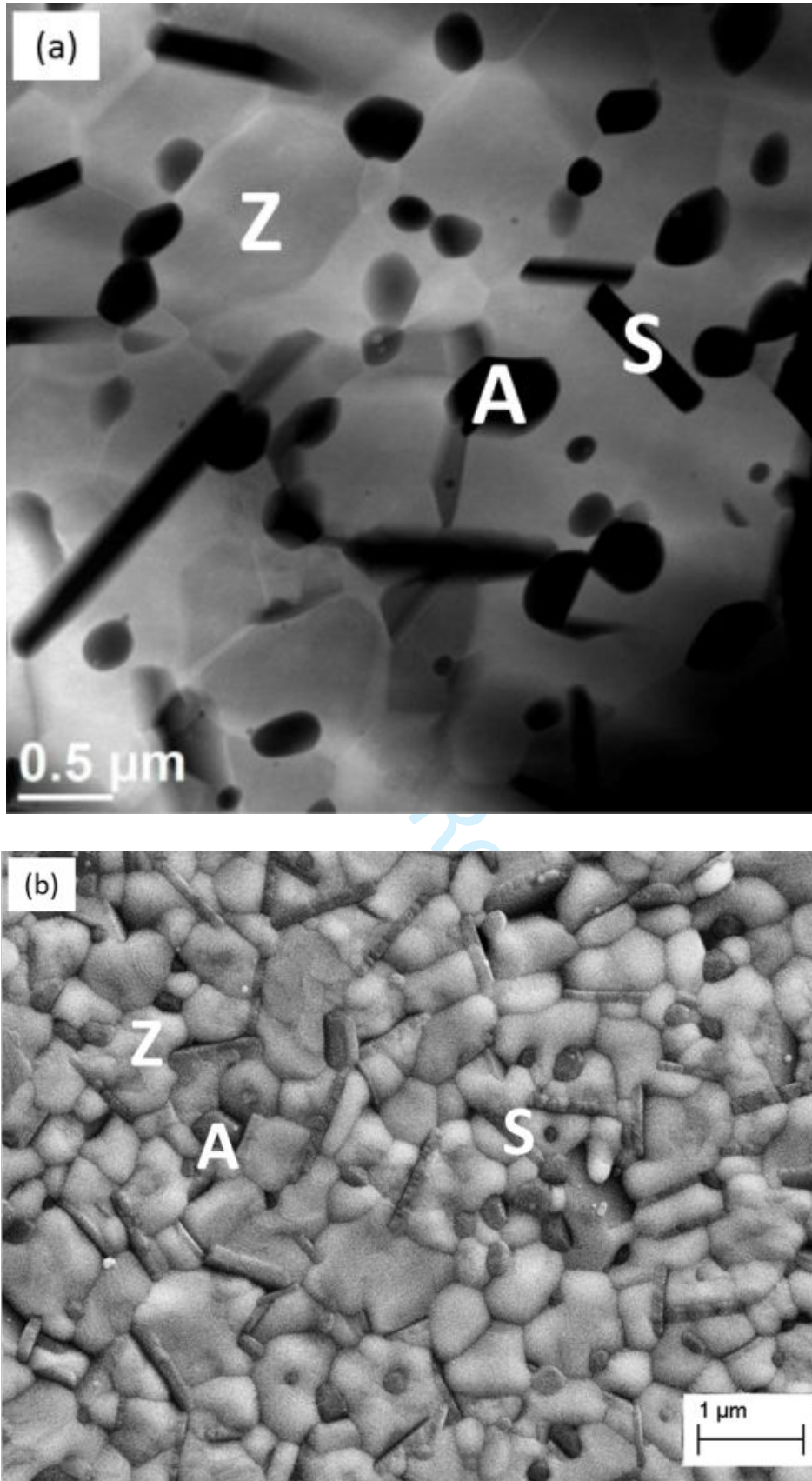


Figure 5.



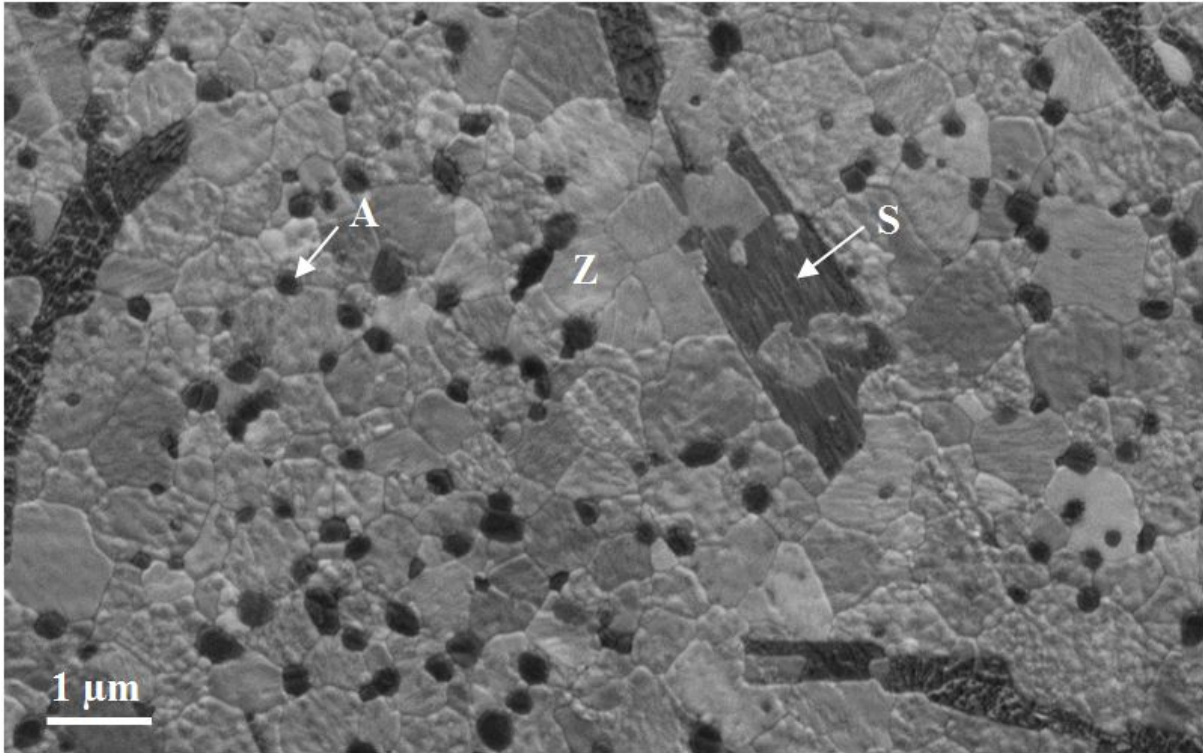


Figure 6.

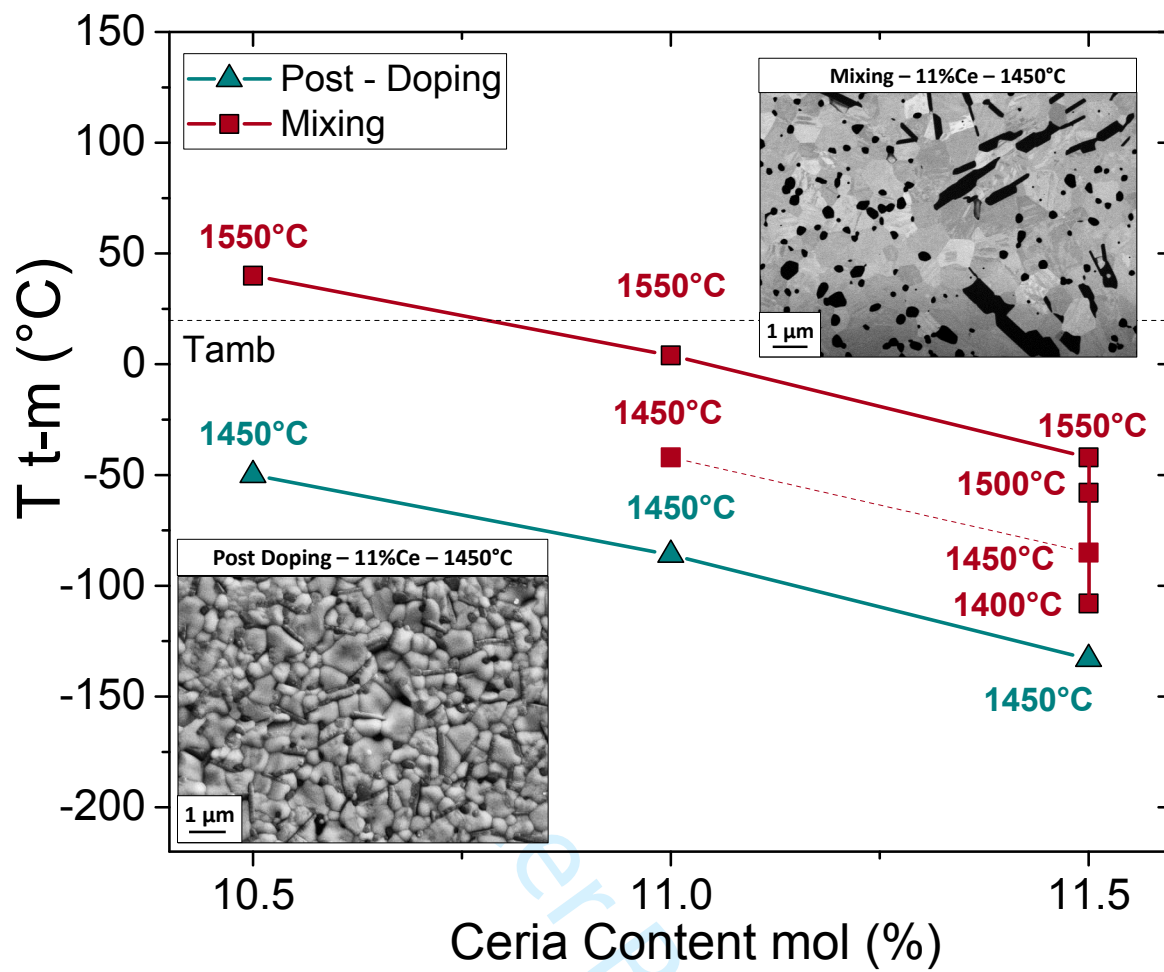


Figure 7.

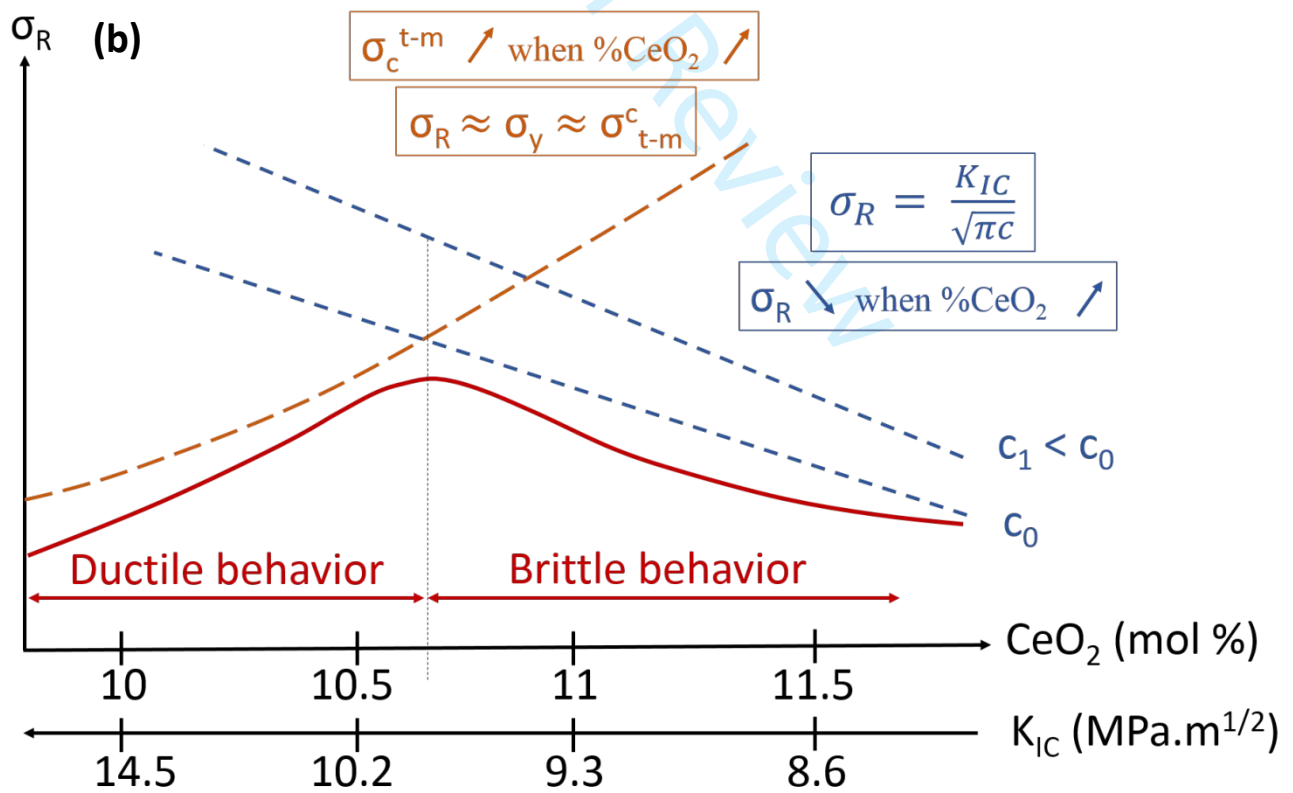
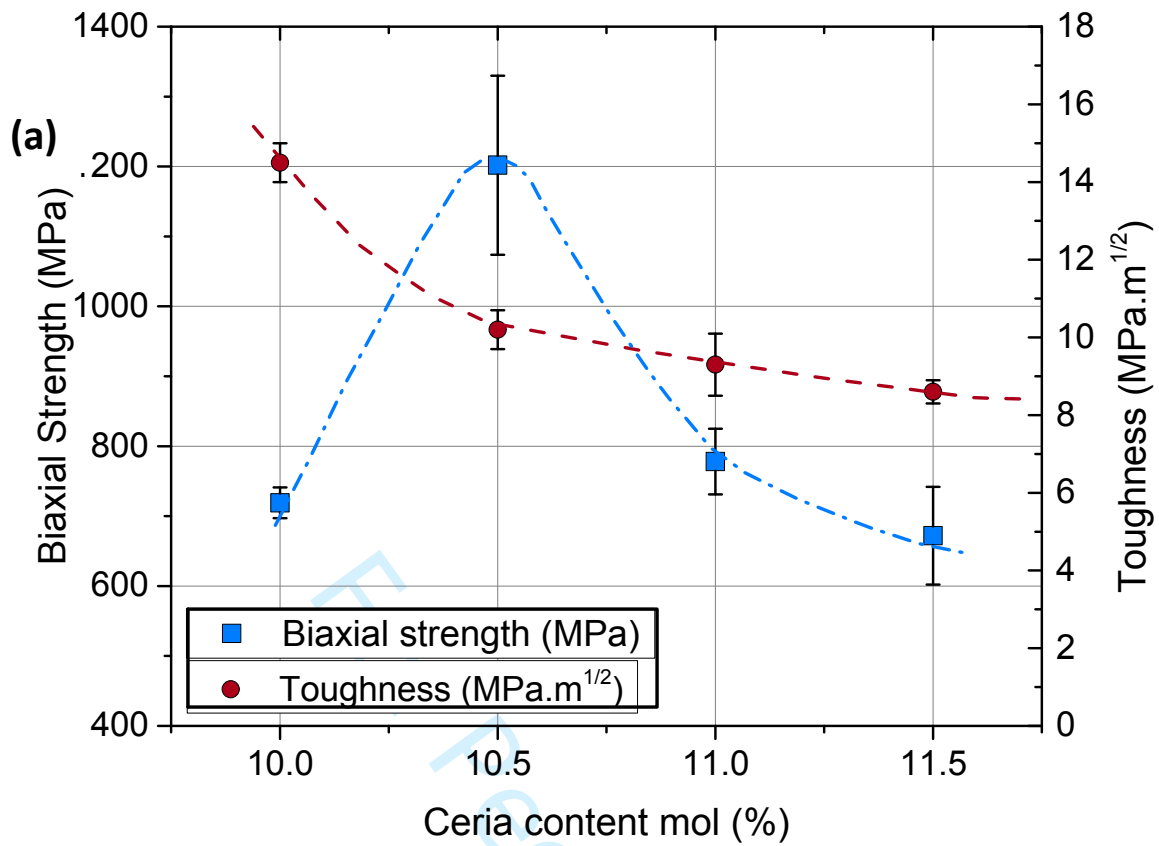


Figure 8.

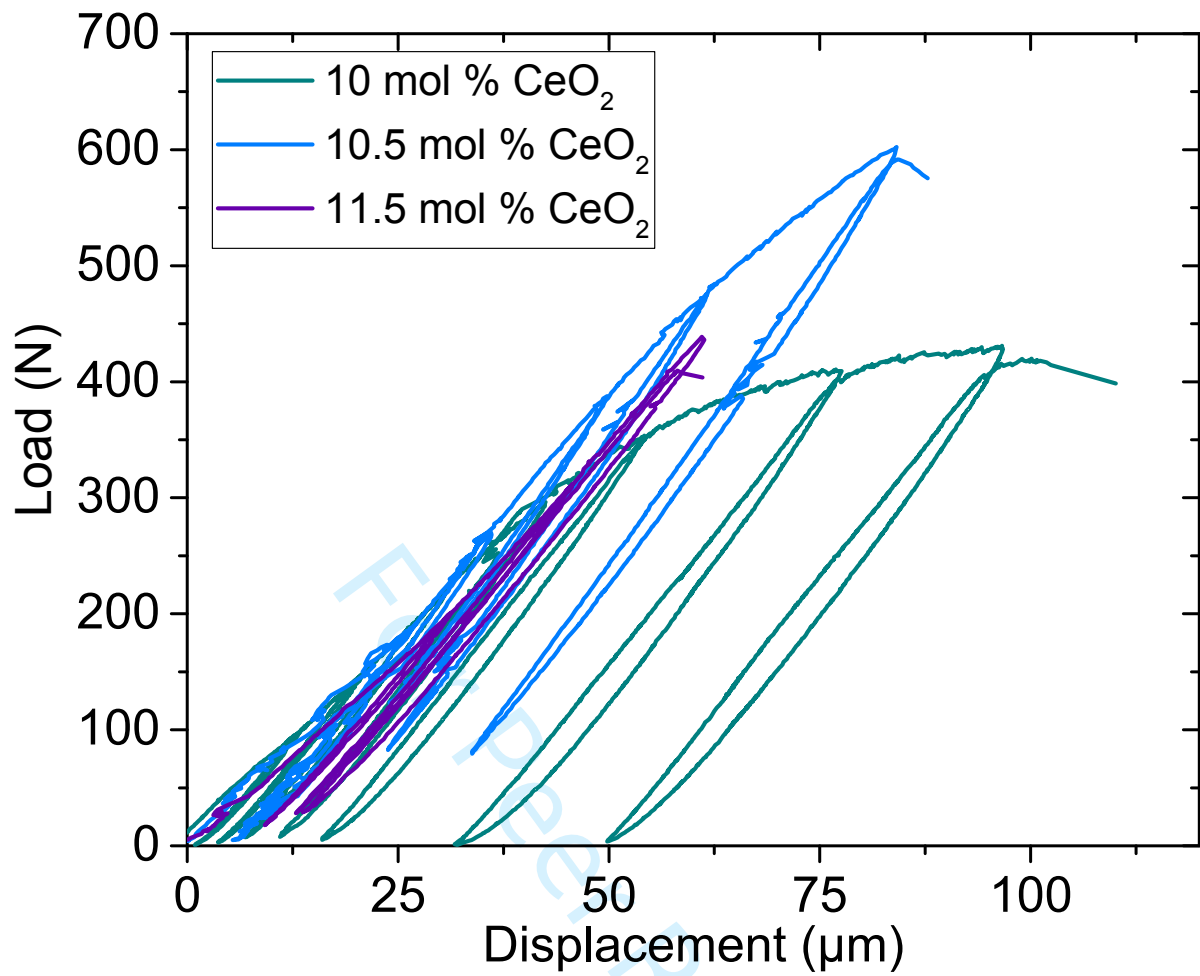


Figure 9.

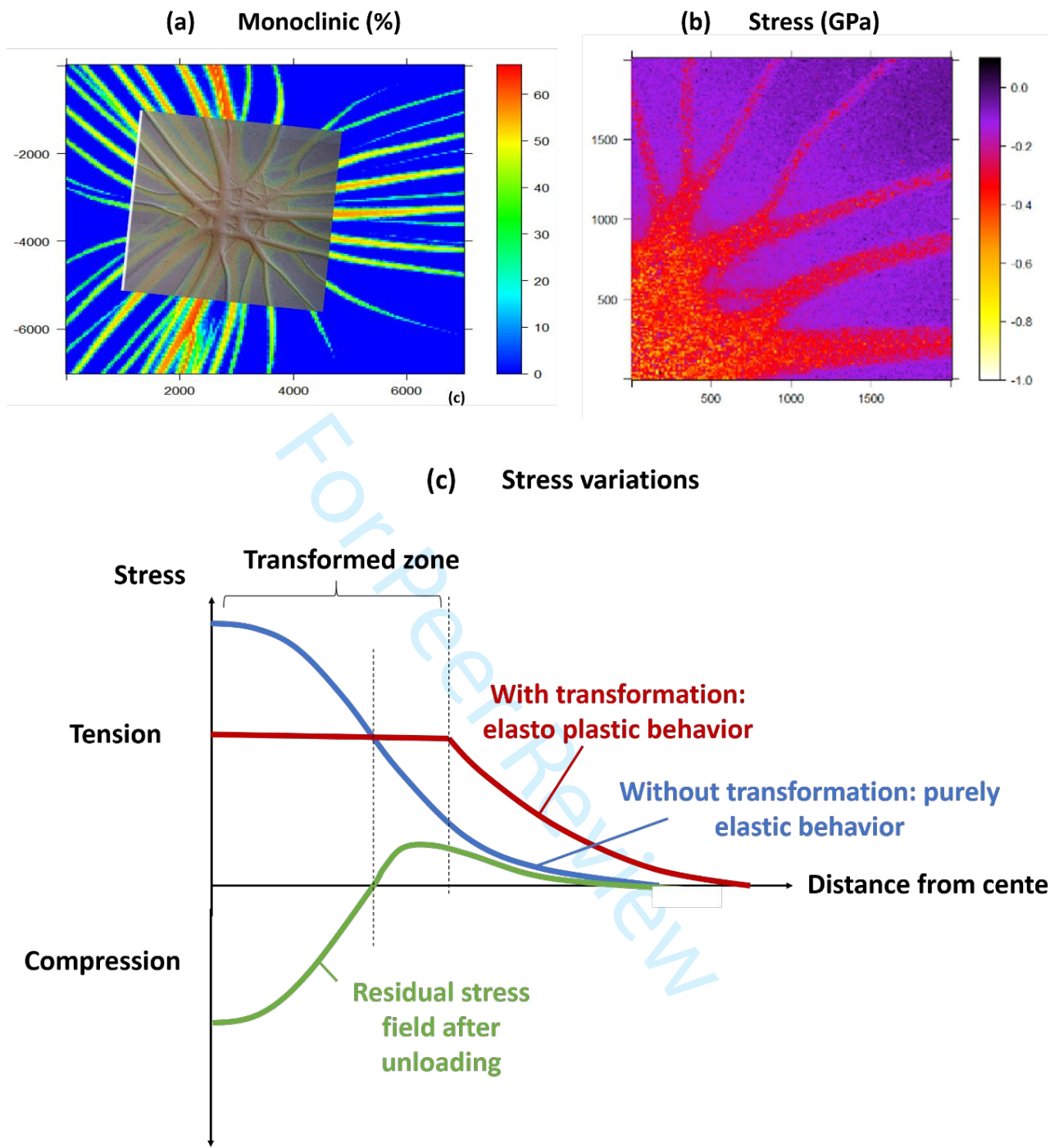


Figure 10.

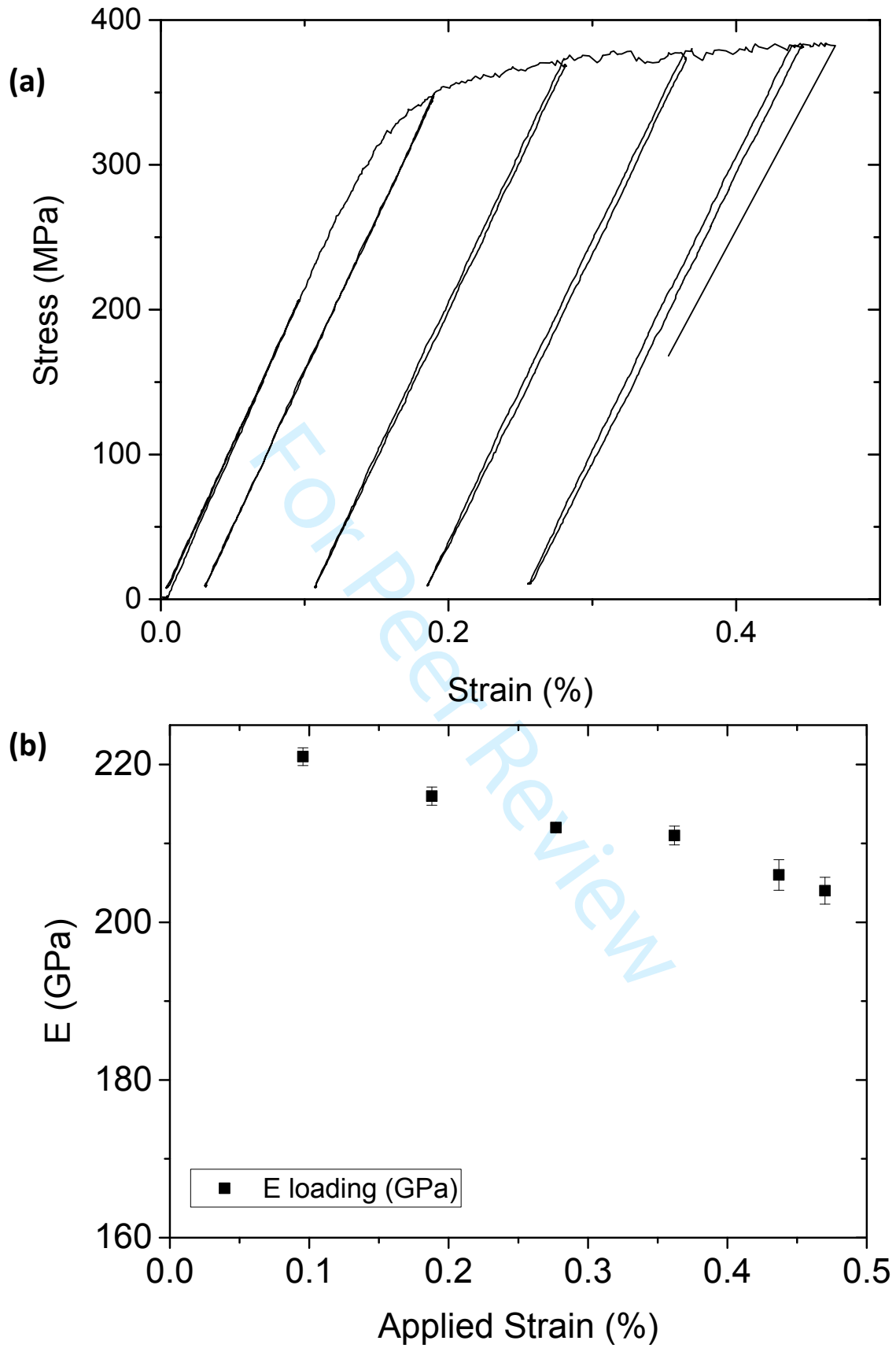


Figure 11.

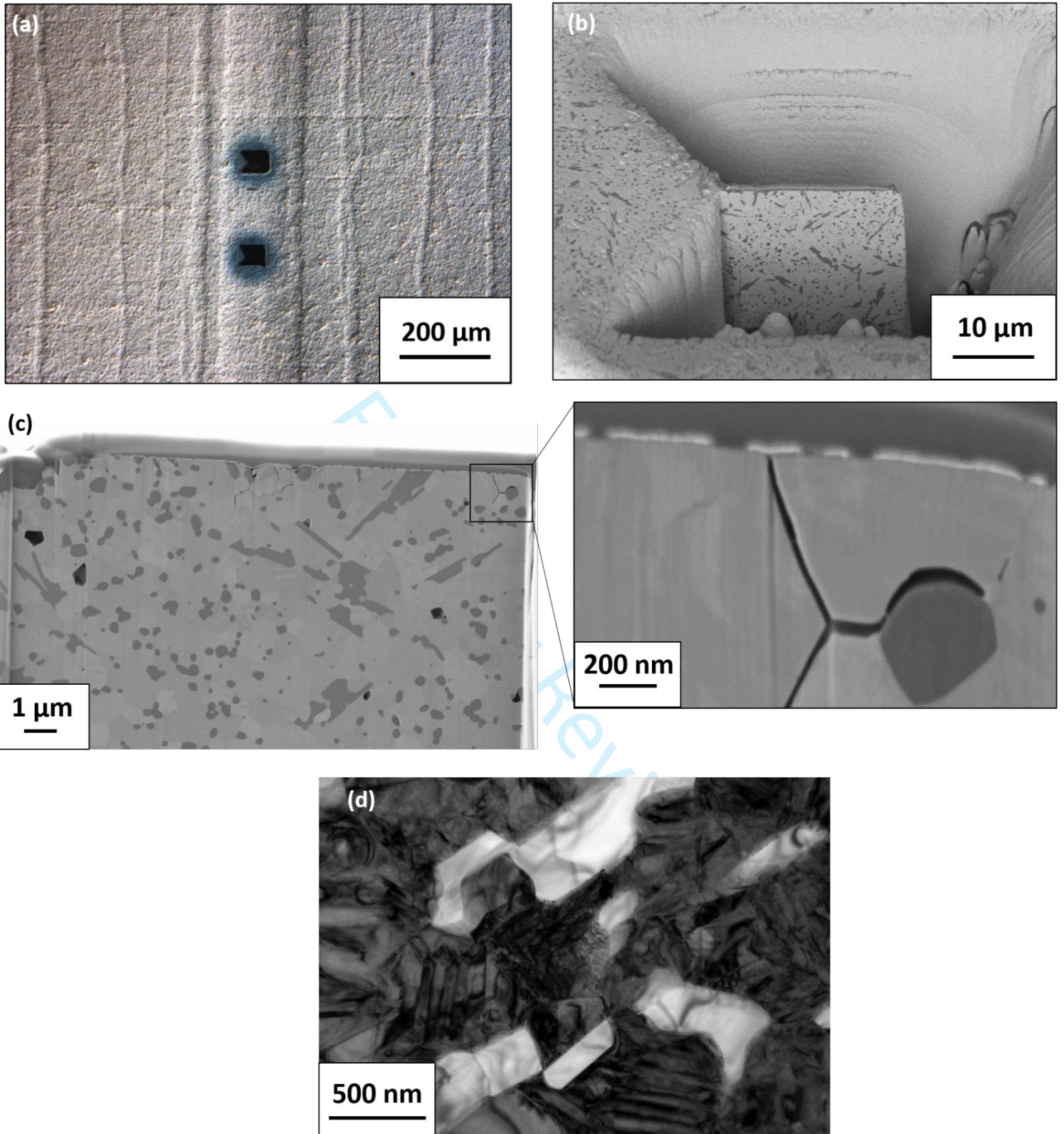


Figure 12.

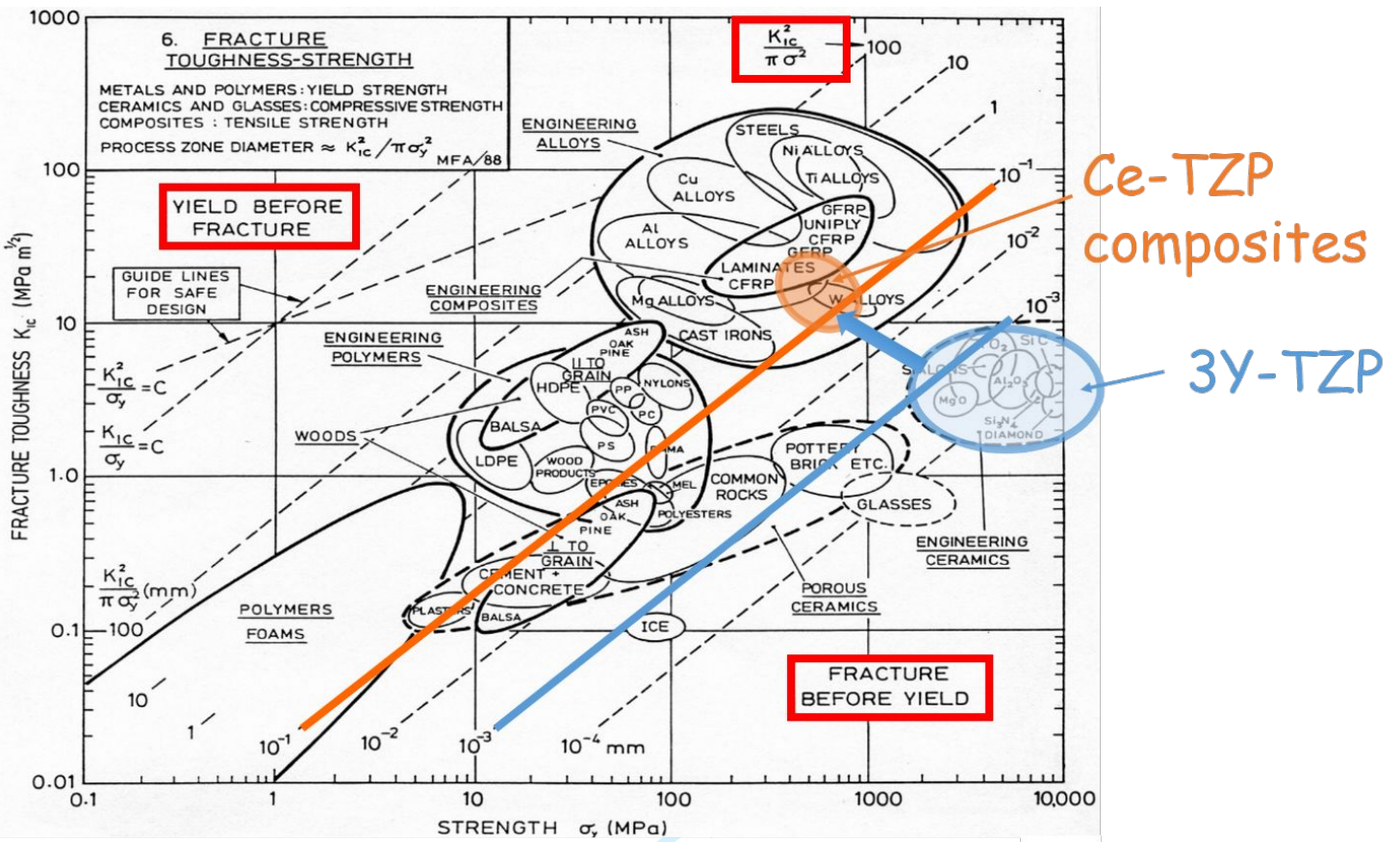


Figure 13.



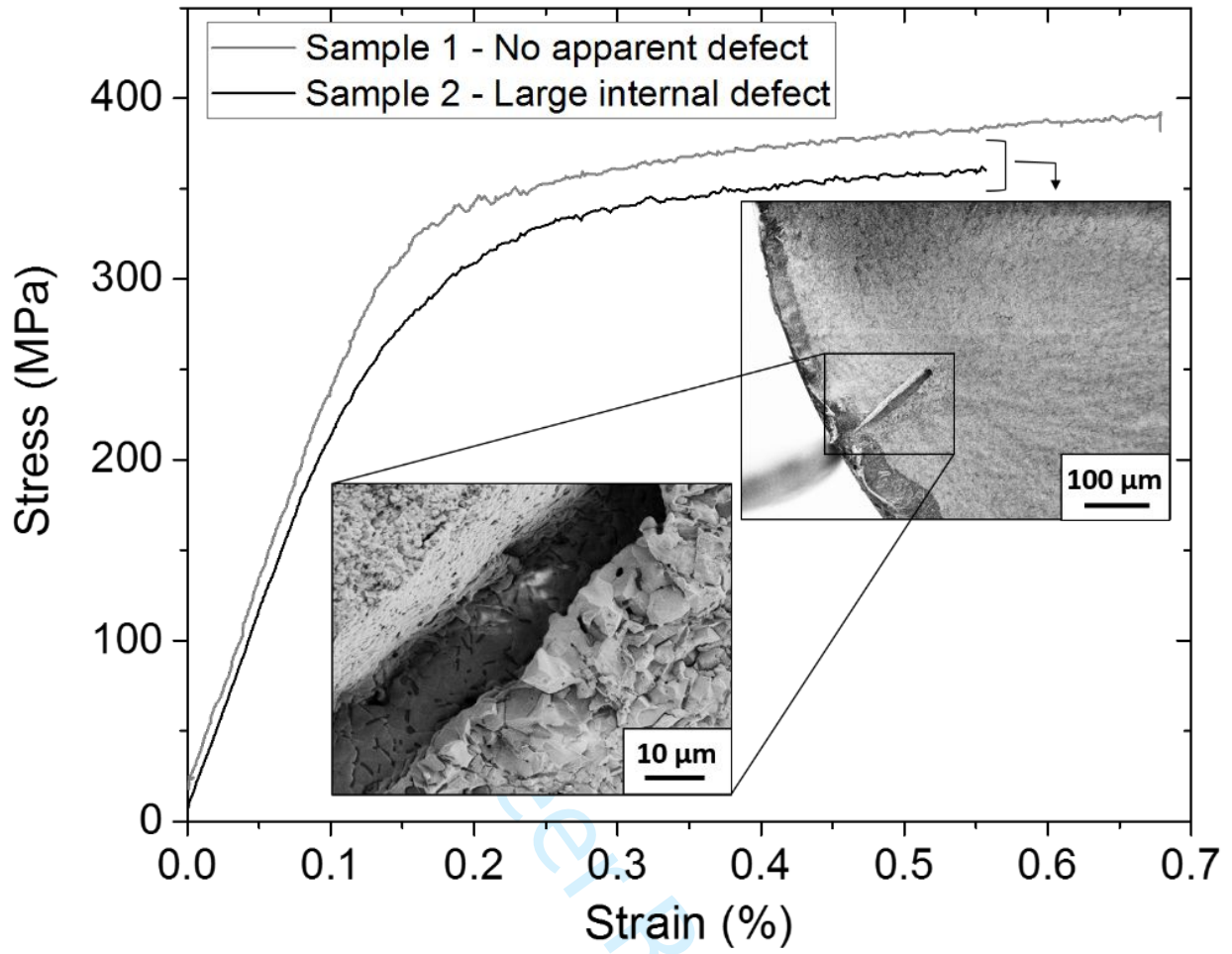


Figure 14.

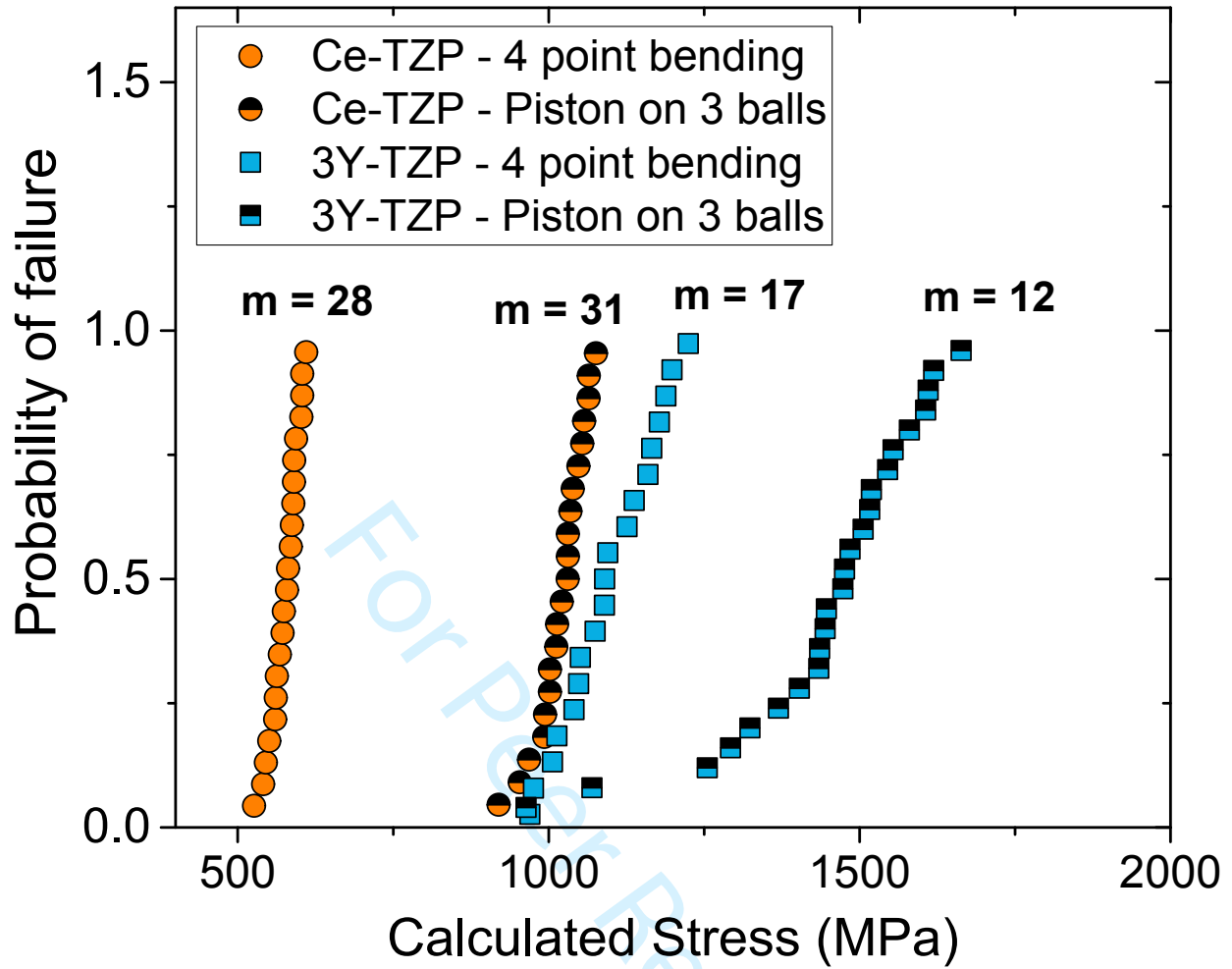


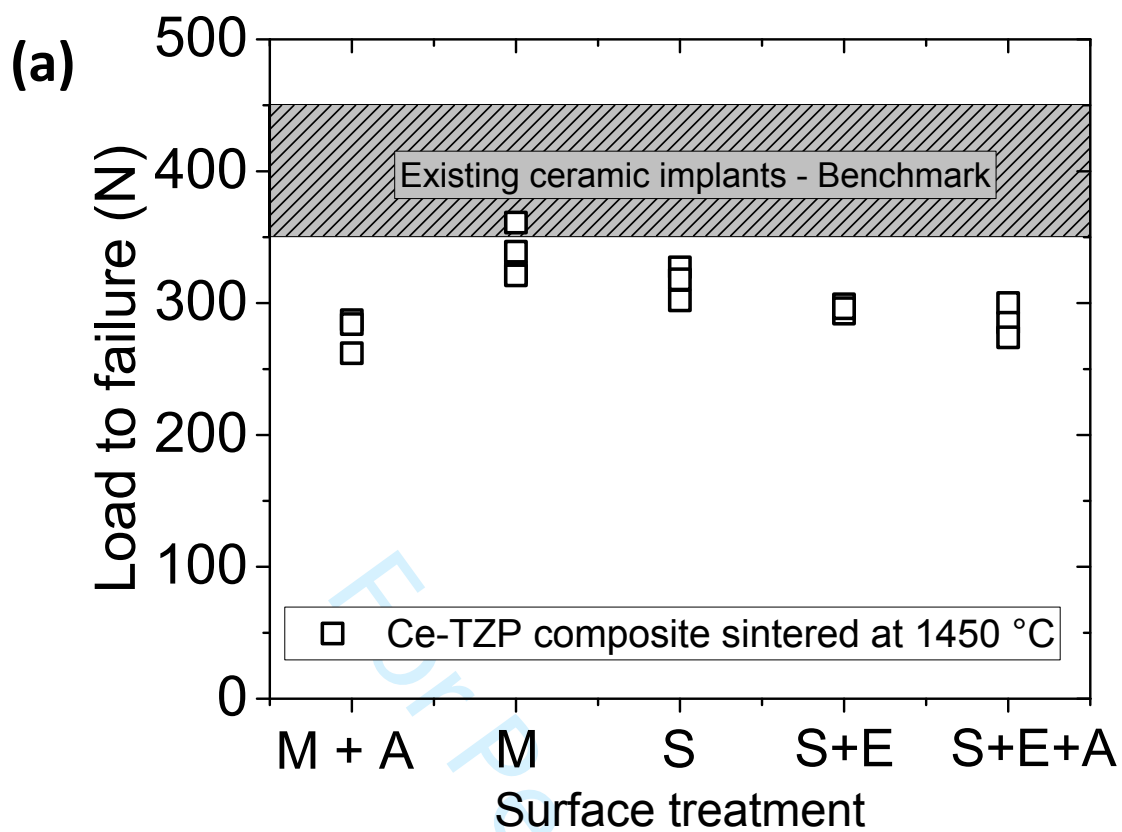
Figure 15.

1  
2  
3  
4  
5  
6  
7  
8  
9  
10  
11  
12  
13  
14  
15  
16  
17  
18  
19  
20  
21  
22  
23  
24  
25  
26  
27  
28  
29  
30  
31  
32  
33  
34  
35  
36  
37  
38  
39  
40  
41  
42  
43  
44  
45  
46  
47  
48  
49  
50  
51  
52  
53  
54  
55  
56  
57  
58  
59  
60



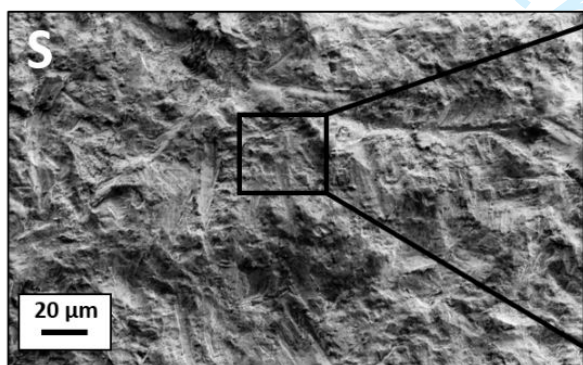
Figure 16.

Peer Review

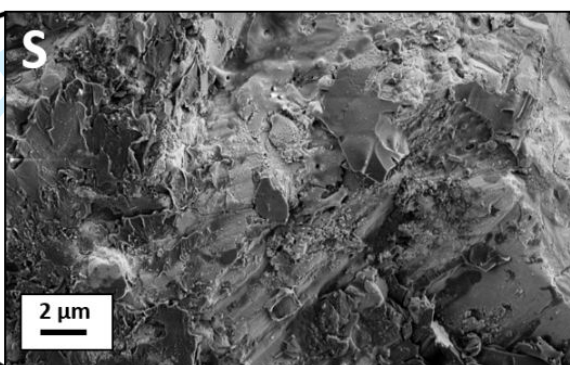


29  
30  
31  
32  
33  
34  
35  
36  
37  
38  
39  
40  
41  
42  
43  
44  
45  
46  
47  
48  
49  
50  
51  
52  
53  
54  
55  
56  
57  
58  
59  
60

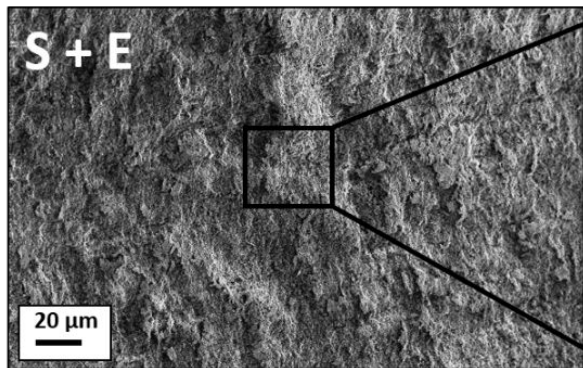
(b)



(c)



(d)

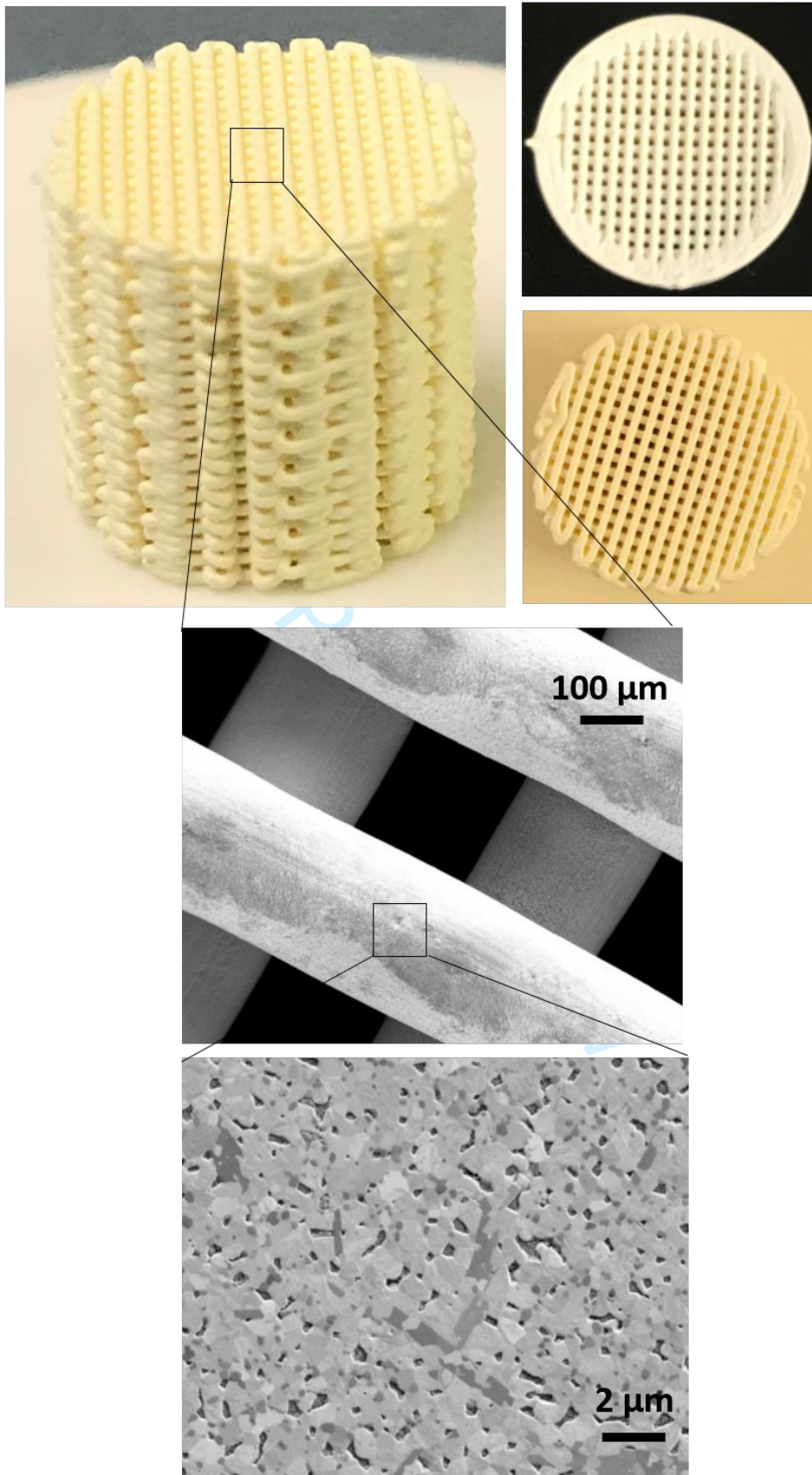


(e)

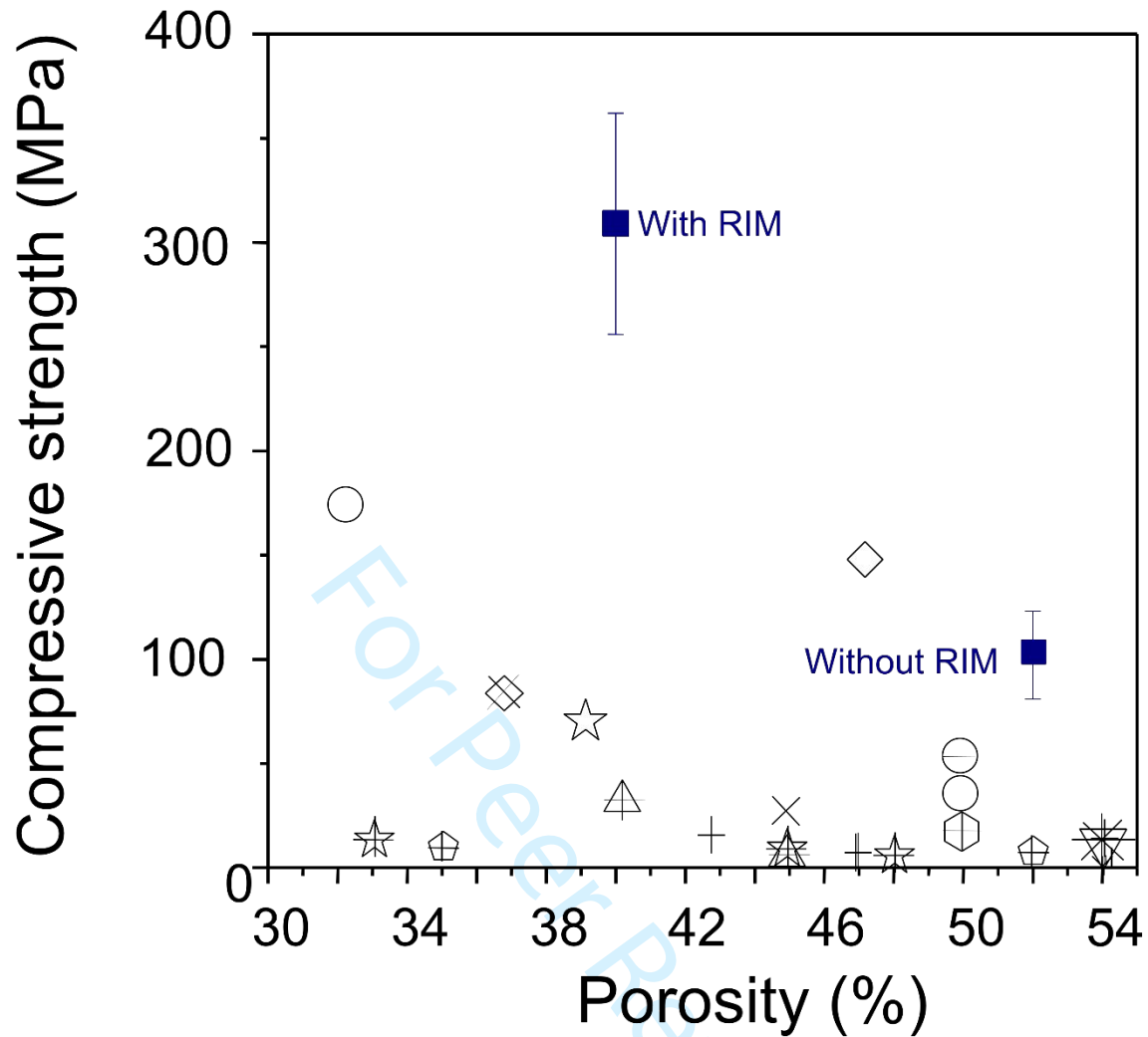


Figure 17.

1  
2  
3  
4  
5  
6  
7  
8  
9  
10  
11  
12  
13  
14  
15  
16  
17  
18  
19  
20  
21  
22  
23  
24  
25  
26  
27  
28  
29  
30  
31  
32  
33  
34  
35  
36  
37  
38  
39  
40  
41  
42  
43  
44  
45  
46  
47  
48  
49  
50  
51  
52  
53  
54  
55  
56  
57  
58  
59  
60



**Figure 18.**



- ZA8Sr8Ce11 DIW, this work
- 10Ce-TZP-Al<sub>2</sub>O<sub>3</sub> DIW [126]
- + TCP, microwave sintering Binder jetting [127]
- ▽ TCP, conventional sintering Binder jetting [127]
- ◇ DLM infiltrated TTCP/b-TCP 3DP [128]
- ☆ HA DIW [129]
- ✱ CaP Binder jetting [130,131]
- ⬠ TCP Binder jetting [131]
- ☆ TCP+ZnO Binder jetting [132]
- ⬠ Bioglass SLS [133]
- △ HA SLA [134]
- × TCP DIW [135]
- ◇ Lamellar HA Freeze casting [136]

Figure 19.

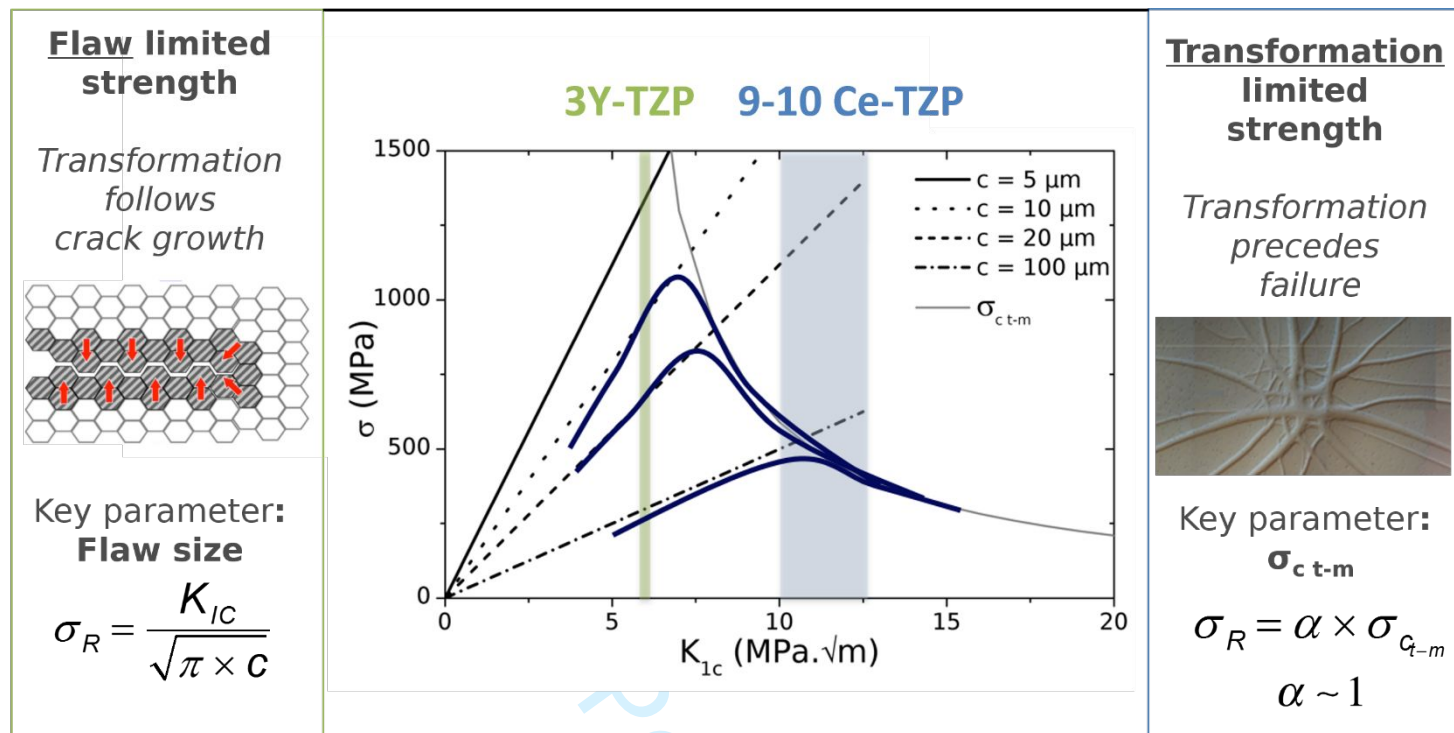


Figure A-1.

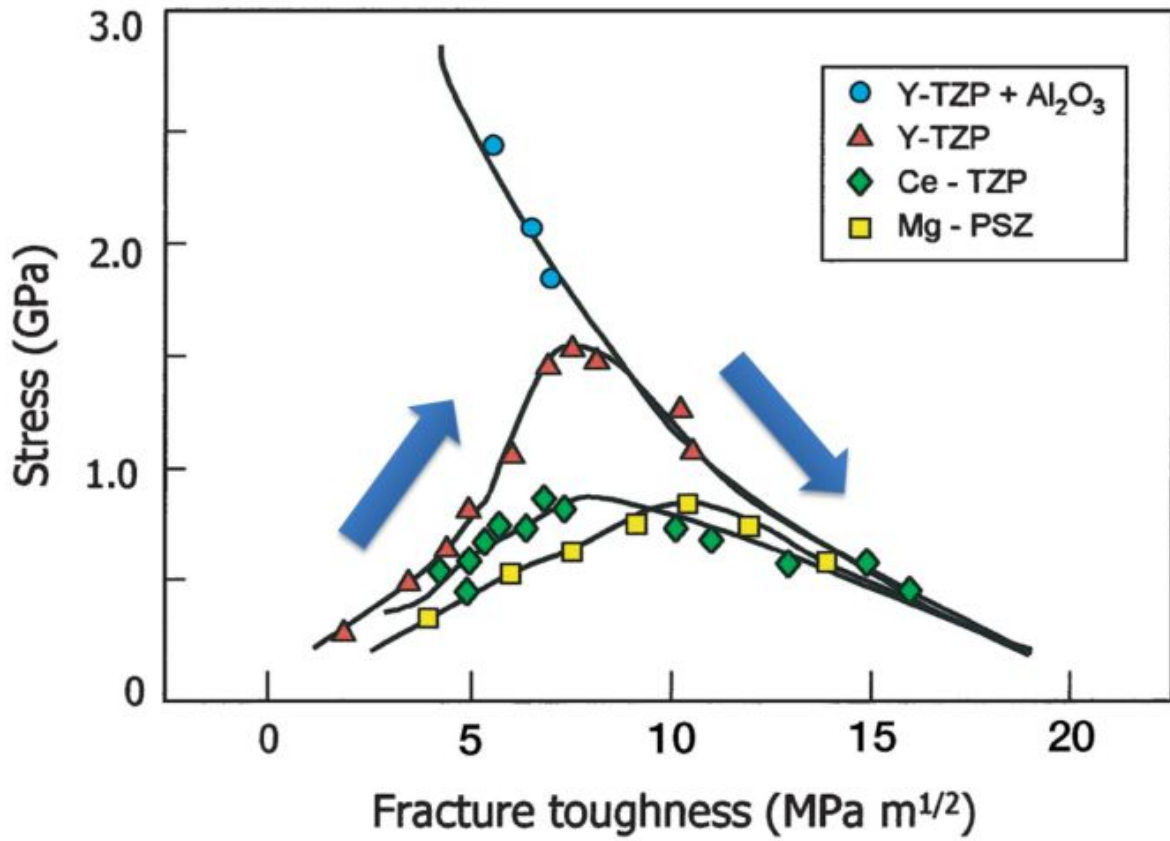


Figure A-2.



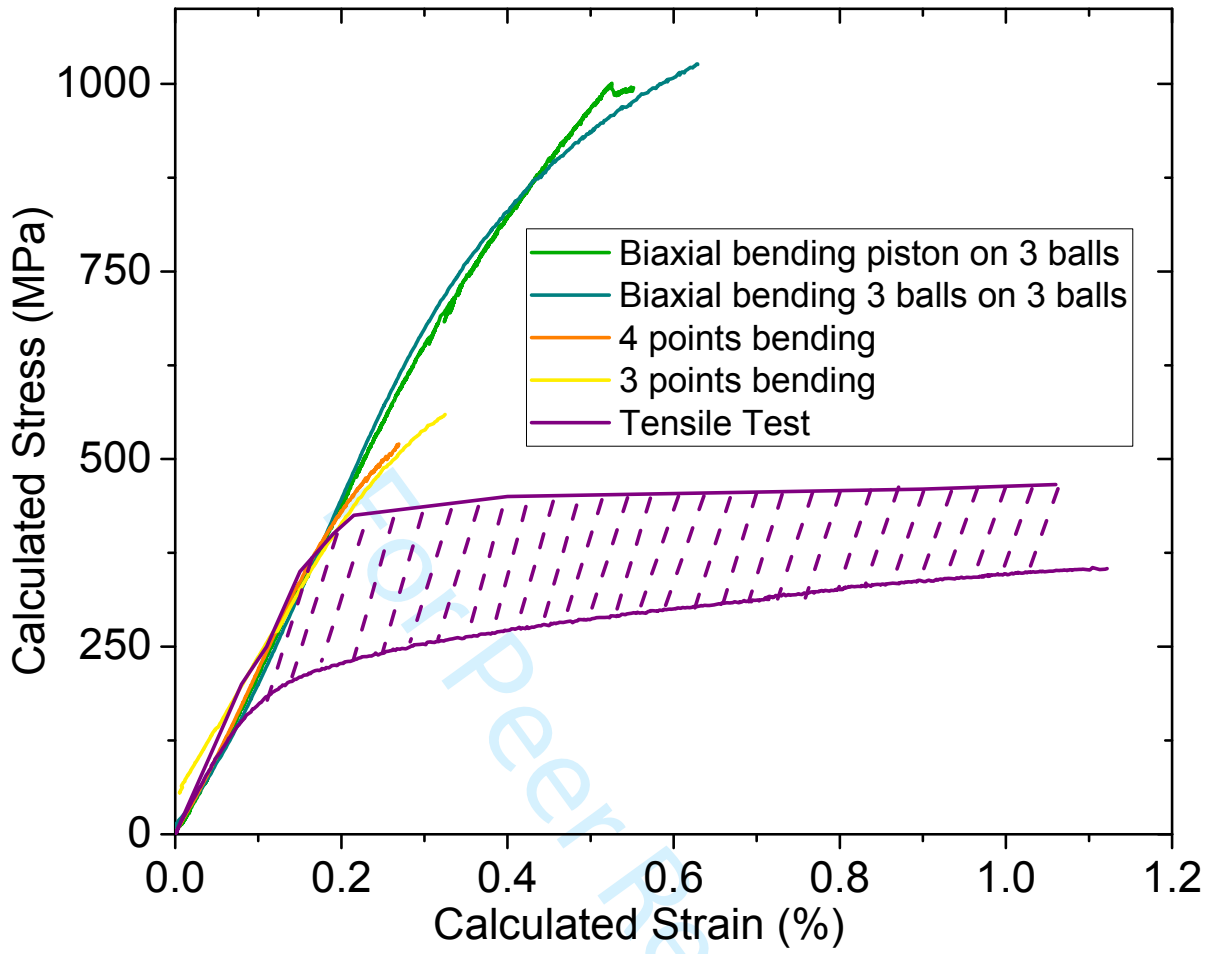


Figure B-1.

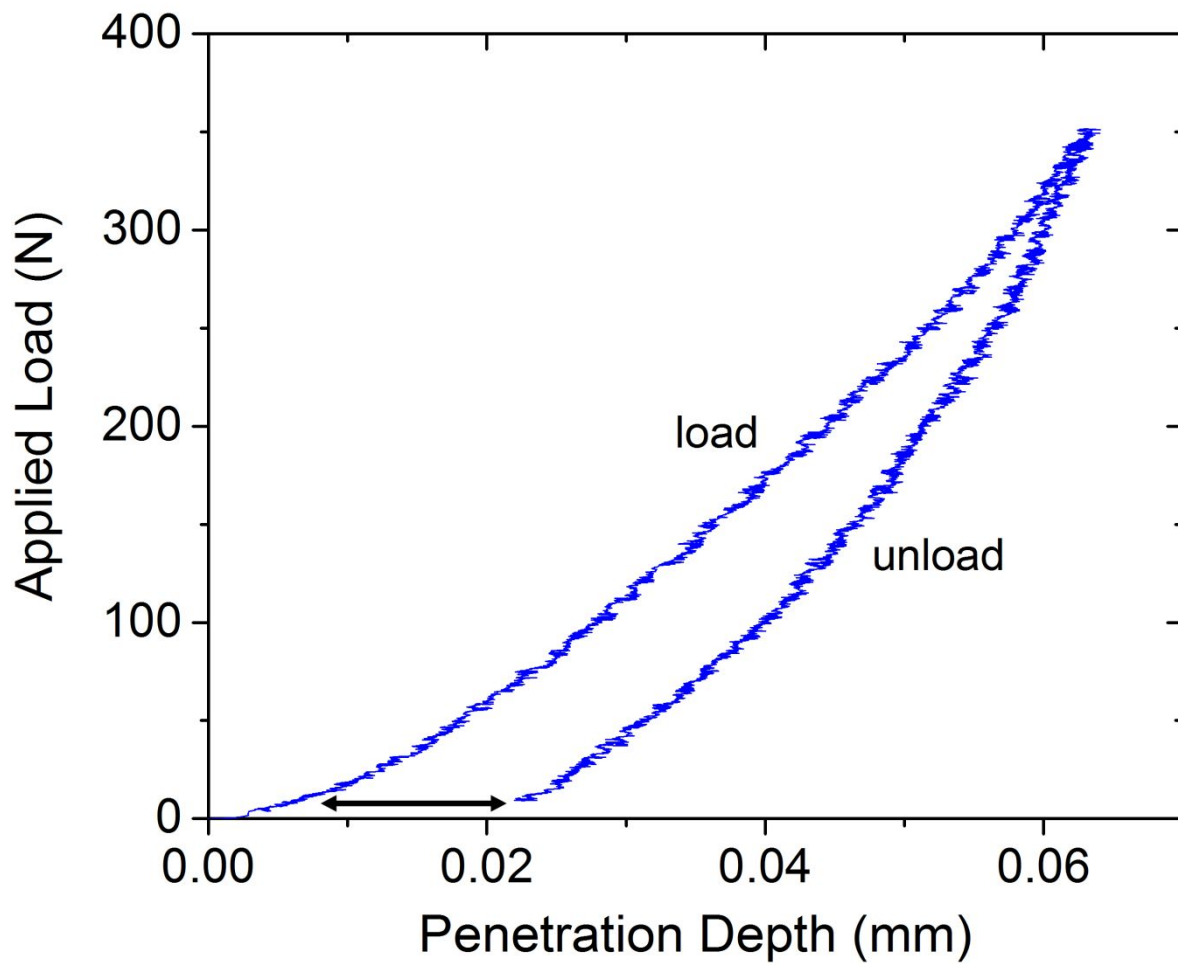


Figure B-2.

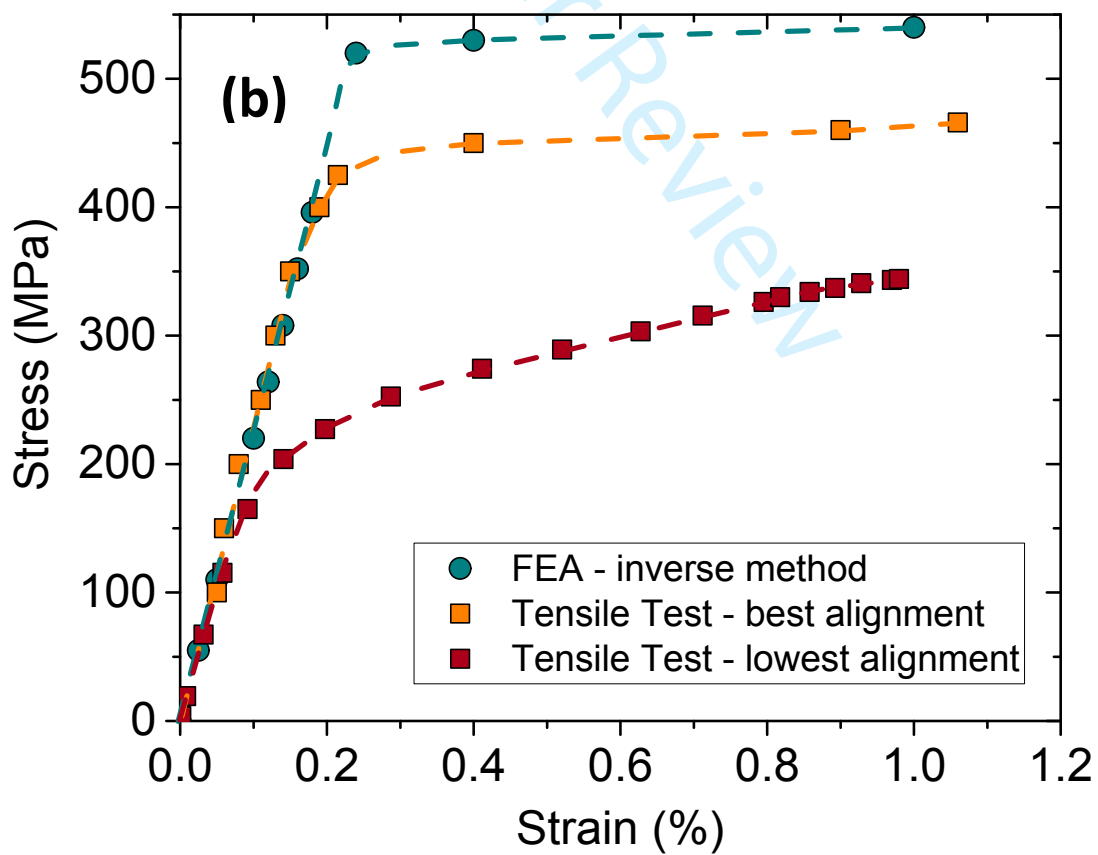
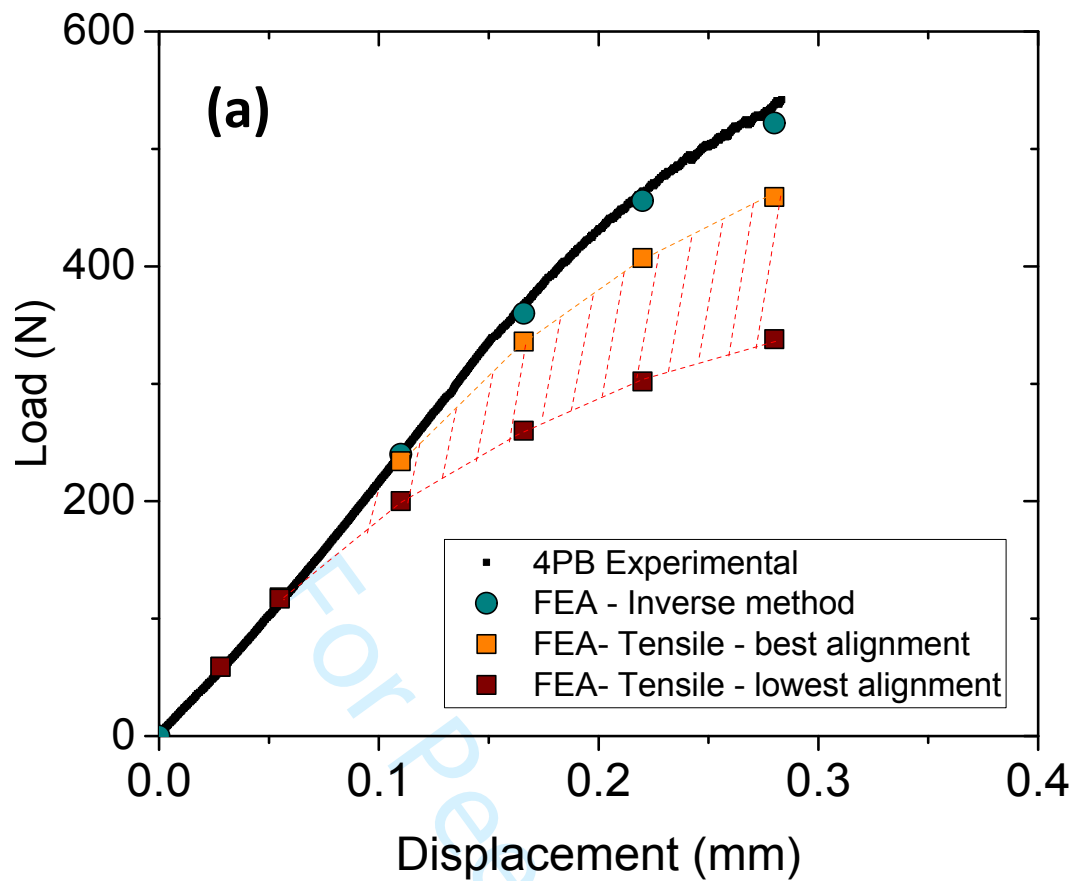


Figure B-3.

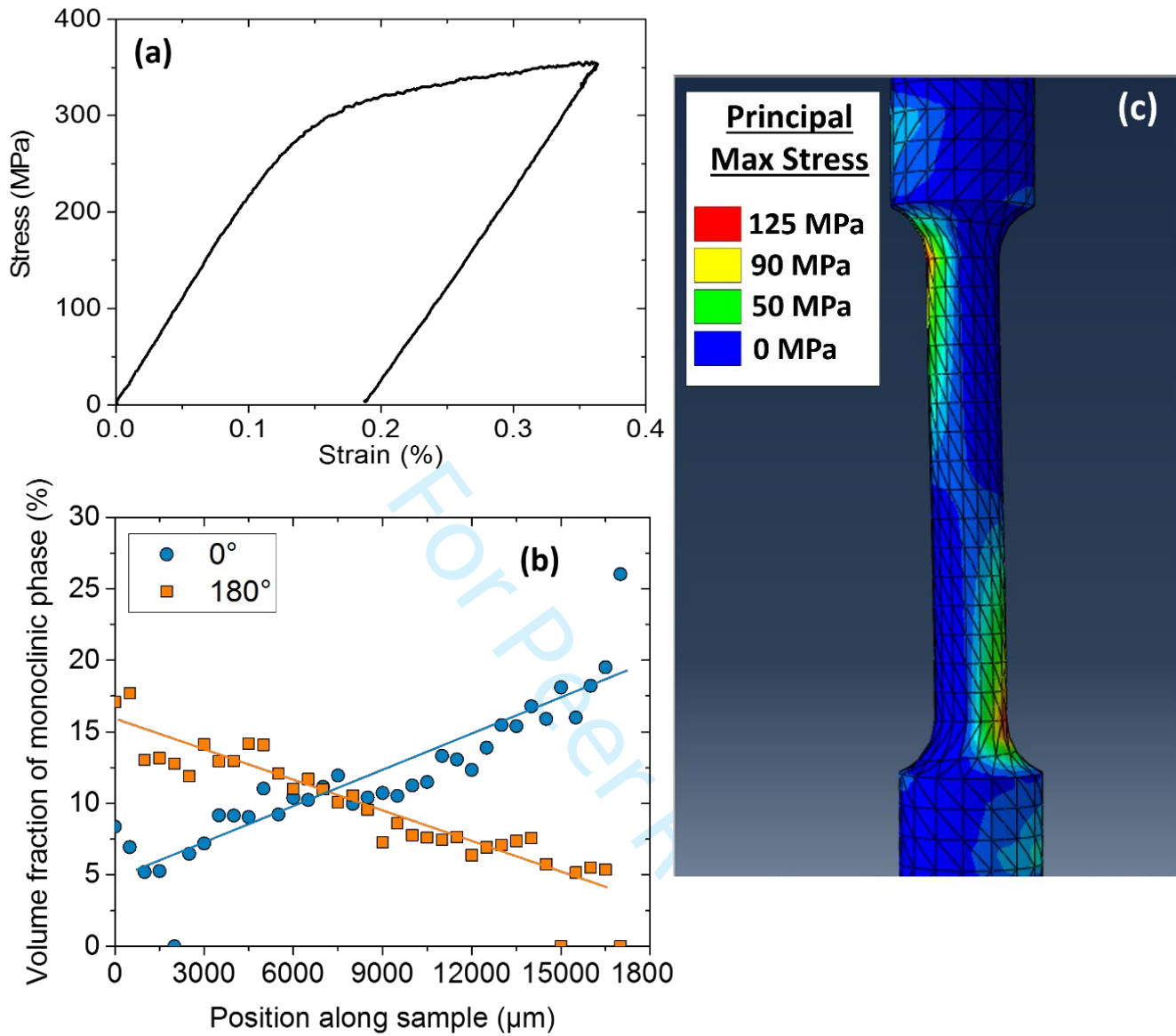
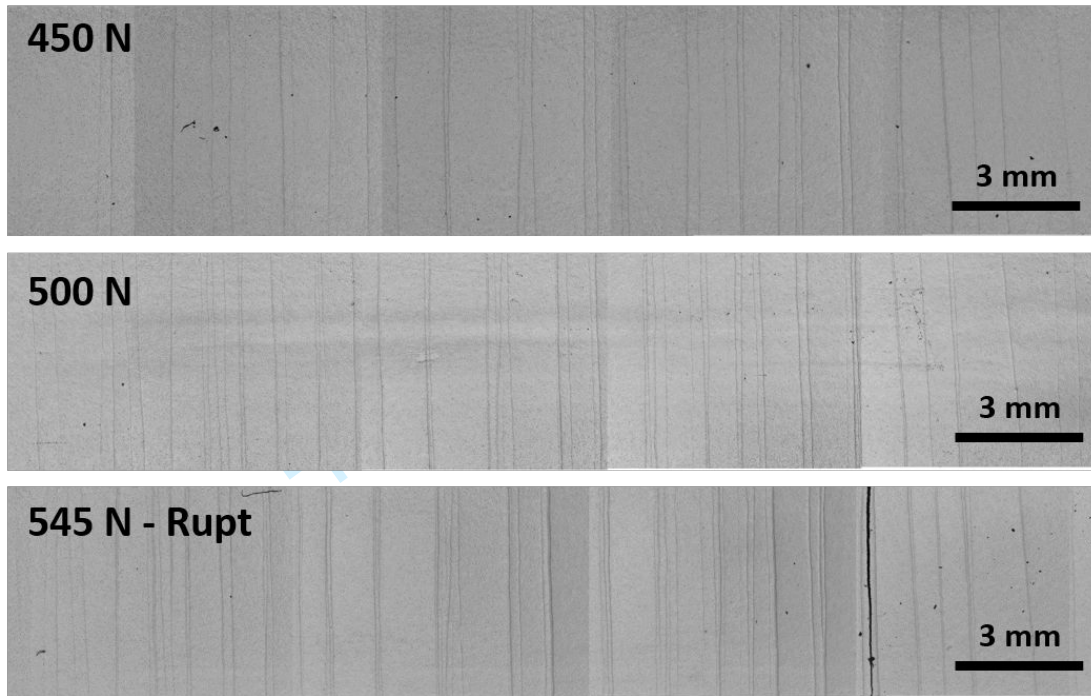


Figure B-4.

1  
2  
3  
4  
5  
6  
7  
8  
9  
10  
11  
12  
13  
14  
15  
16  
17  
18  
19  
20  
21  
22  
23  
24  
25  
26  
27  
28  
29  
30  
31  
32  
33  
34  
35  
36  
37  
38  
39  
40  
41  
42  
43  
44  
45  
46  
47  
48  
49  
50  
51  
52  
53  
54  
55  
56  
57  
58  
59  
60

### (a) 4 Point Bending



### (b) Biaxial Bending – Piston on 3 balls

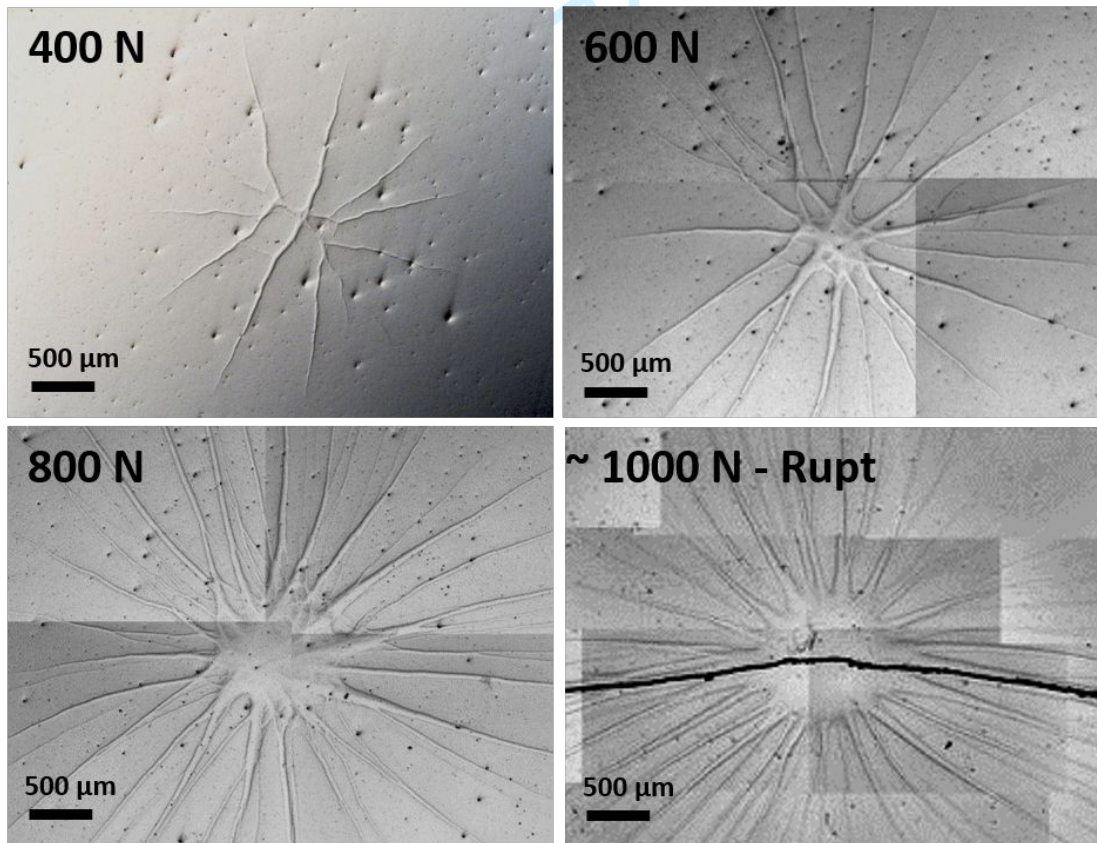
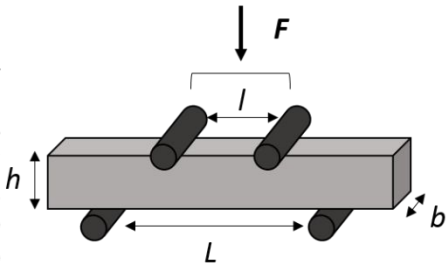


Figure B-5.

## APPENDIX

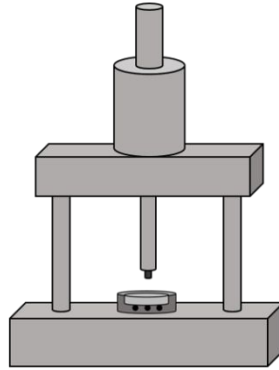
## 4 Point Bending



$$\sigma_{max} = \frac{3 F(L-l)}{2 b h^2} \quad (1)$$

With  $F$  the load to failure,  $b$  the width,  $h$  the thickness of the sample,  $L$  and  $l$  the outer and inner spans

## Biaxial Bending Piston on 3 balls



$$\sigma_{max} = \frac{-0.2387 F(X-Y)}{t^2} \quad (2)$$

$$X = (1 + \nu) \ln\left(\frac{r_2}{r_3}\right)^2 + \left[\frac{(1 - \nu)}{2}\right] \left(\frac{r_2}{r_3}\right)^2$$

$$Y = (1 + \nu) \left[1 + \ln\left(\frac{r_1}{r_3}\right)^2\right] + (1 - \nu) \left(\frac{r_2}{r_3}\right)^2$$

With  $F$  the load to failure,  $t$  the thickness of the disk sample,  $r_1$  the radius of the supported circle,  $r_2$  the radius of the piston,  $r_3$  the radius of the disk sample and  $\nu$  the Poisson's coefficient

## Tensile Test

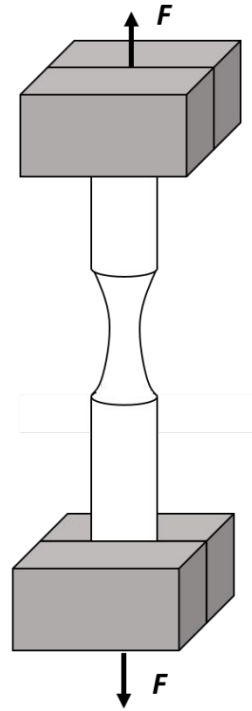


Table 1.

Materials	Toughness (MPa·m <sup>1/2</sup> )	Strength (MPa)	Weibull modulus	Inelastic deformation	Grain size (μm)	
					ZrO <sub>2</sub>	Al <sub>2</sub> O <sub>3</sub>
3Y-TZP <sup>[27]</sup>	4-6	800-1200	~8 <sup>[27]</sup>	-	~ 0.3	-
Ce-TZP <sup>[27, 28]</sup>	7-16	400-600	~20 <sup>[27]</sup>	0.25-0.45 % (4PB) <sup>[28]</sup>	~ 2	-
10Ce-TZP/30Al <sub>2</sub> O <sub>3</sub> nanocomposite <sup>[29, 30, 35]</sup>	9.8*	950	12.6 (4PB) 23.0 (P3B)	~ 0.1-0.3 % (4PB)	0.42 ± 0.08	0.59 ± 0.09
NANOZR <sup>[37]</sup>	8.6	1290	-	-	-	-
10.5Ce-TZP/8Al <sub>2</sub> O <sub>3</sub> / SrAl <sub>12</sub> O <sub>19</sub> <sup>[11, 12]</sup>	10.2*	1100 (P3B)	-	-	0.6 ± 0.2	0.3 ± 0.1 μm
MnO-doped 12Ce- TZP/10Al <sub>2</sub> O <sub>3</sub> <sup>[26, 31]</sup>	7.6-10*	650	40 (4PB)	(4PB) (Uniaxial tension)	1.5-2.5	-
10Ce-TZP/16 vol.% of MgAl <sub>2</sub> O <sub>4</sub> <sup>[38]</sup>	15§	900	-	-	0.5	0.2
12Ce-TZP/SrO/Al <sub>2</sub> O <sub>3</sub> <sup>[21]</sup>	8.3-14.0	500-700	-	0.5%-1.5% (compression)	~ 2	-

\*Measured by single edge V-notch beam (SEVNB); § Measured by double torsion; 4PB: four-point bending; P3B: piston-on-three-balls